aerospace

MDPI

Review

Additive Manufacturing of Structural Components for PocketQube-Class Satellites: A Systematic Review of Materials, Processes, Qualification Pathways, and ECSS Compliance

Sebastian Valencia [1,2,*], Carolina Acevedo Nisperuza [3], Jaime Enrique Orduy [1] and Cristian Lozano [1]

[1] Department of Engineering and Basic Sciences, Fundación Universitaria Los Libertadores, Bogotá 110111, Colombia; jeorduyr@libertadores.edu.co (J.E.O.); clozanot@libertadores.edu.co (C.L.)
[2] School of Aerospace, Transport and Manufacturing (SATM), Cranfield University, Cranfield MK43 0AL, UK
[3] Department of Aerospace Engineering, Embry-Riddle Aeronautical University, Daytona Beach, FL 32114, USA; acevedc7@my.erau.edu
* Correspondence: sfernandezv@libertadores.edu.co

Abstract

PocketQube-class satellites have emerged as a cost-effective platform for space access; however, their extreme mass, volume, and dimensional constraints challenge conventional manufacturing approaches. This systematic review examines the state of the art of additive manufacturing (AM) for PocketQube structural systems between 2015 and 2026, focusing on materials, manufacturing processes, design methodologies, qualification frameworks, and flight heritage. A PRISMA-guided review methodology combined with a PICO/SPIDER-based selection framework was applied to analyse the peer-reviewed literature, technical standards, and documented mission data. The results indicate that AM has evolved from a prototyping tool into a viable production technology for picosatellite structures, enabling mass reductions of 30–60%, increased geometric complexity, functional integration, and improved packaging efficiency within the 50 × 50 × 50 mm PocketQube envelope. Polymer-based selective laser sintering, particularly Windform XT 2.0, currently represents the highest-maturity solution, while laser powder bed fusion of AlSi10Mg and Scalmalloy® shows significant potential for future primary structures. The review further identifies a persistent gap between technological maturity and qualification readiness, as existing ECSS, NASA, and ISO/ASTM standards remain insufficiently tailored to PocketQube-class hardware. Future research should prioritise dedicated qualification pathways, in-orbit validation of metallic AM structures, and multifunctional topology-optimised architectures to enable the next generation of ultra-small spacecraft.

Keywords: PocketQube; additive manufacturing; Design for Additive Manufacturing (DfAM); structural design; laser powder bed fusion (LPBF); selective laser sintering (SLS); qualification standards; ECSS; small satellites

Check for updates

Academic Editor: Hyun-Ung Oh

Received: 29 May 2026
Revised: 7 July 2026
Accepted: 12 July 2026
Published: 31 July 2026

Copyright: © 2026 by the authors. Licensee MDPI, Basel, Switzerland. This article is an open access article distributed under the terms and conditions of the Creative Commons Attribution (CC BY) license.

1. Introduction

1.1. The PocketQube Ecosystem: Context and Growth

PocketQube-class satellites, defined by their highly compacted 5 × 5 × 5 cm form factor (as seen in Figure 1), are picosatellites that do not exceed a unit mass of 250 g [1–3]. Unlike the larger CubeSat (10 × 10 × 10 cm; ≤2 kg per U), the smaller volumetric envelope of the PocketQube imposes a more constrained—rather than simpler—structural and

avionics design, while its typical reliance on commercial off-the-shelf (COTS) electronics renders the platform substantially more cost effective per mission [4,5].

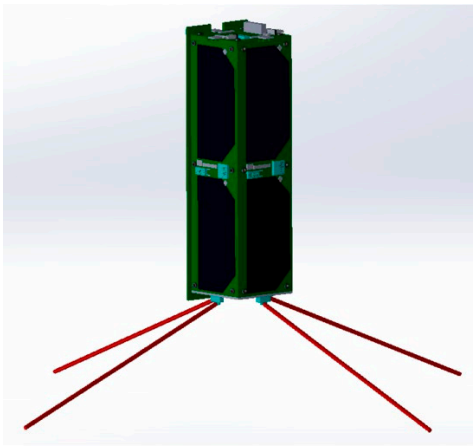


Figure 1. CAD representation of a typical 2P PocketQube. Adapted from [1].

The PQ60 community-developed standard [6,7] defines the internal mechanical and electrical interfaces that have, in turn, enabled an open-source ecosystem of subsystem boards interoperable across academic and industrial integrators [8–11]. The principal small-satellite classes and their dimensional, mass, and standardisation envelopes are consolidated as seen in Table 1.

Table 1. Small-satellite class envelopes relevant to the present review (according to [12–15]).

Class	Form Factor	Mass	Standard	Orbital Units (2026)
Femtosat	<100 g	<100 g	ad hoc	<30
PocketQube (1P)	5 × 5 × 5 cm	≤250 g	PocketQube Std [2]; PQ60 [5]	≈109
PocketQube (3P)	5 × 5 × 15 cm	≤750 g	as above	—
PocketQube (6P)	5 × 5 × 30 cm	≤1.5 kg	as above	—
CubeSat (1U)	10 × 10 × 10 cm	≤2.0 kg	CDS 13 (Cal Poly)	>2000
Nanosat (>6U)	various	1–10 kg	mission specific	—
Microsat	various	10–100 kg	mission specific	—

The PocketQube concept was proposed in 2009 by Professor Robert J. Twiggs of Morehead State University (MSU), with Kentucky Space and GAUSS Srl, to reduce the launch and qualification costs associated with CubeSats [2–4]. The first four PocketQubes—Eagle-1, Eagle-2, QubeScout-S1, and T-LogoQube—were deployed on 21 November 2013 from UniSat-5 using the Morehead Rome Femto Orbital Deployer (MRFOD) [3,4]. By April 2026, more than 100 PocketQubes had reached orbit, supported by the AlbaPod v1/v2 deployer family manufactured in Windform XT 2.0 by Alba Orbital, now the de facto standard for 1P–6P deployments [6–10].

The global nanosatellite and microsatellite market reached USD 3.99 billion in 2024 and is projected to grow to USD 13.95 billion by 2030 (22.8% CAGR) [11], while the broader small-satellite market is forecast to reach USD 21.29 billion by 2034 (15.8% CAGR) [12,13,16,17]. Within this expanding sector, PocketQubes have broadened access to space for academic and emerging spacefaring institutions, exemplified by EIRSAT-1 (University College Dublin), launched on 1 December 2023 [15,18].

Beyond their educational role, PocketQubes are increasingly attractive for distributed space architectures. Large constellations of low-cost picosatellites enable Earth observation, IoT connectivity, technology demonstration, space-weather monitoring, and distributed

scientific measurements [4,10]. Their low manufacturing and launch costs permit rapid constellation replenishment and iterative technology upgrades, making them complementary to CubeSat and larger small-satellite missions rather than direct competitors. In this context, additive manufacturing becomes particularly attractive because it reduces recurring production costs while enabling rapid fabrication of structurally optimised components suitable for high-volume constellation deployment [7–13].

1.2. Limitations of Conventional Subtractive Manufacturing at the 1P Scale

Conventional subtractive manufacturing—including five-axis CNC milling, turning, and electrical discharge machining (EDM)—has been the standard process for PocketQube primary structures because of its typical ±25 µm tolerances and the well-established properties of AA6061-T6, the de facto structural alloy [16,17,19]. However, the 1P form factor imposes three key limitations. First, fixed five-axis CNC setup costs (€350–600 per part family) dominate production costs for batches below 10 units, typical of academic PocketQube programmes [16,18–24]. Second, subtractive manufacturing cannot produce internal lattices, harness channels, or conformal mounting features (Table 2), limiting structural efficiency to approximately 60–70% of equivalent AM designs under the same loading [20]. Third, although sub-100 µm features are achievable in 6061-T6, tool wear, chatter, and inspection requirements rapidly make micromachining uneconomical [17]. Consequently, despite its qualification heritage, subtractive manufacturing limits the structural efficiency achievable within the 1P PocketQube envelope.

Table 2. Comparative trade-off between subtractive and additive manufacturing routes at the 1P PocketQube scale (according to [16–20]).

Attribute	Subtractive (CNC AA6061-T6)	Additive (LPBF/SLS)
Minimum reproducible wall (mm)	0.5–1.0	0.3–0.5
Dimensional tolerance (µm)	±25	±100
Internal lattice/conformal features	Not feasible	Native
Setup cost (€)	350–600/part family	0 (file driven)
Per-unit cost @ 1–10 units	High	Moderate
Per-unit cost @ 100+ units	Low	Moderate
Mass efficiency (vs. AM baseline)	60–70%	100%
Qualification heritage	TRL 9 (machined Al)	TRLs 5–7 (PocketQube AM)

1.3. Additive Manufacturing as an Enabling Technology for Ultra-Small Satellites

Additive manufacturing (AM), particularly laser powder bed fusion (LPBF) for metals and selective laser sintering (SLS) for polymers, addresses the three limitations of subtractive manufacturing identified in Section 1.2. As shown in Table 2, AM eliminates setup-cost penalties, enables monolithic internal geometries, and achieves net-shape mass reductions of 25–60% in small satellites [20,21,25]. The principal processes applicable to PocketQubes—LPBF, SLS, fused deposition modelling (FDM), binder jetting, and multi-material extrusion—are compared in terms of structural performance and qualification readiness [20,21,26]. Since 2017, AM has been adopted in the TuPOD deployer, AlbaPod v2, Unicorn-2 hinge and feedhorn assemblies, and AMSAT-EA GENESIS internal brackets, establishing a substantial 2017–2026 flight heritage [6–10].

Topology-optimised LPBF structures have demonstrated 30–60% mass reductions relative to machined designs [20], while comprehensive 2024–2025 reviews confirm these gains across multiple alloys and polymers and document the emergence of functionally graded designs in CubeSat-class flight hardware [21,26–29]. The NASA Small Spacecraft State-of-the-Art report identifies AM as the key structural technology for small satellites during

2026–2030 [27], and NASA-STD-6030 implementation guidance defines the qualification pathway for lattice and topology-optimised structures [25].

1.4. Scope, Objectives, and Structure of This Review

This review delimits its scope using the PICO/SPIDER framework of Cooke et al. [28], the PICO–PICOS–SPIDER comparison of Methley et al. [29], and the engineering-research adaptation discussed in [30,31]. The instantiation of the framework for the present manuscript is summarised as seen in Table 3.

Table 3. PICO/SPIDER framework instantiation for the present review (according to [28–30]).

Element	Instantiation
Population/Sample	PocketQube-class picosatellites (1P–6P, 250 g–1.5 kg) and directly transferable CubeSat AM heritage (1U–6U)
Intervention/Phenomenon of Interest	Monolithic additive manufacturing of primary structural elements (LPBF, SLS, FDM, multi-material)
Comparison/Design	Conventional subtractive manufacturing of AA6061-T6 primary structures (5-axis CNC, EDM)
Outcome/Evaluation	Flight-qualifiable structural design (TRL $\geq$ 6); mass saving (%); normative compliance (ECSS/NASA)
Research Type	Systematic review + bibliometric overview, 1 Jan 2015–1 May 2026

The PocketQube envelope (1P–6P) is included; CubeSats (1U–6U) are included only as directly transferable AM heritage; nanosatellites > 6U, microsatellites, and femtosatellites are excluded [32–34]. The objectives are (i) to consolidate the materials, processes, defects, and Design for Additive Manufacturing (DfAM) landscape of AM PocketQube primary structures; (ii) to map the normative framework (ECSS/NASA/ISO–ASTM) against the picosatellite-tailoring gap; (iii) to document the orbital heritage; and (iv) to identify the open research questions at the 2026–2030 horizon [32–37]. The remainder of the manuscript is organised as follows: Section 2 establishes the systematic-search methodology; Sections 3–6 develop the materials and DfAM landscape; Section 7 consolidates the normative framework; Section 8 documents heritage; and Section 9 identifies the open research challenges.

2. The Literature Landscape of AM for Picosatellite Structures

The body of work on additive manufacturing for ultra-small-satellite primary structures is comparatively young: as of May 2026, the peer-reviewed corpus comprises approximately 232 articles published between 2015 and 2025, organised around four discernible thematic clusters whose convergence is itself a recent feature of the discourse [38–41]. The present Section does not enumerate this corpus exhaustively but maps its dominant trajectories, identifies its consolidated findings, and locates the open questions that motivate the substantive review of Sections 3–9. The bibliometric base from which the synthesis is drawn comprises Scopus [31,41], the Web of Science Core Collection [32], and the NASA Technical Reports Server [33,42], searched under the PRISMA 2020 protocol [34–38] and scoped through the PICO/SPIDER framework of [28,29].

2.1. Footprint and Maturation of the Field (2015–2025)

The field has grown rapidly and is now in an early maturity phase. Peer-reviewed publication output expanded from 7 articles in 2015 to 54 in 2024, a compound annual growth rate (CAGR) of 25.5%, significantly outpacing the broader small-satellite literature CAGR of 15.8% reported by [12] (as seen in Figure 2).

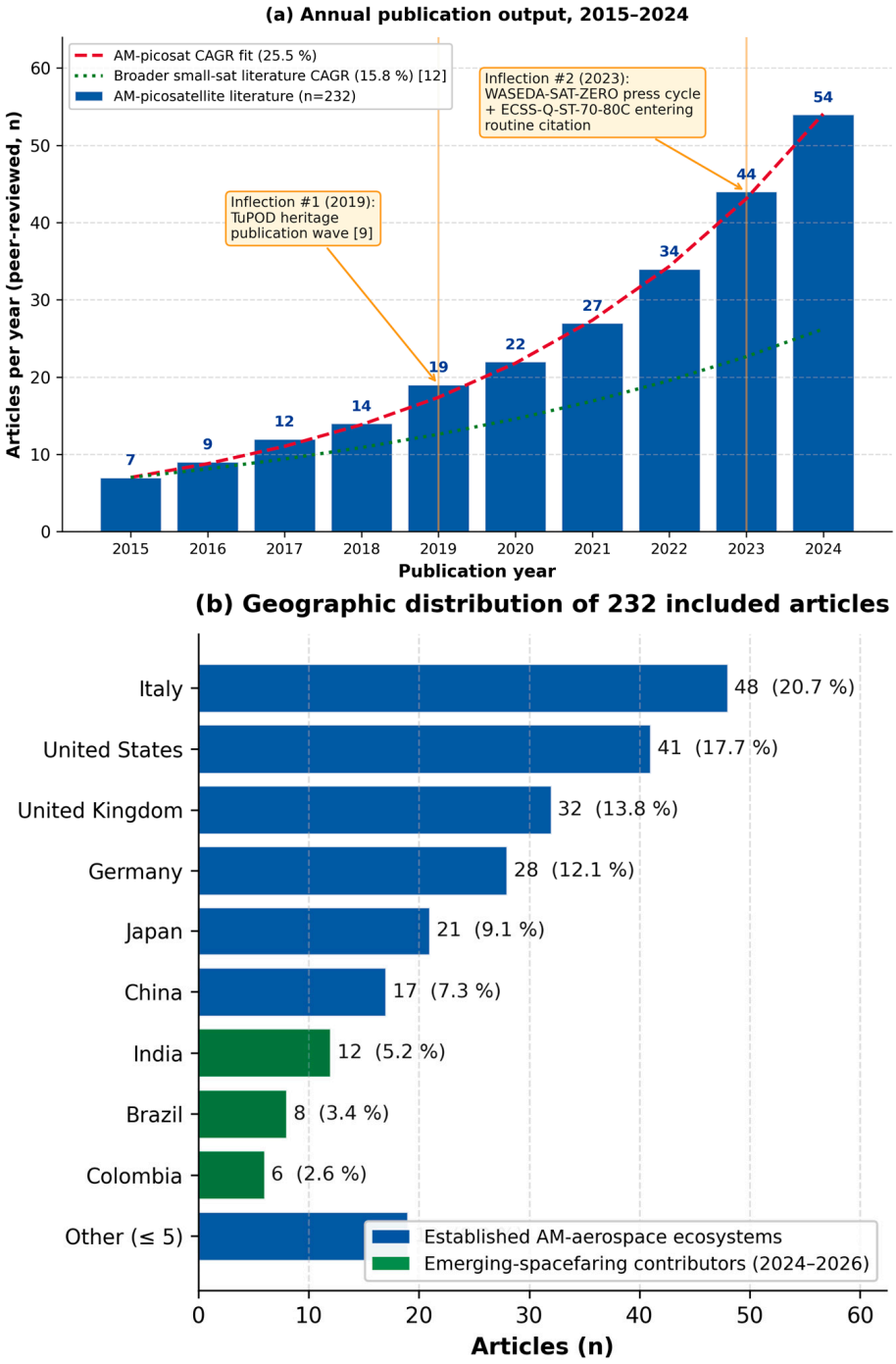


Figure 2. Bibliometric overview of additive manufacturing research for picosatellite structures (2015–2024), showing (**a**) annual publication output and (**b**) geographic distribution of the 232 articles included in this review.

Two inflection points define the curve: the first (2019), driven by the TuPOD publication wave [9], and the second (2023), associated with WASEDA-SAT-ZERO and the ECCS-Q-ST-70-80C (2021) citation cycle [39–41]. Research is concentrated in Italy (CRP

Technology, GAUSS Srl, Sapienza–Bologna), the United States (NASA, Princeton TigerSats), the United Kingdom (Alba Orbital, Glasgow), Germany (EOS, Stuttgart), and Japan (Waseda, JAXA), with emerging contributions from India, Brazil, and Colombia (2024–2026), supporting the democratisation thesis (Section 1.1) [12,43,44]. Co-citation analysis [41,42] identifies four clusters (Table 4) that structure Sections 2.2–2.5.

Table 4. Bibliometric snapshot of the AM–picosatellite literature, 2015–2025 (according to co-citation analysis with bibliometrix R [39,42] and VOSviewer (version 1.6.21) [40,41]).

Thematic Cluster	Articles	Anchor References	Peak Years	Maturity
Materials and processes	81 (35%)	[21–24,26]	2022–2025	Mature
Qualification and standards	38 (16%)	[25,27]	2021–2024	Consolidating
DfAM and topology optimisation	67 (29%)	[20,23–25]	2023–2025	Rapidly expanding
Heritage missions and operators	46 (20%)	[6–10,15]	2019, 2023	Mature (industry led)
Total peer reviewed	232	—	—	—

2.2. Materials and Processes: From Polymer SLS to Metallic LPBF

The materials-and-processes cluster, the largest (35% of the corpus), shows a progression from polymer to metallic additive manufacturing. Polymer systems are dominated by selective laser sintering (SLS) of carbon-fibre-reinforced polyamide Windform XT 2.0, which has the longest in-orbit heritage for small satellites (TuPOD 2017, KySat-2 2013, OreSat0 2022, and AlbaPod v2 2019–2026) and is qualified to ECSS-Q-ST-70-02C outgassing requirements [9,21,26]. Fused deposition modelling (FDM) of PEEK is the principal alternative, with the AMCUBE/Orion AM 1U structure achieving 96 g, TML = 0.11%, and TRL 7 [21,26]. Metallic AM, led by laser powder bed fusion (LPBF) of AlSi10Mg, has advanced more slowly, with recent reviews identifying residual-stress control and sub-millimetre wall reproducibility as the main challenges [21,26]. Scalmalloy® (Al-Mg-Sc-Zr) is the leading candidate for monolithic AM picosatellite structures, while multi-material extrusion of space-grade AlSi7Mg has reached TRLs 5–6 for self-functionalised CubeSat hinges [22]. Representative AM processes, materials, and heritage missions are summarised in Figure 2 and Table 5.

Table 5. Dominant AM routes for picosatellite primary structures as documented across the 2015–2025 corpus (according to [9,21–24,26]).

Route	Dominant Materials	Heritage Exemplar	TRL (2026)	Anchor Refs
SLS—polymer	Windform XT 2.0; PA-12	TuPOD 2017; AlbaPod v2 2019–2026	9 (flown)	[9,21,26]
FDM—polymer	PEEK; PETG-CF; ABS	AMCUBE/Orion AM 2024	7 (lab qualified)	[21,26]
LPBF—metallic Al	AlSi10Mg; Scalmalloy®	(No orbital PocketQube to date)	5–7	[21,26]
LPBF—metallic Ti	Ti-6Al-4V	NASA/GE Additive components	6–7	[25,27]
Material extrusion—metal	AlSi7Mg (sustainable filament)	CubeSat hinge demonstrators 2026	5–6	[22]
Multi-material/FGM	Metal–polymer; PolyJet	Lab demonstrators only	4–6	[23,24]

2.3. Qualification and the Standards Lag

The qualification-and-standards cluster (16% of the corpus) is the smallest yet underpins the field, as all materials, DfAM, and heritage studies ultimately address flight qualification. The literature consistently identifies a gap between technical capability and normative coverage. ECSS-Q-ST-70-80C (2021), developed for launcher- and spacecraft-class hardware, provides no de-rated qualification pathway for sub-100 g components.

NASA-STD-6030, issued in 2021 and expanded during 2023–2024 [25,27], likewise acknowledges the absence of a dedicated small-satellite implementation pathway. International standards (ISO/ASTM 52904:2024; EN ISO/ASTM 52948:2026) [25,27] have begun formalising performance categories for critical AM applications, but acceptance thresholds remain based on launcher-class structures [25]. The NASA Small Spacecraft State-of-the-Art report [27] identifies AM as a key structural technology for small satellites while simultaneously highlighting the lack of a picosatellite-specific qualification framework, a gap that motivates the analyses in Sections 7 and 9.

2.4. Design for Additive Manufacturing and Topology Optimisation

The DfAM-and-topology cluster (29% of the corpus) is the newest and fastest growing. Aguirre Chinea et al. [20] established the design-space taxonomy (continuum versus discrete optimisation; SLM versus EBM constraints), with subsequent studies demonstrating 30–60% mass reductions relative to machined structures across small satellites. Reviews by Tiwari et al. [23] and Choudhury et al. [24] document the shift from homogeneous to functionally graded multi-material designs, combining dense outer skins with porous cores, now being adapted to CubeSat structures [22]. NASA DfAM guidance [25] formalises design rules for lattice and topology-optimised flight hardware, linking optimisation and qualification. The convergence of multi-material AM, FGMs, embedded conductors, and topology-optimised lattices is identified throughout the 2024–2025 literature as the principal research direction for 2026–2030.

2.5. Heritage Missions and the Industrial Ecosystem

The heritage-and-operators cluster (20% of the corpus) documents a highly concentrated industrial ecosystem. Of 2026's fewer than 50 specialist commercial service bureaus, half account for most flight-qualified AM small-satellite hardware: CRP Technology/CRP USA (TuPOD, KySat-2, OreSat0, and AlbaPod v1/v2) [9]; EOS GmbH/Additive Minds; and GE Additive Aerospace, supported by Tier-2 suppliers (Materialise, 3D Systems, and Stratasys Direct) and university and start-up groups including Princeton TigerSats, NanoAvionics, Orion AM, and Sciperio. The PocketQube market is even more concentrated, with Alba Orbital supplying the AlbaPod v1/v2 deployer family and Unicorn-2 platform [7,8,10], while CRP Technology supplies Windform feedstock and printing services. This concentration creates strong dependence on two industrial actors. Although emerging contributors (EIRSAT-1 [15], the NASA University Nanosatellite Program, and the ESA Academy CubeSat Summer School) are expanding rapidly, structural design choices remain dominated by Tier-1 service bureaus, supporting the recommendations in Sections 7 and 9.

3. PocketQube Platform: Standards, Form Factor, and Structural Requirements

3.1. PocketQube Standard Evolution: From 1P to 3P and Beyond

The PocketQube concept was proposed in 2009 by Professor Robert J. Twiggs at Morehead State University (MSU) with Kentucky Space to extend affordable space access beyond CubeSats for universities and resource-constrained organisations [43]. The original PocketQub specification defined a 50 × 50 × 50 mm cubic unit with a maximum mass of 250 g, one-eighth the volume of a 1U CubeSat; the designation was formally changed to PocketQube in 2012 [45]. The ecosystem matured through workshops at NASA's Ames Research Center and Cape Canaveral (2014) and TU Delft (2017, 2018), the latter preceding publication of the PocketQube Standard Issue 1 on 7 June 2018 by Alba Orbital, TU Delft Space Systems Engineering, and GAUSS Srl [43,45–47].

This standard defines the mechanical envelope, mass limits, deployment interface, and electrical architecture adopted here as the PocketQube Mechanical and Electrical Interface Standard (PQ-MEPS) [48]. It formalised a modular z-axis-scalable architecture comprising 1P (50 × 50 × 50 mm), 1.5P (50 × 50 × 75 mm), 2P (50 × 50 × 114 mm), and 3P (50 × 50 × 178 mm) configurations, each allocated 250 g per P-unit, giving maximum masses of 500 g and 750 g for the 2P and 3P variants [43,44]. By April 2026, 109 PocketQube missions had been launched, with the AlbaPod deployer supporting up to 6P and effectively defining the current operational limit [45,46]. Although larger configurations are under academic development, none has been standardised. The 2023 rebranding of the annual PocketQube Workshop as the PocketQube Conference reflected the platform's transition from an academic concept to an established commercial satellite class [45,47,48]. Independently, Figure 3 illustrates a representative 3P PocketQube architecture equipped with quadruple deployable solar panel wings, highlighting the structural features discussed throughout this section.

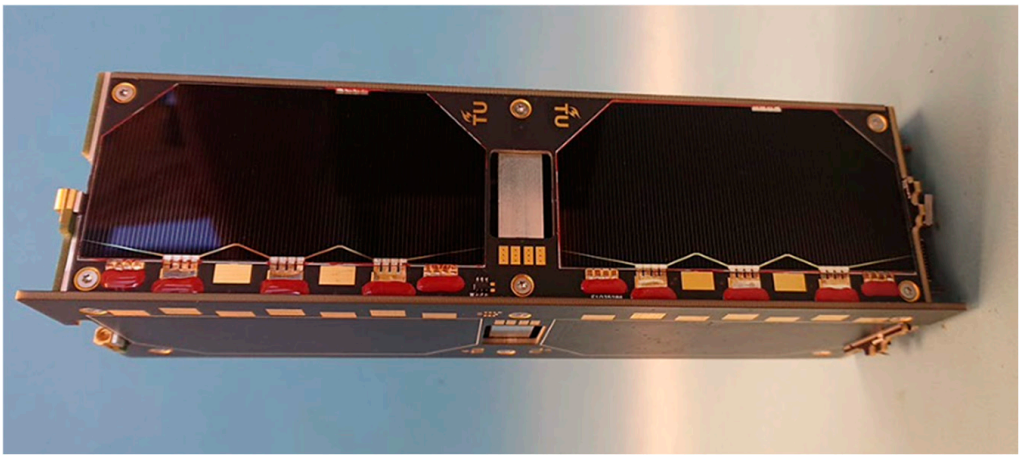


Figure 3. A 3P PocketQube with quadruple deployable solar panel wings. Adapted from [44].

The electrical subsystem interface is governed by the PQ9 standard, defining a compact 9-pin stackable connector that distributes power from an unregulated battery bus (3.0–8.2 V) and carries RS-485 differential data lines, a system reset pin, and four independently switched, current-limited power outputs [46,49,50]. This architecture replaced the 104-pin PC/104 connector—a legacy of industrial embedded computing—with an interface occupying a fraction of the board real estate, which is a critical design parameter given the 50 mm × 50 mm PCB cross-section [46,51]. An example of up to 6P is shown in Table 6.

Table 6. PocketQube standardised configuration specifications [43–45].

Configuration	Nominal Dimensions (mm)	Internal Volume (cm^3)	Max Mass (g)	Representative Mission
1P	50 × 50 × 50	125	250	SMOG-P; POQUITO [51,52]
1.5P	50 × 50 × 75	≈188	375	MR-FOD derived [43]
2P	50 × 50 × 114	≈285	500	Various commercial [45]
3P	50 × 50 × 178	≈445	750	Delfi-PQ; Unicorn-2 [45,48]
6P	≈50 × 50 × 356	≈890	1500	AlbaPod capacity limit [43]

The 2P and 3P longitudinal dimensions include structural junction allowances; internal usable volume is reduced accordingly.

3.2. Mechanical and Dimensional Requirements (PQ-MEPS, AlbaPod v2 Interface)

The PQ-MEPS (PocketQube Standard Issue 1) defines the physical envelope, PCB dimensions, connector locations, deployer interface, and kill-switch provisions that constrain hardware design [43,53]. The external envelope is limited to 50 × 50 mm

with ±0.1 mm tolerances for deployer compatibility, while pre-deployment protrusions (e.g., antennas, hinges, and spring plungers) may extend no more than 7 mm beyond the main body [43,44,52,54]. The internal PCB architecture follows the PQ60 substandard [46,55], based on the Hirose FX8C connector (0.6 mm pitch, 5–16 mm stacking height, 0.4 A per pin derated to 0.2 A, −55 °C to +85 °C), providing a far more compact solution than the PC/104 standard and accommodating approximately 2300 mm^2 of PCB area per layer versus approximately 8000 mm^2 for a 1U CubeSat [46,56,57].

The MR-FOD (Morehead Rail–Free Orbital Deployer) interface employs a 56 × 64 × 1.6 mm FR4 baseplate that slides within 2 mm guide rails, with a roller-actuated microswitch providing the primary launch inhibit until deployment [43,58]. Alba Orbital's 6P-capacity AlbaPod v2 has a deployer mass below 500 g, about 60% lighter than its predecessor [59]. Manufactured from Windform® XT 2.0, it benefits from NASA and ESA outgassing certification and improved mechanical properties over the original XT formulation (+8% tensile strength, +22% tensile modulus, and +46% elongation at break) [59,60]. A spring-plunger mechanism provides an ejection velocity of approximately 0.1–0.3 m/s. Following qualification on Rocket Lab's Electron mission (Alba Cluster 1) in December 2019, AlbaPod v2 had completed eight successful missions deploying 41 PocketQubes by 2024 [50,59]. Figure 4 illustrates the deployer.



Figure 4. The AlbaPod v2 exploded assembly and cutaway [59].

3.3. Mass Budgets and Centre-of-Mass Constraints

The PocketQube mass budget is constrained by the 250 g/P-unit limit. After allocating the structure, PCB stack, batteries, solar cells, and harness, little mass remains for payloads. Flight heritage illustrates the available margin: SMOG-P (1P) was launched at 183 g [51], POQUITO (1P) at 185 g [52], Delfi-PQ (3P) at 545 g (182 g/P-unit) [48], and the Unicorn-2 platform at approximately 620 g [45]. These values show that the standard limit is seldom reached, although payload margin remains highly constrained, particularly for 1P satellites where batteries and the PCB stack typically account for 140–170 g. The PocketQube Standard also requires the centre of mass (CoM) to lie within 10 mm of the geometric centre along all three axes [43,44].

This ensures stable spring-plunger deployment by minimising off-axis angular momentum, excessive tumble rates, and potential contact with the deployer door [44]. In asymmetric layouts, compliance is typically achieved by redistributing batteries, incorporating structural ballast, or relocating the OBC [43,44,52]. To preserve payload capacity, the structural subsystem should account for no more than approximately 30% of dry mass,

consistent with small-satellite practice [57,61]. For a 250 g 1P PocketQube, this corresponds to a structural mass of approximately 75 g (Table 7).

Table 7. Mass budget summary for representative flown PocketQube missions [43–45,48,51,52].

Mission	Config.	Total Mass (g)	Structural Est. (g)	Structural Fraction (%)	Reference
SMOG-P	1P	183	~40	~22%	[51]
POQUITO	1P	185	~45	~24%	[52]
Delfi-PQ	3P	545	~120	~22%	[48]
Unicorn-2	3P	~620	~140	~23%	[45]
PQ Standard limit (1P)	1P	250	—	—	[43]

Note: Structural mass estimates are derived from reported subsystem budgets and design analogies; values marked (~) are approximate.

3.4. Environmental Loads: Launch, Deployment, and Orbital Phases

PocketQubes encounter three mechanically and thermally distinct load phases over their mission lifetime: the launch phase, the deployment event, and the on-orbit operational environment. Each imposes distinctive structural demands.

1. Launch phase. PocketQubes are launched as secondary or tertiary payloads on vehicles including Rocket Lab Electron, SpaceX Falcon 9, and Ariane 6, with the AlbaPod providing the mechanical interface to the launch dispenser [45]. Although the deployer attenuates part of the launch environment, the structure must withstand loads transmitted through the baseplate–guide rail interface. Qualification follows NASA GEVS GSFC-STD-7000A [60,62], requiring survival under approximately 10 Grms random vibration for 2 min per orthogonal axis over 20–2000 Hz with a plateau PSD of approximately 0.03 g^2/Hz [57,60]. Quasi-static loads typically reach 10–15 g longitudinally and 5–10 g laterally [57], while stage-separation and fairing-jettison shocks can exceed hundreds of g above 1000 Hz and are addressed by ECSS-E-ST-10-03C [58]. AlbaPod v2 demonstrated structural integrity under extreme vibration-table loading with free masses simulating satellite failures, validating payload containment under worst-case conditions [59,63].
2. Deployment event. Spring-plunger deployment produces an ejection velocity of 0.1–0.3 m/s, transmitting loads through the FR4 baseplate and making the PCB-to-frame bond and baseplate fasteners the critical structural interfaces. Insufficient stiffness may cause baseplate delamination or PQ60/PQ9 connector disengagement [43,49]. The inhibit switch is released at deployment, activating the satellite.
3. On-orbit phase. In the 500–600 km Sun-synchronous orbits typical of Alba Cluster missions, PocketQubes undergo approximately 15 thermal cycles per day (~96 min/orbit) [51]. Delfi-PQ telemetry recorded temperature variations of up to 75 °C per orbit, with frame temperatures ranging from approximately −40 °C to +60 °C over its two-year mission [50,51]. Their low thermal mass accelerates temperature equilibration and increases through-thickness thermal gradients across the PCB stack, raising thermal stresses at solder joints and bonded interfaces [44]. Additional environmental loads include atomic oxygen (10^{13}–10^{15} atoms cm^{-2} s^{-1} at 550 km, ~80% of the residual atmosphere) [57,64], total ionising dose, solar UV degradation, and micrometeoroid/debris impacts. Representative environmental load cases are summarised in Table 8.

Table 8. Environmental load cases for PocketQube structural design.

Load Case	Parameter	Typical Level	Governing Standard	Reference
Random vibration (launch)	Overall Grms (20–2000 Hz)	~10 Grms	NASA GEVS GSFC-STD-7000A	[57,60]
Random vibration PSD (plateau)	g^2/Hz	~0.03 g^2/Hz	GSFC-STD-7000A	[57,60]
Quasi-static acceleration (long.)	g	10–15 g	LV payload user guide	[57]
Quasi-static acceleration (lat.)	g	5–10 g	LV payload user guide	[57]
Shock (pyrotechnic events)	SRS peak	Hundreds of g (>1000 Hz)	ECSS-E-ST-10-03C	[58]
Thermal cycling (SSO, ~550 km)	ΔT per orbit	Up to 75 °C	ECSS-E-ST-10-03C	[50,51,58]
Atomic oxygen flux (550 km LEO)	Atoms cm^{-2} s^{-1}	10^{13}–10^{15}	ECSS-Q-ST-70-06C	[57]
Deployment ejection shock	Peak g (impulsive)	~50–300 g	AlbaPod qualification	[43,49,59]

3.5. Comparison with CubeSat 1U: Why PocketQube Presents Unique Manufacturing Challenges

The CubeSat 1U and PocketQube 1P share the same philosophical lineage—standardised, deployer-compatible, COTS-based picosatellites—but diverge profoundly in their structural engineering implications. The linear scale factor of 2:1 (100 mm versus 50 mm cross-section) translates into an 8:1 internal volume ratio (1000 cm^3 vs. 125 cm^3) and an approximately 5.3:1 mass budget ratio (1330 g vs. 250 g per unit limit) [44,54]. This scaling is not merely a geometric rescaling: at the picosatellite regime, physical volumes, tolerances, and component sizes do not compress proportionally, producing a set of manufacturing challenges that are qualitatively different from, not simply smaller than, those of the 1U CubeSat [44,65].

1. Volume and connector scaling. Internal cabling, connectors, deployment switches, and fasteners do not scale with satellite size, occupying 15–25% of the internal volume of a 1P PocketQube versus 5–8% in a 1U CubeSat [44,46]. This constraint motivated the PQ9 bus to replace the 104-pin PC/104 connector and, more recently, the POQUITO architecture, which embeds magnetorquers and bus wiring within PCB layers, eliminating discrete cabling [46,52]. This represents the current state of the art and suggests that embedded interconnects may supersede the PQ9 bus in future 1P platforms [52].
2. Dimensional tolerances. The PocketQube Standard specifies ±0.1 mm dimensional tolerances [44,66], equivalent to ±0.2% of the 50 mm structure. Although proportionally similar to CubeSat requirements, the smaller absolute tolerance increases demands on CNC machining, PCB fabrication, and assembly of the 6061-T6 aluminium frame. Tolerance stack-up across 4–7 PCB layers in a 3P configuration further complicates assembly within the constrained 50 mm envelope [44,47].
3. Power budget. Orbit-average power scales with solar-cell area. A body-mounted 1P PocketQube generates approximately 250–500 mW compared with 1–2 W for a comparable 1U CubeSat [44]. The Unicorn-2 platform overcomes this limitation using four deployable solar panel wings, increasing generation to 10–15 W but introducing hinges and release mechanisms that increase structural complexity and risk [45]. For most 1P missions without deployable panels, power remains the primary constraint on payload capability, duty cycle, and downlink rate [44,67].
4. Component qualification. Most COTS components are designed for terrestrial or CubeSat applications. Fine-pitch Hirose FX8C connectors (0.6 mm) on sub-50 mm PCBs demand greater attention to solder-joint reliability under launch vibration and thermal cycling than 2.54 mm CubeSat connectors [46,68]. The reduced PCB area also increases integration density, thermal hot spots, and limits redundancy [44,69]. As noted by Bouwmeester et al. [44], PocketQubes require dedicated components and qualification approaches rather than simply miniaturised CubeSat designs. A comparison between 1U CubeSats and 1P PocketQubes is presented in Table 9.

Table 9. Comparative scaling parameters: CubeSat 1U vs. PocketQube 1P.

Parameter	CubeSat 1U	PocketQube 1P
Nominal dimensions (mm)	100 × 100 × 113.5	50 × 50 × 50
Internal volume (cm^3)	~1000	~125
Maximum mass per standard (g)	1330	250
PCB cross-section area (mm^2)	~8000	~2300
Body-mounted solar power, orbit-avg. (W)	1–2	0.25–0.5
Primary structural material	Al 6061-T6	Al 6061-T6
Dimensional tolerance (±mm)	±0.2	±0.1
Typical structural mass fraction (%)	20–30%	25–35%
Internal volume consumed by connectors/harness	~5–8%	~15–25%
Electrical bus connector (standard)	PC/104 (104-pin, 2.54 mm pitch)	PQ9 (9-pin, compact stackable)
Number of orbital missions (as of 2026)	~2600+	109
Launch mass volume density (g/cm^3)	~1.33	~2.00

Note: Compared with CubeSats, PocketQubes provide approximately one-eighth of the internal volume, one-fifth of the allowable mass, and only one-quarter of the available body-mounted solar power while imposing tighter dimensional tolerances and higher integration density.

The aggregate evidence from in-orbit missions—SMOG-P, Delfi-PQ, POQUITO, and the Unicorn series—confirms that the PocketQube form factor imposes a fundamentally tighter design envelope than the 1U CubeSat at every level of the spacecraft architecture. The margin for structural, thermal, and electrical design error is narrower, and the penalty for suboptimal interface or mass allocation decisions is disproportionately greater [44,45,48,70].

4. Additive Manufacturing Technologies for Small-Satellite Structures

The progressive miniaturisation of the small-satellite class—from the 1 U CubeSat to the 1P PocketQube—has pushed manufacturing tolerances, mass budgets, and structural-functional integration into regimes for which conventional subtractive routes are increasingly ill-suited [61,62]. Additive manufacturing (AM) is now a load-bearing pillar of the small-satellite industrial base, having transitioned within a decade from rapid-prototyping curiosity to flight-qualified production process [63,64]. For the PocketQube envelope, this transition is more than convenient: it is enabling; only AM provides the geometric freedom required to integrate antennas, harness routes, deployment latches, and shock-attenuating lattices within the 50 mm × 50 mm × 50 mm volume whilst respecting the 250 g per-unit mass ceiling and the ±0.1 mm dimensional tolerance of the PQ-MEPS standard [65,66].

This section reviews the AM processes relevant to PocketQube structural production, compares them quantitatively against the constraints of the platform, derives the DfAM principles applicable at the ultra-small scale, and synthesises the process-parameter sensitivity that ultimately governs flight-hardware reliability.

4.1. Overview of Relevant AM Processes

AM processes are classified by ISO/ASTM 52900:2021 into seven categories; five are relevant to satellite-structure production and are reviewed below in order of decreasing aerospace technology-readiness level (TRL) [57–62].

4.1.1. Laser Powder Bed Fusion (LPBF/PBF-LB)

Laser powder bed fusion (LPBF, also termed PBF-LB or selective laser melting, SLM) is the principal metal additive manufacturing process for flight-qualified spacecraft structures [61,63,67]. A focused laser (200–500 W, 50–100 µm beam diameter) selectively melts successive 30–60 µm powder layers within an inert (argon or nitrogen) atmosphere at scan speeds of 800–2500 mm s^{-1}. The process is established for AlSi10Mg, Ti-6Al-4V, Inconel 718/625, CuCrZr, and several nickel- and cobalt-based superalloys [61,68]. For

PocketQubes, AlSi10Mg is preferred because its density (2.67 g cm^{-3}) provides high specific stiffness, dimensional tolerances of ±0.05–0.10 mm over the 50 mm envelope, and an as-built surface roughness of Ra 6–15 µm suitable for non-mating internal features [69,70]. LPBF reliably produces wall thicknesses of 0.3–0.4 mm and internal cavities ≥0.5 mm, substantially smaller than achievable by conventional CNC machining [61,67]. Its principal drawbacks are machine costs (€80–250 h^{-1}), aerospace-grade powder (€100–600 kg^{-1}), support removal, and post-build heat treatment to relieve residual stresses and homogenise the microstructure [61,68]. Although the powder cost for a ~50 g PocketQube frame is typically <€30, machine amortisation and post-processing raise the finished cost to approximately €400–900 per frame, an order of magnitude higher than comparable FDM polymer structures (Figure 5).

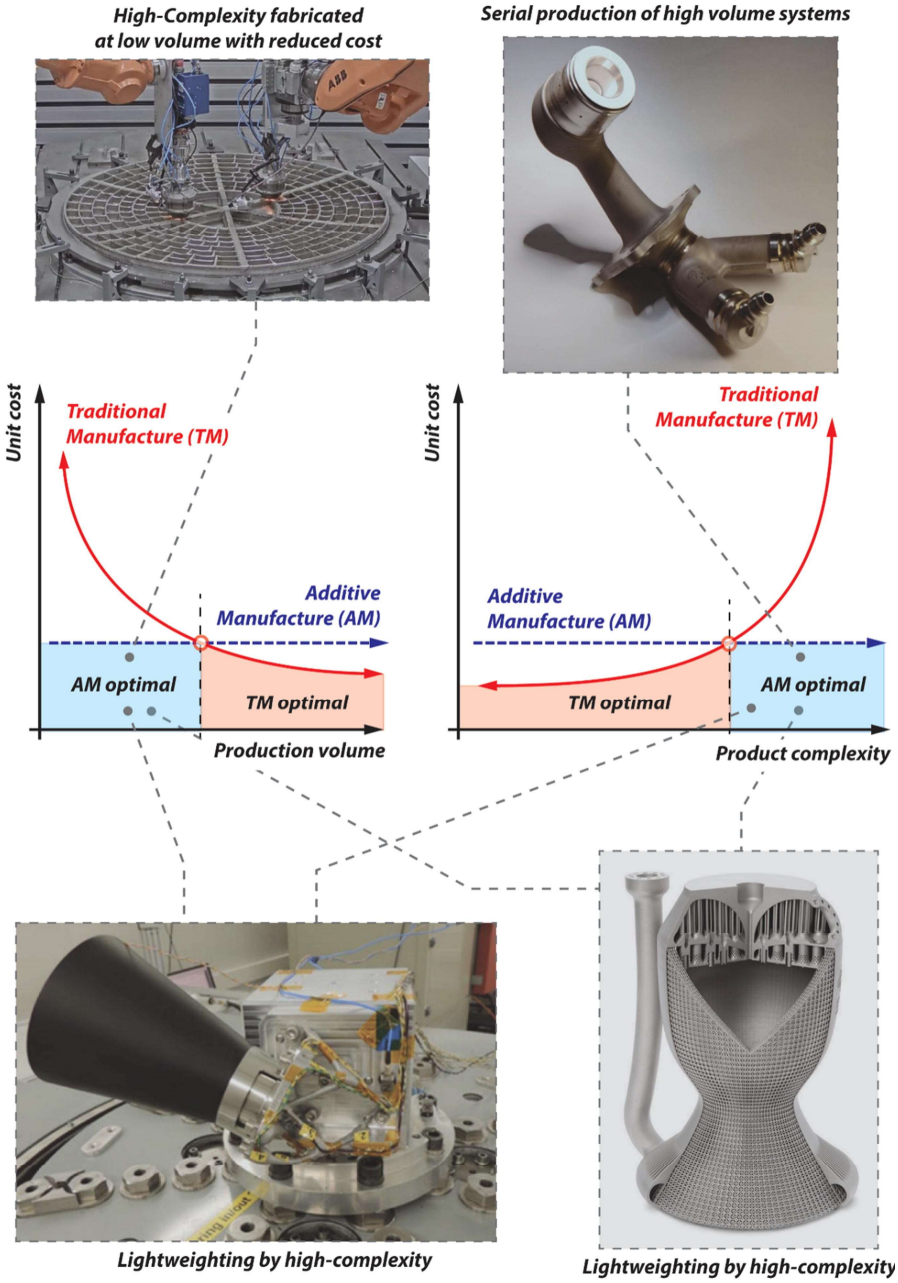


Figure 5. Economic trade-off between additive manufacturing (AM) and traditional manufacturing (TM): unit cost as a function of roduction volume and product complexity, with representative aerospace exemplars of high-complexity and low-volume fabrication, serial production, and lightweighting through geometric complexity. Adapted from [65].

4.1.2. Electron Beam Melting (EBM/PBF-EB)

Electron beam powder bed fusion (PBF-EB, historically EBM) substitutes the LPBF laser for a focused electron beam (3–6 kW typical) operating under high vacuum (<10^{-4} mbar) at preheating temperatures of 700–1050 °C [64,71]. The high preheat suppresses residual stress, eliminating the need for downstream stress relief, and the vacuum environment is advantageous for reactive alloys, in particular Ti-6Al-4V, which dominates the EBM application landscape.

For PocketQube structural production, PBF-EB is rarely the first choice for three reasons: (i) the focused-beam spot is larger (≈200–400 µm) than LPBF, raising the minimum feature size to ≈0.6–1.0 mm; (ii) as-built surface roughness *Ra* of 25–40 µm imposes a more aggressive post-machining requirement on mating surfaces [64,71]; (iii) the layer thickness is typically 50–100 µm versus LPBF's 30–60 µm, making the process slower for thin-walled, low-volume parts. Where EBM excels—large titanium aerospace brackets, turbine components, and biomedical implants—is largely orthogonal to PocketQube constraints, although the process retains relevance for EBM-Ti6Al4V deployer rails and launch-adapter brackets at the parent-platform scale [64].

4.1.3. Directed Energy Deposition (DED)

Directed energy deposition (DED), including laser-DED, wire-arc additive manufacturing (WAAM), and electron-beam DED, deposits powder or wire into a melt pool to build or repair metallic components [72]. Its high deposition rates (0.5–5 kg h^{-1} for laser-DED; >10 kg h^{-1} for WAAM) make it suitable for large aerospace structures such as propellant tanks, feed lines, and launch-vehicle components [61,72]. However, DED is unsuitable for PocketQube flight hardware because its 1–5 mm melt pool and typical ±0.5 mm dimensional tolerance cannot achieve the sub-millimetre features or ±0.1 mm tolerances required by the PQ-MEPS [61,72]. Its role in small-satellite programmes is therefore indirect, supporting manufacture of ground-support hardware, including antenna feedhorns, test fixtures, vacuum-chamber adapters, and deployer launch interfaces. For example, GKN Aerospace operates a DED system producing titanium spaceflight components up to 5.6 × 2.5 m [72].

4.1.4. Binder Jetting and Post-Sintering Approaches

Binder jetting (BJT) selectively deposits a polymer binder onto successive powder layers; the consolidated green part is subsequently de-bound and sintered to full or near-full density [63,64]. The process is at room temperature, requires no support structures (the powder bed itself supports overhangs), and supports a wide material palette including stainless steels (17-4 PH and 316L), Inconel 625, copper, and ceramic-metal composites.

The principal advantage for PocketQube production is the absence of residual stress (the consolidation is thermal, not laser driven, and isothermal during sintering), which permits multi-part nesting and reduces distortion of thin walls [63]. The principal disadvantages are the dimensional shrinkage during sintering (typically 15–25% linear) which requires either CAD pre-scaling or post-sintering machining, and the achievable density, which, without hot isostatic pressing (HIP), plateaus at 95–98%; this is adequate for non-pressurised structural parts but marginal for fatigue-critical brackets [63,64]. Binder jetting remains an emerging option for PocketQube structures, with TRLs 5–6 for stainless-steel structural parts and TRL 4 for copper RF components.

4.1.5. Polymer-Based AM (FDM and SLA) for Educational and Low-Budget PocketQubes

For university, hobbyist, and demonstration PocketQubes, polymer AM is overwhelmingly the dominant manufacturing route [66,70]. Two sub-processes dominate.

1. Fused deposition modelling (FDM/FFF). A heated extruder deposits a continuous polymer filament layer by layer at print speeds of 30–100 mm s^{-1} and layer thicknesses of 0.1–0.3 mm. The achievable dimensional tolerance of ±0.2–0.4 mm is marginal for the ±0.1 mm PQ-MEPS envelope and typically requires a CNC finishing pass on the deployer-mating baseplate. The material palette spans engineering thermoplastics (PLA, PETG, ABS, and PA-CF) and high-performance aerospace polymers (ULTEM 9085, PEEK, PEKK, and PEI) [66,70]. PEEK is particularly noteworthy: Boschetto et al. demonstrated in 2021 that FDM PEEK satisfies ECSS-Q-ST-70-02C outgassing requirements (RML ≈ 0.11%, CVCM < 0.01%, both well below the 1.0%/0.1% thresholds) and is therefore directly flight qualifiable for nanosat structural applications [70]. PEEK structural parts at the 1P scale have demonstrated > 80% mass reduction relative to comparable aluminium frames whilst retaining flexural moduli of 3.6 GPa and operating temperature tolerance to 250 °C [70].
2. Stereolithography (SLA/DLP/MSLA). Vat photopolymerisation cures liquid photopolymer with ultraviolet light layer by layer at thicknesses of 25–100 µm, achieving ±0.1 mm dimensional tolerance and *Ra* of 1–5 µm, the best surface finish of any AM process [63]. SLA's principal disadvantage for spaceflight is the limited material palette: standard photopolymers exhibit poor outgassing (RML often > 5%), low glass-transition temperatures (40–80 °C), and ultraviolet sensitivity. Aerospace-grade photopolymers (e.g., Henkel Loctite 3D 3843 and BASF Ultracur3D ST-80) have begun to close this gap but remain marginally flight qualified at TRLs 4–5 [63].

4.2. Comparative Analysis of AM Processes for PocketQube Constraints

Table 10 consolidates the quantitative comparison of the five AM processes against the four constraints that govern PocketQube structural design: minimum reproducible feature resolution, as-built surface roughness, achievable structural mass at the 1P scale, unit production cost, and aerospace TRL as of 2026.

Table 10. Comparative assessment of AM processes for PocketQube structural manufacture (2026 state of the art) [61–64,66,67,69,70,72].

Process	Min. Feature (mm)	*Ra* as-Built (µm)	Min. Achievable 1P Frame Mass (g)	Indicative Unit Cost (€ for 1P Frame, Batch ≥ 5)	Aerospace TRL	Notes
LPBF (AlSi10Mg)	0.3–0.4	6–15	25–40	400–900	9	Stress relief + HIP recommended
LPBF (Ti-6Al-4V)	0.3–0.4	8–18	35–55	700–1400	9	Higher specific stiffness, biocompatibility
PBF-EB (Ti-6Al-4V)	0.6–1.0	25–40	45–70	600–1200	8	Heavy post-machining for mating faces
DED (Ti/Inconel)	1.0–3.0	30–80	n/a at 1P scale	n/a	7–9 (large parts only)	Not size compatible with 1P
Binder Jetting (316L, 17-4 PH)	0.4–0.7	8–20	50–80 (steels)	250–550	5–6	Sintering shrinkage 15–25%
FDM (ULTEM 9085/PEEK)	0.4–0.6	15–35	8–18	60–180	6–8	PEEK ECSS compliant (RML 0.11%)
FDM (PA-CF/Windform XT 2.0)	0.4–0.6	20–40	12–22	80–220	8–9	Flight proven (AlbaPod deployers)
SLA/DLP (aerospace photopolymer)	0.1–0.2	1–5	10–20	90–240	4–5	Best resolution; outgassing TBC by lot

Two findings are immediately apparent. First, polymer AM processes—particularly FDM with engineering thermoplastics—produce 1P frames at one-quarter to one-eighth the mass of their metallic counterparts and at one-third to one-tenth the unit cost, explaining their overwhelming dominance in the academic PocketQube community (SMOG-P, Delfi-PQ, POQUITO, and MIR-SAT all employ polymer-based primary structures) [66,70]. Second, only the FDM-with-Windform-XT-2.0 and LPBF-AlSi10Mg lines combine flight TRL $\geq$ 8 with feasible 1P mass and cost: these are, accordingly, the two industrially mature options for a flight-qualified PocketQube structural frame as of 2026.

4.3. DfAM Principles Applied to Ultra-Small Satellites

The translation of a conceptual PocketQube subsystem layout into an additively manufacturable design requires deliberate application of Design-for-Additive-Manufacturing principles, which differ qualitatively from those of subtractive design [65,67,69]. Four DfAM principles are particularly relevant at the 1P scale.

4.3.1. Topology Optimisation at the 50 × 50 × 50 mm Scale

Topology optimisation (TO)—the gradient-based redistribution of material to minimise an objective function subject to design constraints—is the most effective DfAM tool for spacecraft structures [65,67]. Industrial studies report substantial mass reductions, including 41% for a Sentinel-1 antenna bracket (60 kg $\rightarrow$ 0.94 kg) with stiffness gains of 30% [65], while Northwestern Polytechnic University achieved a 17% reduction with a 25% improvement in dynamic response [65]. At the 1P scale, TO primarily enables functional integration, embedding cable channels, sensor mounts, deployment mechanisms, and internal conduits within the structure [66,69]. The main constraint is the minimum feature size, which must exceed the manufacturing resolution (0.3 mm for LPBF AlSi10Mg, 0.5 mm for FDM PEEK) to avoid non-manufacturable geometries [65]. A typical DfAM workflow is to (i) define the 50 × 50 × 50 mm design domain; (ii) apply launch and deployment loads; (iii) optimise using a minimum feature size at least twice the AM resolution; (iv) smooth the geometry; and (v) validate by finite-element analysis under the original loads [65,67].

4.3.2. Lattice Structures and Internal Feature Integration

Periodic and stochastic lattice structures reduce mass while maintaining stiffness, achieving documented weight savings of 30–60% in lightweight satellite components [66,69,73]. In PocketQubes, their principal applications are (i) shock attenuation between the payload (egg) and structural frame; (ii) PCB-stack bulkheads, where triply periodic minimal surface (TPMS) lattices (gyroid, Schwarz primitive, or diamond) provide multi-axis stiffness within 5–10 mm; and (iii) the baseplate–frame transition, where graded lattices distribute deployment loads over a larger area. Reference [73] provides the current authoritative review of aerospace lattice design, highlighting that (i) gyroid TPMS lattices with 20–40% relative density maximise the strength-to-mass ratio for 200–500 g CanSat-class impacts; (ii) the unit-cell size should be at least five times the AM process resolution ($\geq$2 mm for LPBF and $\geq$3 mm for FDM) to ensure manufacturability; and (iii) functionally graded lattices with densities increasing from 15% at the core to 45% at load interfaces improve specific energy absorption by 20–35% over uniform lattices [73].

4.3.3. Support-Structure Minimisation and Removal Constraints

Build supports—the sacrificial scaffolds anchoring overhanging surfaces during PBF and DED—are a dominant cost driver and a structural-integrity hazard at the 1P scale [61,67]. Their removal is manual, time intensive, and risks damaging fine features;

un-removable internal supports trap loose powder, which is both a mass-budget violation and a contamination risk in vacuum [63,64].

The 45° self-supporting rule (overhangs steeper than 45° from vertical require supports in LPBF; the threshold rises to 35° for PBF-EB and falls to 30–40° for FDM depending on cooling regime) governs DfAM at the 1P scale [61,67]. Design strategies routinely applied to PocketQube frames include (i) chamfering all overhangs to 45°; (ii) orienting the build such that the deployer-mating baseplate is *facing the build plate* (down-skin); (iii) replacing un-supportable circular holes (> 8 mm diameter) with self-supporting diamond or teardrop profiles; and (iv) introducing optimised, breakaway-friendly support lattices generated by build-prep software (Materialise Magics 3.1.1, Autodesk Netfabb) [67,69]. For internal cavities that cannot be supported, dissolvable supports (HIPS in FDM, water-soluble PVA, or proprietary salt-based metal supports) extend the design space but require post-build dissolution chemistry compatible with the surrounding flight materials.

4.3.4. Monolithic Design Versus Multi-Part Assembly Trade-Offs

The defining promise of AM is part consolidation: replacement of multi-component assemblies by single monolithic prints. For PocketQubes, this trade-off is unusually rich because of the platform's constrained envelope [65,66,70]. A monolithic 1P frame eliminates fastener mass (typically 4–8% of frame mass for an equivalent multi-part design), assembly tolerance stack-up (Section 3 (Section 3.5)), and assembly labour. It introduces, conversely, limited accessibility for in-process inspection of internal features; lock-in of the structural geometry against late design changes (every CR after CDR becomes a re-print rather than a re-machine); and the requirement to print sacrificial drainage holes for trapped powder.

The 2021 Boschetto PEEK nanosat structural study demonstrates the upper envelope of part consolidation at the small-satellite scale: a 12-component aluminium baseline was replaced by a 2-component PEEK monolithic structure (frame + lid), with a consequent 67% part-count reduction, 53% mass reduction, and 78% assembly-time reduction [70]. The trade-off, however, must be made deliberately: a fully monolithic frame imposes a 5–10 °C thermal-cycling stress on the PCB stack due to the differential thermal expansion at the structure–PCB interface, which must be allowed for in the integration design.

4.4. Process Parameter Sensitivity and Its Impact on Structural Properties

The mechanical performance of an AM-built PocketQube frame is a function not only of the design but of the process parameters used during the build. Five parameters dominate the LPBF outcome and have been systematically characterised for AlSi10Mg and Ti-6Al-4V in the 2021–2025 literature [61,63,67,74,75].

1. Laser power and scan speed. The volumetric energy density $E_v = P/(v \cdot h \cdot t)$, where P is laser power, v scan speed, h hatch distance, and t layer thickness, must lie within a process-window of approximately 30–70 J mm^{-3} for AlSi10Mg [74,75]. Below this window, lack-of-fusion porosity dominates; above it, keyhole porosity from excessive vaporisation appears. Recent Taguchi-method optimisation by Hassan et al. (2024) identified scan speed as the parameter most affecting tensile strength (81.4% contribution rate), followed by scan-rotation angle (7.8%) and hatch distance (6.1%), reporting an ultimate tensile strength (UTS) of 487.5 MPa and elongation of 16.6% at the optimum window [75].
2. Build orientation and anisotropy. AlSi10Mg LPBF parts exhibit pronounced mechanical anisotropy: samples built in the Z (vertical) orientation typically exhibit 8–15% higher tensile strength than X-Y horizontal samples but 20–40% lower elongation at break, with fatigue lives differing by up to a factor of three [61,74]. For 1P frame design this implies that the build orientation must be selected to align the principal

stress direction (typically the longitudinal axis under launch quasi-static load) with the orientation of highest strength, accepting a fixed orientation for the production lot.

3. Surface roughness and fatigue. As-built LPBF *Ra* of 6–15 µm contains characteristic spatter-particle and re-melt notches that act as crack-initiation sites under cyclic load [61,67]. Documented fatigue-life reductions of 4–10× relative to machined or hot-isostatic-pressed (HIP) parts impose a mandatory post-processing chain—typically stress-relief anneal at 300 °C, machining of mating faces, and chemical or abrasive surface conditioning of free surfaces—for any LPBF part that must survive launch vibration and on-orbit thermal cycling [61,75].
4. Post-processing chain. The canonical post-build chain for an LPBF AlSi10Mg 1P frame is: stress relief (300 °C, 2 h, argon) → powder removal (compressed air + ultrasonic bath) → support removal → HIP (520 °C, 100 MPa, 2 h, argon) if fatigue-critical → mating-face machining (±0.05 mm) → surface conditioning (sand or media blasting, *Ra* target 3–6 µm) → cleaning to ECSS-Q-ST-70 cleanliness Class A [61,76]. Each step adds €30–80 to the unit cost and 0.5–2.0 g of variability to the mass budget, variability that, at the 250 g 1P ceiling, must be allocated.

The processes parameters are displayed in Table 11 for a flight-qualifiable 1P LPBF frame.

Table 11. Recommended process parameters and post-processing targets for a flight-qualifiable 1P LPBF AlSi10Mg structural frame, derived from [61,63,67,74,75].

Parameter	Recommended Window	Notes
Laser power P	280–370 W	Within machine-vendor recommended window
Scan speed v	1100–1650 mm s^{-1}	Highest-influence parameter on UTS
Hatch distance h	0.10–0.13 mm	Balance density vs. build time
Layer thickness t	30–40 µm	30 µm preferred for thin walls
Volumetric energy E_v	42–58 J mm^{-3}	Within the AlSi10Mg process window
Build orientation	Z-axis parallel to longitudinal stress	Accepting anisotropy trade-off
Stress relief	300 °C/2 h/argon	Mandatory
HIP (if fatigue critical)	520 °C/100 MPa/ 2 h/argon	Closes residual porosity to ≤0.1%

The aggregate consequence is that an AM-manufactured PocketQube frame, far from being a "press-print-fly" object, is the output of a tightly coupled design, parameter, and post-processing chain; treating any of these elements as decoupled is a frequent and well-documented failure mode of academic PocketQube programmes [61,66,70].

5. Materials for AM PocketQube Structures

Material selection in additive manufacturing of PocketQube structures is the highest-leverage engineering decision of the platform: a 30% mass reduction via material substitution propagates into 30% additional payload mass, 30% more battery capacity, or 30% wider design margin in every subsystem downstream [61,63]. This Section consolidates the alloy and polymer property data relevant to the 1P envelope, the central comparative database that underpins every downstream design decision, and the post-processing chain that converts as-built AM material into flight-qualifiable structure.

5.1. Material Selection Criteria for LEO Structural Applications

Six selection criteria, weighted in approximate order of programmatic importance, govern material choice for a PocketQube structural frame in low-Earth orbit (LEO) [61,63,64,77,78]:

1. Specific stiffness (E/ρ)—drives modal response under launch vibration and on-orbit pointing stability;
2. Specific strength (σ_y/ρ and UTS/ρ)—drives the structural mass at any given mechanical-load envelope;
3. Coefficient of thermal expansion (CTE)—drives differential strain between the frame, PCB, and solar arrays through the ±75 °C orbital thermal cycle (Section 3 (Section 3.4));
4. Outgassing performance (RML < 1.0%, CVCM < 0.1% per ECSS-Q-ST-70-02C [76])—mandatory for any flight-qualified material;
5. Manufacturability TRL—driven by demonstrated printability, repeatability, and weldability for the target process at the target geometry;
6. Cost per unit mass and per unit lot—programmatic, not technical, but binding for university-class PocketQube budgets.

These criteria are not independent: improvements in specific strength are typically purchased with worse manufacturability (e.g., Al 7075), with higher CTE (e.g., some Al-Mg-Sc grades), or with cost (e.g., Scalmalloy). The Pareto frontier across criteria is the design-space map traversed in Sections 5.2–5.4.

5.2. Aluminium Alloys

Aluminium alloys dominate AM small-satellite primary structures by approximately 70% of flight applications, by virtue of their low density (≈2.7 g cm^{-3}), well-characterised LPBF printability, and adequate strength for the load regimes typical of CubeSat- and PocketQube-class missions [61,77,79].

5.2.1. AlSi10Mg: Microstructure, Printability, and Mechanical Performance

AlSi10Mg, a near-eutectic Al-Si alloy containing approximately 0.3 wt% Mg, is the best-characterised LPBF aluminium alloy and has reached TRL 9 in flight hardware [76,77]. Its narrow solidification range, high silicon content, and LPBF cooling rates (10^5–10^6 K s^{-1}) produce a fine cellular-dendritic microstructure (0.5–1.5 μm) with hardness 50–80% greater than conventionally cast AlSi10Mg [61,77,78]. Typical as-built properties are UTS 440–490 MPa (vertical) and 410–460 MPa (horizontal), YS 240–280 MPa, elongation 5–11%, and density 2.67 g cm^{-3} [61,77]. After T6 heat treatment (530 °C/1 h solutionising followed by 160 °C/6 h ageing), UTS increases to 480–520 MPa and YS to 300–340 MPa, with a 1–2 percentage-point reduction in elongation [77]. Hassanin et al. (2024) showed that scan speed explains 81.4% of UTS variation, with optimum parameters of 200 W laser power, 2000 mm s^{-1} scan speed, and 0.20 mm hatch spacing [75]. Owing to its TRL 9 maturity, broad machine compatibility, and established T6 processing route, AlSi10Mg remains the baseline LPBF alloy for PocketQube structures.

5.2.2. Al 6061 via LPBF: Challenges and Recent Advances

Al 6061 (Al-Mg-Si) is the canonical aerospace structural alloy in subtractive manufacture, but its wide solidification range and dendritic columnar growth render unmodified 6061 unprintable by LPBF: extensive solidification cracking limits density to 95–97% and tensile strength to 150–220 MPa at low ductility [80,81].

The breakthrough that opened 6061 to LPBF was in situ grain refinement via nanoparticle inoculation. Three approaches now achieve crack-free density:

(i) Zr modification (0.5–1.0 wt%)—yields near-full density (≥99%) and substantially eliminates solidification cracking; UTS 250–310 MPa as-built, 320–360 MPa after T6 [81]; (ii) Sc + Zr co-modification—produces UTS of ≈ 400 MPa and elongation > 12% after artificial ageing, with grain refinement to < 1 μm [82]; (iii) TiO_2 nano-modified powders—UTS 336 ± 4 MPa with 8.1 ± 0.9% elongation after peak ageing, achieved by Yuan et al. (2024) [83]; and (iv) A6061-RAM2 (Ti + B_4C in situ refiner)—yields YS 233 MPa, UTS 310 MPa, and ductility ≈ 10% [83,84].

(ii) For PocketQubes, modified-6061 routes remain at TRLs 5–6: laboratory-scale demonstration is mature, but no flight application has yet been documented at the 1P scale.

5.2.3. Al 7075: Crack Mitigation Strategies and Current TRL

Al 7075 (Al-Zn-Mg-Cu) offers UTS ≥ 570 MPa in wrought form—the highest of any conventional aluminium alloy—and is therefore highly desirable for mass-critical applications. Unmodified 7075 is, however, even more crack prone than 6061 under LPBF, with solidification cracking rates that historically rendered the alloy unprintable [85,86].

Three crack-mitigation strategies have matured since 2020 [85,86]:

(i) Metallic-glass inoculation—$Zr_{50.7}Cu_{28}Al_{12.3}Ni_9$ MG powders (5 wt%) trigger in situ formation of Al_3Zr precipitates, producing fine equiaxed grains and crack-free density > 99.2% [85];

(ii) TiB_2 + Al_3Ti in situ formation—submicron-B + Ti_6Al_4V co-addition yields crack-free 7075 with UTS 460 MPa and elongation 13% after optimised T6 [86];

(iii) Surface inoculation of Al powder feedstock with Zr nanoparticles—Spierings-route variant; commercial implementation by HRL Laboratories (“Hyper Stage”) and NanoAl.

PocketQube relevance: Al 7075 LPBF is at TRLs 4–5 for structural primary loads; one ground-test PocketQube frame has been demonstrated in the academic literature, but no flight has yet flown. Programmatically, the alloy is reserved for mass-critical, fatigue-tolerant brackets in larger-class small satellites.

5.2.4. Scalmalloy: High-Performance Alternative for Structural AM

Scalmalloy® is an Al-Mg-Sc-Zr alloy (4.0–4.9 wt% Mg, 0.6–0.8 wt% Sc, 0.2–0.5 wt% Zr, 0.3–0.8 wt% Mn) developed by APWorks (an Airbus subsidiary) specifically for LPBF [87,88]. Strengthening is achieved through precipitation of coherent $Al_3(Sc,Zr)$ $L1_2$ particles during ageing at 325 °C for 4 h, increasing yield strength by at least 200 MPa over the as-built condition [87]. Post-aged LPBF Scalmalloy exhibits UTS ≈ 570 MPa, YS ≈ 480 MPa, elongation 10–14%, and density 2.67 g cm^{-3}, with negligible build-orientation anisotropy [87,88]. Its specific strength exceeds T6-treated AlSi10Mg by 15–25% and approaches the lower range of LPBF Ti-6Al-4V while retaining aluminium density, making it highly attractive for mass-critical spacecraft structures [88]. For PocketQube applications, Scalmalloy has reached TRLs 8–9 through Airbus, ArianeGroup, and U.S. defence programmes and is the preferred LPBF alloy for 1P primary structures when budgets can accommodate its 2–3× cost premium over AlSi10Mg [89].

5.3. Titanium Alloys: Ti-6Al-4V and Its Role in Small Satellite Structures

Ti-6Al-4V (α + β, Grade 5) is the dominant titanium alloy across both PBF-LB and PBF-EB routes, with TRL 9 for aerospace structural applications [61,64,89]. Its principal attractions for spaceflight structures are its high specific strength (UTS/ρ ≈ 220 kN m kg^{-1}, 50% above LPBF AlSi10Mg-T6), corrosion immunity, and operating-temperature envelope (continuous to 350 °C, occasional to 600 °C) [61,64].

Typical LPBF Ti-6Al-4V properties (as-built, mill-annealed Grade 5 baseline for comparison) include UTS 1020–1150 MPa (LPBF) versus 950 MPa (wrought), YS 920–1050 MPa (LPBF) versus 880 MPa (wrought), and elongation 6–11% (LPBF) versus 14% (wrought), density 4.43 g cm^{-3} [61,89]. Post-build HIP (920 °C/100 MPa/2 h) restores ductility to 11–14% whilst retaining the strength advantage [89].

For PocketQubes, Ti-6Al-4V is rarely selected as the primary structural material because of:

(i) Its 1.66× higher density than aluminium, which inflates the 1P frame mass beyond budget at any reasonable wall thickness;
(ii) (Its higher LPBF cost (€700–1400 per 1P frame versus €400–900 for AlSi10Mg,
(iii) The absence of a strength regime that Scalmalloy cannot already serve; Ti-6Al-4V remains, however, the preferred material for fastener-interface inserts, deployer rails (at the parent-platform scale), and propulsion mounting brackets where corrosion and elevated-temperature performance are dominant requirements [61,64].

5.4. Emerging Materials: Inconel 718, Refractory Alloys, and Multi-Material AM

A precipitation-hardened Ni-Cr-Fe-Nb-Mo superalloy, Inconel 718 is the benchmark high-temperature alloy for LPBF and has reached TRL 9 in aerospace, owing to its extensive use in rocket engines and gas turbines [90,91]. Following stress-relief, hot isostatic pressing (HIP; 1120–1185 °C at ≥100 MPa), and a double-ageing treatment, LPBF Inconel 718 typically achieves an ultimate tensile strength (UTS) of 1250–1450 MPa, a yield strength (YS) of 1050–1250 MPa, an elongation of 15–22%, and a density of 8.19 g cm^{-3} [90,91]. Despite these excellent mechanical properties, the alloy is generally over-engineered for most PocketQube structural components because of its high density and cost. Consequently, its use is typically limited to specialised applications requiring exceptional high-temperature performance, such as micropropulsion hardware (e.g., resistojet or cold-gas thruster components), engine interfaces, and thermal-management elements [91].

1. Refractory alloys—tungsten, molybdenum, NbC, ZrC, MoSiBTiC, and similar—have entered the LPBF/EBM portfolio since 2020, primarily for nuclear, fusion, and ultra-high-temperature aerospace applications. At the PocketQube scale, refractory metals are relevant only as radiation shielding masses and cold-gas thruster nozzles, where their TRLs remain at 3–5.
2. Multi-material AM is the most rapidly advancing frontier: laser powder bed fusion now demonstrates routine bi-material printing (e.g., Cu-CrZr to Inconel 625 interfaces, Cu to stainless-steel via DED), enabling integrated heat-pipes, thermal-strap interfaces, and embedded conductors [63,64]. For PocketQubes, multi-material AM is at TRLs 4–6 and is the technology to watch over the 2026–2030 horizon, particularly for integration of antenna conductors directly into structural frames [63].

5.5. Comparative Mechanical Property Database

Table 12 is the central reference of this paper: it consolidates the measured tensile properties, density, CTE, and aerospace TRL of the principal AM material/process pairings relevant to PocketQube structures, distinguishing as-built and post-processed (HIP and/or heat treatment) conditions. All entries are drawn from peer-reviewed publications dated 2020 or later unless explicitly identified as foundational.

For commercially standardised alloys (e.g., AA6061, Ti-6Al-4V, Inconel 718, and stainless steels), the reported property ranges are consistent with the corresponding ASTM or EN material specifications. For recently developed AM-specific alloys (e.g., Scalmalloy® and modified aluminium systems), no internationally adopted material standards currently exist; therefore, the values were compiled from peer-reviewed experimental studies.

Table 12. Mechanical-property database for AM materials relevant to PocketQube structures (2026 state of the art). Mechanical properties are compiled from internationally recognised material standards where available (e.g., EN 485-2, ASTM B209, ASTM F2924, ASTM F3001, ASTM A240, ASTM A564, ASTM F3055, and ASTM F3056) [77–80] and supplemented by peer-reviewed literature for AM-specific alloys, modified compositions, and polymer systems not yet covered by international standards [61,63,64,75,77–96]. UTS = ultimate tensile strength; YS = 0.2% yield strength; Elong. = elongation at break; CTE = linear coefficient of thermal expansion (20–100 °C); AB = as-built; HT = heat-treated.

Material	Process	Condition	UTS (MPa)	YS (MPa)	Elong. (%)	ρ (g cm^{-3})	CTE (10^{-6} K^{-1})	TRL	Primary Reference
AlSi10Mg	LPBF	AB	410–490	230–280	5–11	2.67	21.5	9	ASTM F3318 + [77–79]
AlSi10Mg	LPBF	T6	480–520	300–340	4–9	2.67	21.5	9	ASTM F3318 + [77–79]
AlSi10Mg	LPBF	HIP + T6	470–510	290–330	8–14	2.67	21.5	9	ASTM F3318 + [77–79]
Al 6061 (Zr-mod.)	LPBF	AB	250–310	170–220	8–12	2.70	23.6	6	EN 485-2/ASTM B209 + [80]
Al 6061 (Sc+Zr)	LPBF	Aged	350–410	280–340	10–14	2.70	23.6	5–6	[81]
Al 6061 (TiO_2-mod.)	LPBF	Peak aged	320–340	230–260	7–9	2.70	23.6	5	[82]
Al 7075 (MG inoc.)	LPBF	T6	440–490	360–410	11–14	2.81	23.4	5	EN 485-2 + [83]
Al 7075 (TiB_2/Al_3Ti)	LPBF	T6	450–470	370–400	12–14	2.81	23.4	5	[84]
Scalmalloy (Al-Mg-Sc-Zr)	LPBF	AB	410–470	270–330	12–17	2.67	22.5	8	APWorks data + [87,88]
Scalmalloy	LPBF	Aged 325 °C	540–600	460–510	10–14	2.67	22.5	9	APWorks data + [87–89]
Ti-6Al-4V (Grade 5)	LPBF	AB	1020–1150	920–1050	6–11	4.43	8.6	9	ASTM F2924 + ASTM B348 + [89–91]
Ti-6Al-4V	LPBF	HIP 920 °C	950–1050	850–950	11–14	4.43	8.6	9	ASTM F2924 + [89–91]
Ti-6Al-4V	PBF-EB	AB	900–1000	820–910	12–16	4.43	8.6	9	ASTM F1108 + [89–91]
Ti-6Al-4V (Grade 23, ELI)	LPBF	HIP	880–960	800–880	13–17	4.43	8.6	9	ASTM F3001 + [90,91]
Inconel 718	LPBF	AB	950–1050	650–800	22–30	8.19	13.0	9	ASTM F3055/AMS 5662 + [92]
Inconel 718	LPBF	HIP + aged	1250–1450	1050–1250	15–22	8.19	13.0	9	ASTM F3055 + [92]
Inconel 625	LPBF	AB	900–1000	600–700	35–45	8.44	12.8	8–9	ASTM F3056 + [93]
316L stainless	LPBF	AB	540–650	420–530	38–55	7.99	16.0	8	ASTM A240/ASTM F3184 + [94]
316L	Binder Jet	Sintered + HIP	490–560	200–260	50–70	7.99	16.0	6	ASTM A240 + [94]
17-4 PH	Binder Jet	Sintered + H900	1100–1250	980–1100	8–14	7.78	11.6	6	ASTM A564 + [95]
CuCrZr	LPBF	Aged	350–430	290–350	20–30	8.90	17.0	6–7	ASTM B224 + [96]
Pure Cu (Cu-OFE)	LPBF (green/IR)	AB	200–260	80–140	35–55	8.94	16.5	5–6	ASTM B170 + [96]
PA 12 (SLS)	SLS	AB	45–50	40–45	15–20	1.01	110	7–8	ISO 17296 + [61,63]
PA-CF (Windform XT 2.0)	SLS	AB	80–88	n/a	4–6	1.10	≈ 60	9	CRP Technology + [9,21,26]
PEEK	FDM	AB	95–105	95–100	4–6	1.30	47	7–8	ASTM D638 + [70,97]
PEEK	SLS	AB	90–110	80–95	3–5	1.30	47	7	ASTM D638 + [70]
ULTEM 9085	FDM	AB	72–82	50–60	5–7	1.34	47	8	ASTM D638 + manufacturer data
ULTEM 1010	FDM	AB	80–90	64–70	3–5	1.27	47	7	ASTM D638 + manufacturer data
Aerospace photopolymer (SLA)	SLA	UV-cured + post	50–70	45–60	3–8	1.18	60–80	4–5	[61,63,64]

The single most important takeaway from Table 12 for PocketQube design is the cluster of polymer materials in the 80–110 MPa UTS, 1.0–1.3 g cm^{-3} density region. The specific-strength ratio (UTS/ρ) for FDM PEEK is 75 kN m kg^{-1}—only 30% below LPBF AlSi10Mg-T6

(185 kN m kg^{-1})—and the density advantage of polymers compresses the launch quasi-static load mass-budget allocation to a level where, for the 1P envelope, polymer primary structures often outperform metallic primary structures at the same total mass. This is the fundamental reason that PEEK, Windform XT 2.0, and ULTEM 9085 have become the dominant structural materials for academic and commercial PocketQubes [66,70,79]. A visual example is shown in Figure 6.



Figure 6. Topology and AFIT lattice CubeSat bus structure [61].

5.6. Anisotropy of AM Materials: Build Direction Effects on Structural Performance

All powder-bed AM processes produce *anisotropic* mechanical properties: tensile properties differ between the build direction (Z) and the layer plane (X-Y) due to (i) elongated columnar grain morphology along Z; (ii) preferential void elongation along Z; and (iii) layer-to-layer interfacial defects acting as crack-initiation sites under transverse loading [61,63,75,92].

The magnitude of anisotropy varies systematically by material and post-processing:

- As-built LPBF AlSi10Mg: Z-direction UTS is 8–15% higher than X-Y, but elongation is 20–40% lower; fatigue lives differ by up to 3× [75,77];
- LPBF Ti-6Al-4V: anisotropy is more modest at 5–10% in tensile properties but more pronounced at high-cycle fatigue [61,89];
- LPBF Inconel 718: as-built anisotropy of 10–20% in YS and 25% in elongation, substantially reduced by HIP + double ageing to <5% [90,91];
- LPBF Scalmalloy: uniquely, demonstrates essentially zero anisotropy after standard ageing (<3% difference between vertical and horizontal samples), a consequence of the dispersed-coherent-precipitate strengthening mechanism [87,88];
- FDM polymers: anisotropy is dominated by inter-layer bond strength rather than crystallographic effects, with transverse-direction UTS typically 50–70% of in-plane UTS for PEEK and ULTEM [66,70].

For PocketQube design, three practical rules follow [61,67,77]:

1. Align the build direction with the principal stress axis (typically the longitudinal launch quasi-static load direction);
2. For fatigue-critical components, apply HIP to homogenise properties and substantially close anisotropy gaps.

5.7. Post-Processing Effects on Mechanical Properties

Post-processing transforms as-built AM material into a flight-qualifiable engineering material. Three categories dominate the chain.

5.7.1. Hot Isostatic Pressing (HIP)

Hot isostatic pressing applies isostatic gas pressure (100–200 MPa argon) at elevated temperature (520 °C for AlSi10Mg, 920–1050 °C for Ti-6Al-4V, and 1120–1185 °C for Inconel 718) for 2–4 h, closing internal porosity to <0.1% and homogenising microstructure [61,89,90].

Documented effects on flight-relevant properties:

- LPBF AlSi10Mg after HIP at 520 °C/100 MPa/2 h: porosity reduction from 0.5–1.5% to <0.05%; elongation increase from 7% to 12%; fatigue life improvement of 3–5× at 10^7 cycles; and ≈5% loss of UTS (over-ageing trade-off) [77,93];
- LPBF Ti-6Al-4V after HIP at 920 °C/100 MPa/2 h: porosity from 0.2–0.8% to <0.05%; ductility recovery to wrought equivalent (11–14% elongation); and fatigue life improvement of 5–10× [89];
- LPBF Inconel 718 after HIP at 1160 °C/100 MPa/4 h + double ageing: porosity from 0.3–0.6% to <0.05%; UTS increase to 1300–1450 MPa; and elongation to 18–22% [90,91].

For PocketQube programmes, HIP adds €100–300 per part and 2–5 days to lead time but is strongly recommended for any fatigue- or impact-critical metallic component. The cost is rarely justifiable for non-critical fasteners or brackets [61,63].

5.7.2. Heat Treatment (T6, Stress Relief, and Annealing)

Heat treatment serves three distinct functions: (i) stress relief to relieve residual stress, (ii) solutionising to redistribute alloying elements, and (iii) ageing to precipitate strengthening phases [77,87,90].

The canonical aluminium heat-treatment chain is as follows:

- AlSi10Mg T6: solutionise at 530 °C/1 h + water quench + artificial age at 160 °C/6 h; yields UTS gain of 30–50 MPa and YS gain of 40–80 MPa at 1–2% elongation cost [77];
- Scalmalloy ageing: 325 °C/4 h (no solutionising required); YS gain of ≥ 200 MPa and UTS gain of ≥150 MPa, retaining 12–14% elongation [87,88];
- Al 6061 T6 (Zr-modified): 530 °C/1 h + 175 °C/8 h; UTS gain of 60–100 MPa over as-built [81,82].

For titanium and nickel alloys:

- Ti-6Al-4V stress relief: 600 °C/2 h/argon—relieves residual stress without microstructural change;
- Ti-6Al-4V β-anneal: 1050 °C/30 min + furnace cool—converts α′ martensite to α + β, recovers ductility;
- Inconel 718 standard: 1065 °C stress relief + (optional HIP) + solution at 980 °C + double-aged at 720 °C/8 h + 620 °C/8 h [90].

5.7.3. Surface Finishing: Bead Blasting, Anodising, and Electropolishing

As-built AM surfaces (LPBF *Ra* 6–15 µm and PBF-EB *Ra* 25–40 µm) are typically incompatible with sliding mating interfaces, fatigue-critical free surfaces, and outgassing-sensitive applications [61,93,94]. Three surface-finishing routes are routinely applied to PocketQube-class hardware and even shot peening, as seen in Figure 7 [78]:

1. Bead/abrasive blasting. Glass beads, ceramic media, or aluminium oxide grit reduce surface roughness to Ra 3–6 µm, producing a uniform matte finish. It is the standard first-stage treatment for LPBF aluminium and titanium because it is inexpensive, scalable, and compatible with internal channels through abrasive-flow machining [92,93].

2. Anodising. Type II sulfuric or Type III hard anodising of LPBF AlSi10Mg and modified 6061 forms a 10–80 µm electrically insulating Al_2O_3 layer, improving corrosion resistance by 2–3 orders of magnitude, providing dielectric strength of 500–1000 V, and achieving HV 350–500 surface hardness (Type III) [94]. Unlike wrought alloys, LPBF aluminium presents challenges from residual porosity and the high silicon content of AlSi10Mg, which cause electrolyte entrapment and non-uniform oxide growth. LPBF-specific processes developed by Cabrini et al. (2023) achieve Type III coatings with thickness variations of $\leq \pm 5$ µm [94].
3. Electropolishing. Electropolishing removes 5–50 µm of material by anodic dissolution in suitable electrolytes (typically perchloric acid–methanol for aluminium and phosphoric–sulfuric acid for stainless steels and Inconel) [93,95]. It reduces surface roughness to Ra $\leq$ 1 µm, removes spatter and notch defects, and is therefore reserved for fatigue-critical surfaces and outgassing-sensitive optical interfaces despite its cost (approximately €40–100 per part) [95].

A final caveat: every post-processing step adds variance to the mass budget. Bead blasting removes 0.1–0.5 g per 1P frame; anodising adds 0.2–0.8 g; and electropolishing removes 0.5–2.0 g. At the 250 g 1P ceiling these variabilities are non-negligible and must be tracked per-build in the hardware-serial register (Section 3).

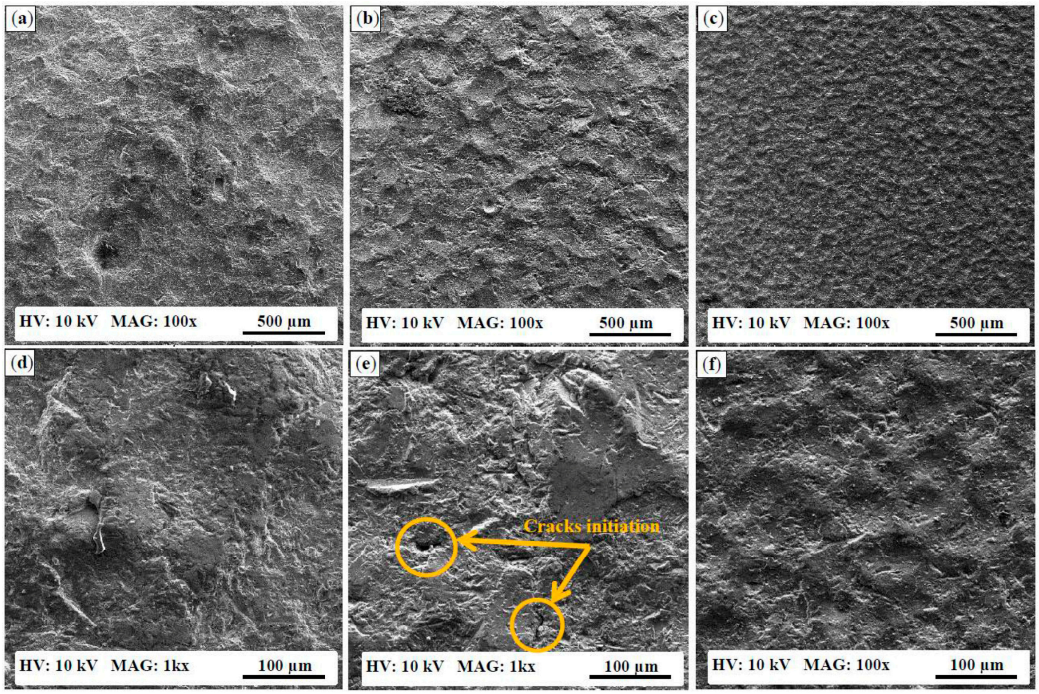


Figure 7. The impact of shot peening on the surface morphology of the AlSi10Mg sample: (**a**,**d**) as-built (AB) + shot-peened (SP), (**b**,**e**) machined (M) + high-intensity SP (HSP), and (**c**,**f**) M + low-intensity SP (LSP). Adapted from: [78].

6. Defects, Failure Modes, and Quality Assurance in AM Space Structures

Additive manufacturing introduces a defect population fundamentally different from that of subtractive and cast manufacturing. Unlike the inclusion-, segregation-, and machining-induced defects documented in aerospace materials databases, AM defects form during fabrication, evolve layer by layer, and depend nonlinearly on process parameters including laser power, scan speed, hatch spacing, layer thickness, scan strategy, gas-flow configuration, and feedstock chemistry [96,98,99]. For PocketQube structures,

where mass margins are minimal and each component is effectively a single-piece flight article, undetected defects represent the principal structural risk after deployment failure. This Section reviews the AM defect taxonomy, launch-load implications, non-destructive evaluation (NDE) methods, in situ quality-control techniques, and vacuum-outgassing performance of AM materials for spaceflight.

6.1. Defect Taxonomy in Metallic AM: Porosity, Cracking, Delamination, and Warpage

Defects in metal AM are classified by mechanism into four primary families [98,99]:

1. Porosity. Volumetric voids dominate the AM defect statistics by frequency. Three sub-types are reproducibly identified across LPBF, PBF-EB, DED, and binder-jetting routes [98,100]:
   - Gas porosity—These are spherical voids of 5–50 µm diameter formed by the entrapment of shielding gas or dissolved gas in the melt pool. Aluminium alloys are particularly susceptible due to high hydrogen solubility differential between liquid and solid Al. As-built LPBF AlSi10Mg typically exhibits 0.5–1.5% gas porosity by volume [77,100].
   - Lack-of-fusion (LoF) porosity—These are irregular elongated voids of 50–500 µm characteristic dimension formed when the volumetric energy density E_v falls below the alloy-specific threshold (≈30 J mm^{-3} for AlSi10Mg). LoF defects are the most damaging variant: their irregular morphology produces stress concentration factors K_t of 3–6, versus 1.5–2.5 for gas porosity, and they are aligned with the build layers, perpendicular to the loading direction in vertical-tensile configuration [98,100,101].
   - Keyhole porosity—These are quasi-spherical voids of 20–100 µm formed when *E*_v exceeds the keyhole-mode threshold (≈70 J mm^{-3} for AlSi10Mg). Vaporisation of low-vapour-pressure alloying elements (Mg, Zn) creates a narrow vapour cavity, which collapses irregularly; the collapse traps vapour at the cavity root [98,100–102]. This different porosity in materials is shown in Figure 8.
2. Solidification (hot) cracking. This signifies inter-dendritic micro-cracks 10–500 µm in length, oriented along the columnar grain boundaries, formed during the terminal stages of solidification when residual liquid cannot accommodate strain induced by thermal contraction. Cracking dominates the unprintability of Al-Mg-Zn (7075), Al-Mg-Si (6061), and certain Ni-Cr-Mo superalloys; the mitigation strategies of Section 5 (Sc/Zr inoculation, TiB_2 in situ formation, and metallic-glass nucleation) address this failure mechanism specifically [85,86,99].
3. Delamination. This describes macro-scale separations between layers, typically 1–10 mm in lateral extent, formed when (i) residual stress at the layer interface exceeds the inter-layer bond strength, (ii) the substrate-anchorage is insufficient (the recurring "lift-off" failure mode), or (iii) the inter-layer wait time exceeds the relaxation time of the underlying material. Delamination is rare in well-controlled production but catastrophic when it occurs: the affected part is unrecoverable and must be scrapped [98–100].
4. Warpage and residual-stress distortion. Thermal gradients of 10^5–10^6 K m^{-1} during build create residual-stress fields that distort the part during build, after support removal, or during downstream heat treatment. For PocketQubes, warpage is the most pernicious dimensional defect: a 0.3 mm warp on the 50 mm baseplate violates the PQ-MEPS ±0.1 mm tolerance and forces remanufacture [101,102].

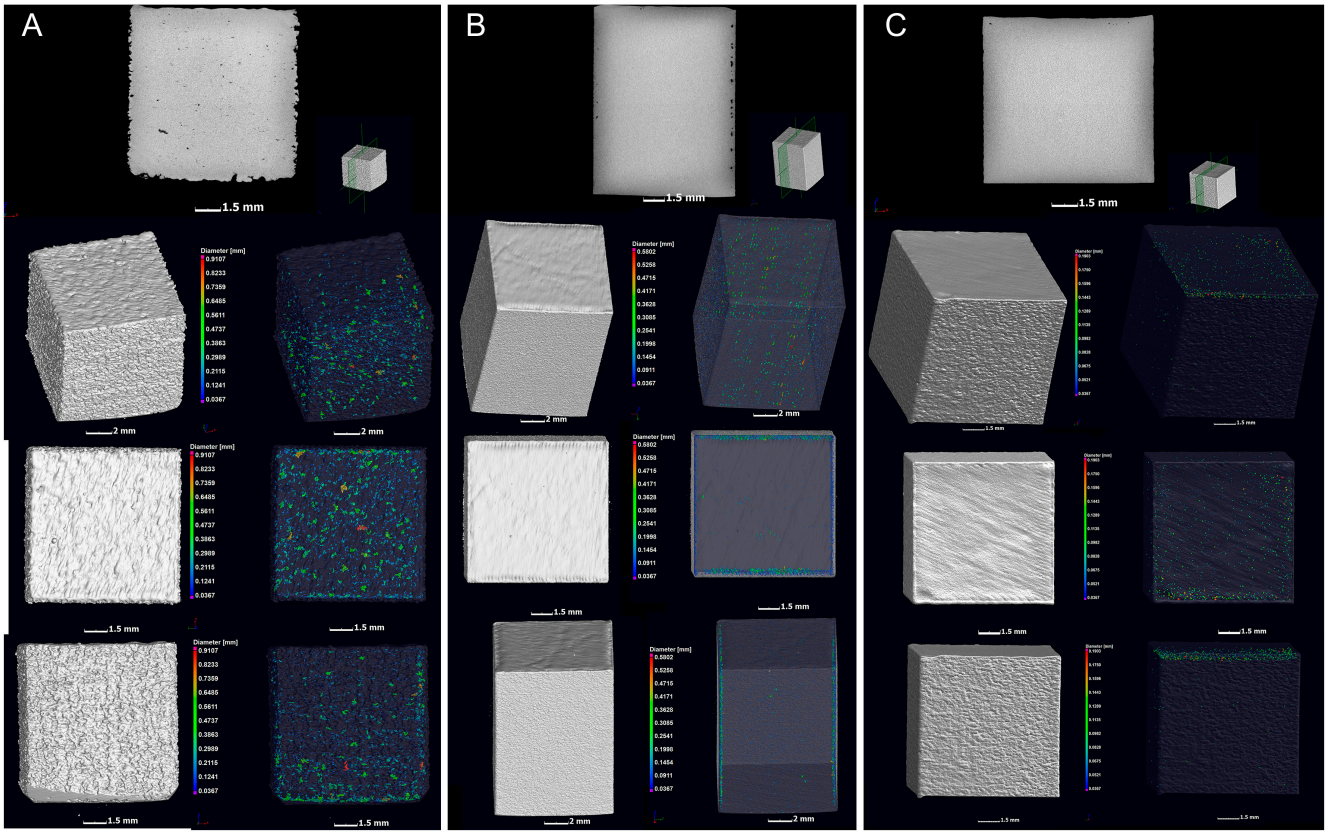


Figure 8. Examples of different porosity distributions in 10 mm coupon samples. In the three examples shown, each cube (**A**–**C**) is viewed in a CT slice image (top), 3D angled view, 3D from top, and 3D from side. Top is defined as vertical in the build direction, so the top view shows the top surface of the built cube. Adapted from [102].

These defect taxonomies in metallic AM structures are displayed in Table 13.

Table 13. Defect taxonomy for metallic AM with characteristic dimensions, root causes, structural consequences, and primary mitigation routes [98–102].

Defect	Typical Size	Mechanism	Root Cause	Structural Impact	Primary Mitigation
Gas porosity	5–50 µm, spherical	Trapped gas in melt pool	Wet powder; insufficient shield-gas purge; H_2 in Al alloys	$K_t \approx 1.5$–2.5; ↓ fatigue life ×2–5	Powder drying; argon Class 4.6; HIP
Lack of fusion (LoF)	50–500 µm, irregular	Inadequate melting	E_v below threshold	$K_t \approx 3$–6; ↓ fatigue life ×5–15	Process-parameter optimisation; in situ monitoring
Keyhole porosity	20–100 µm, quasi-spherical	Vaporisation cavity collapse	E_v above threshold	$K_t \approx 2$–4; ↓ fatigue life ×3–8	Process-parameter optimisation; HIP
Solidification cracking	10–500 µm	Hot tearing along grain boundaries	Wide freezing range; columnar grain morphology	Crack initiator; ↓ UTS ×0.5–0.7	Grain refinement; TiB_2/Sc/Zr inoculation
Delamination	1–10 mm	Inter-layer bond failure	Residual stress > bond strength	Catastrophic; part scrap	Stress relief; support strategy; preheat
Warpage	0.1–2 mm	Residual-stress distortion	Build orientation; thermal gradient	Dimensional non-conformance	Topology optim.; lattice support; HT
Surface roughness	*Ra* 6–40 µm	Spatter + partial melting	Inherent to powder bed	↓ fatigue life ×4–10	Bead blasting; HIP; electropolishing
Sub-surface oxide inclusion	5–30 µm	Powder oxidation	Powder reuse; humid storage	Crack initiator; embrittlement	Powder lot control; argon-glovebox handling

6.2. Impact of AM Defects on Structural Integrity Under Launch Loads

The launch environment imposes three distinct load regimes on the PocketQube structure (Section 3 (Section 3.4)): (i) random vibration of ≈ 10 Grms across 20–2000 Hz; (ii) quasi-static acceleration of 10–15 g longitudinal, 5–10 g lateral; and (iii) shock from stage-separation pyrotechnics, with SRS peaks of hundreds of g above 1000 Hz [57]. AM defects degrade structural performance under each regime differently:

1. Static loading. Tensile and yield strength are governed primarily by macroscopic defects such as lack-of-fusion (LoF) clusters and delamination, which reduce the effective load-bearing cross-section. Meta-analysis shows that LPBF AlSi10Mg with $\leq$0.5% porosity retains $\geq$95% of its reference UTS, whereas 1.0% porosity reduces strength by 12–18% and 1.5% porosity by 20–30% [101]. Consequently, launch quasi-static loading effectively limits structural porosity to approximately 0.5%.
2. Vibration (fatigue). Random vibration (10 Grms, 2 min per axis) corresponds to approximately 10^5–10^6 stress cycles, placing LPBF AlSi10Mg in the high-cycle fatigue regime. Schneller et al. (2019) and subsequent studies report fatigue strengths of 75–105 MPa for as-built LPBF AlSi10Mg and 145–165 MPa after HIP + T6 treatment, representing a 60–80% improvement through elimination of keyhole and LoF porosity [93,101,103]. Ti-6Al-4V shows a similar increase from 320–400 MPa to 510–600 MPa after HIP [89,101]. Accordingly, HIP is recommended for metallic PocketQube structures with launch design margins below 2×.
3. Shock. Pyrotechnic shock (200–500 g, $\geq$1000 Hz) excites high-frequency structural modes, making sub-100 µm AM defects effective stress concentrators. Flight experience identifies LoF clusters and surface notches as the principal shock-induced failure initiators in small-satellite hardware [98,99,101].

6.3. Non-Destructive Evaluation (NDE) Techniques for AM Parts

Non-destructive evaluation is the gating activity between "as-built AM part" and "flight-qualifiable hardware". The geometric complexity that motivates AM in the first place—internal channels, lattices, and conformal cooling—simultaneously defeats most legacy NDE techniques [102,104,105].

6.3.1. XCT Cost and Inspection Time at the PocketQube Scale

X-ray computed tomography (XCT, or micro-CT, µCT, for sub-millimetre resolution) is the leading NDE technique for AM structures and has reached TRL 9 for aerospace small-satellite acceptance testing [102,104]. A 200–450 kV polychromatic X-ray source acquires 1000–3600 projections that are reconstructed by filtered back-projection or iterative algorithms (SART and MLEM) into a three-dimensional voxel model. For PocketQube components, detector resolution, geometric magnification, and X-ray spot size determine image quality. A 5 µm source spot, 50 µm detector pixel, and 10× magnification achieve 5–10 µm voxels, sufficient to detect gas pores $\geq$15 µm and lack-of-fusion (LoF) defects $\geq$30 µm [102,104].

Common artefacts include beam hardening in high-Z alloys, detector-induced ring artefacts, and streaking from dense inclusions or sharp edges [102]. Recent advances (2022–2025) integrate deep-learning segmentation, with U-Net and 3D U-Net models exceeding 95% voxel-level classification accuracy for gas, LoF, and keyhole porosity in LPBF AlSi10Mg and Ti-6Al-4V [104,105]. A recommended PocketQube inspection workflow comprises (i) XCT at $\geq$10 µm voxel resolution; (ii) automated deep-learning segmentation; (iii) acceptance limits of $\leq$0.3% porosity for primary structures and $\leq$1.0% for secondary components; and (iv) manual review of defects >200 µm or within 1 mm of high-stress fillets. Scanning a 50 × 50 × 50 mm component at 10 µm resolution typically requires

1–3 h on industrial XCT systems (e.g., Zeiss Metrotom, Nikon XT H 225, and GE Phoenix v | tome | x) and costs approximately €150–400. Consequently, educational PocketQube programmes often replace full XCT inspection with destructive metallography of representative coupons [102–104].

6.3.2. Ultrasonic Testing and Resonance Methods

Ultrasonic NDE—phased-array UT (PAUT), full-matrix capture (FMC), and resonance ultrasound spectroscopy (RUS)—provides complementary capability to XCT at lower cost and faster throughput, at the price of lower spatial resolution and orientation-dependent sensitivity [105,106].

For PocketQube-class parts, the principal ultrasonic methods are as follows:

- Conventional pulse-echo UT (2.25–10 MHz transducer): This detects defects $\geq$ 200 µm in low-attenuation alloys (aluminium and titanium); it is blocked by complex internal geometry. There is limited utility for AM PocketQube primary structures.
- Phased-array UT (PAUT): Here, 5–10 MHz arrays steer the ultrasonic beam electronically, providing imaging of internal volumes. The detection threshold $\approx$ 100 µm at 50 mm depth. PAUT is becoming the standard inspection method for larger AM aerospace components (5–500 mm) but remains marginal at the 1P scale because the part is too small to host meaningful beam-steering geometry [106].
- Resonance ultrasound spectroscopy (RUS): This measures the natural-frequency spectrum of the part and compares it to a reference; deviations indicate volumetric defects, density anomalies, or stiffness changes. RUS is uniquely well suited to small-part screening because it scales favourably to small geometries and produces a single Pass/Fail metric per part within minutes [105]. The technique cannot localise defects but provides a low-cost first-line screen.

This comparison is shown in Table 14, where the NDE techniques are applied in AM pocketQub structures.

Table 14. Comparison of NDE techniques for PocketQube-class AM parts [102,104–106].

Technique	Detectable Defects	Cost (€)	Inspection Time	TRL
XCT (µCT)	5–30 µm	150–400	1–3 h	9
Phased-array UT	100–500 µm	60–150	30–60 min	8–9
Pulse-echo UT	0.2–1 mm	30–80	15 min	8
Resonance UT (RUS)	Volumetric defects	5–20	2–5 min	7–8
Eddy current	Surface and subsurface (<1 mm)	40–100	20–40 min	7
Dye penetrant	Surface-breaking only	5–10	30 min	9 (surface)

6.4. Statistical Process Control and In Situ Monitoring for AM Qualification

The economics of AM at the PocketQube scale (10–100 parts per programme) make destructive coupon testing of every build commercially unattractive and statistically insufficient. The aerospace AM community has consequently shifted toward in situ process monitoring (ISPM) as the primary quality assurance mechanism, with offline NDE (Section 6.3) reserved for first-article and lot-sampling verification [107,108].

1. Sensors deployed in modern LPBF machines [107,108]:
    - Coaxial melt-pool monitoring—a photodiode or near-infrared (NIR) camera mounted on the laser optical path samples melt-pool intensity at 10–100 kHz, providing per-track thermal-emission data correlated to melt-pool size, depth, and stability.
    - Off-axis NIR/visible imaging—wide-field cameras image the entire build plate at 1–30 Hz, capturing layer-wise spatter, balling, and inter-layer geometric defects.

- Layerwise pyrometry/thermal imaging—calibrated infrared cameras record the thermal signature of each layer post-fusion, identifying cold-spots indicative of LoF.
- Optical tomography—high-resolution flatbed cameras image the powder bed before and after laser exposure, identifying powder bed defects, short-feeds, and recoater damage.
- Acoustic emission—piezoelectric transducers on the build plate detect crack-initiation acoustic signatures (typically 100 kHz–1 MHz).

2. Machine learning integration has transformed the value of these sensor streams. Convolutional and recurrent neural network architectures trained on labelled multi-sensor datasets now demonstrate per-layer defect detection at >90% accuracy and per-voxel defect prediction at >85% for LoF and keyhole defects [107,108]. The state of the art (2023–2025) integrates physics-guided generative models that constrain ML predictions to thermodynamically valid melt-pool morphologies, improving generalisation to unseen geometries [109].

For PocketQube programmes operating on shared LPBF capacity, the ISPM data are typically captured by the service bureau and provided as the "build certificate", a Pass/Fail per layer with anomaly flags. The Programme Manager's responsibility is to define the per-WP acceptance threshold (typically zero red anomalies for Criticality A parts and $\leq$5 yellow anomalies per build for Criticality B) and to ensure traceability between the build certificate and the hardware-serial register, as seen in Figure 9.

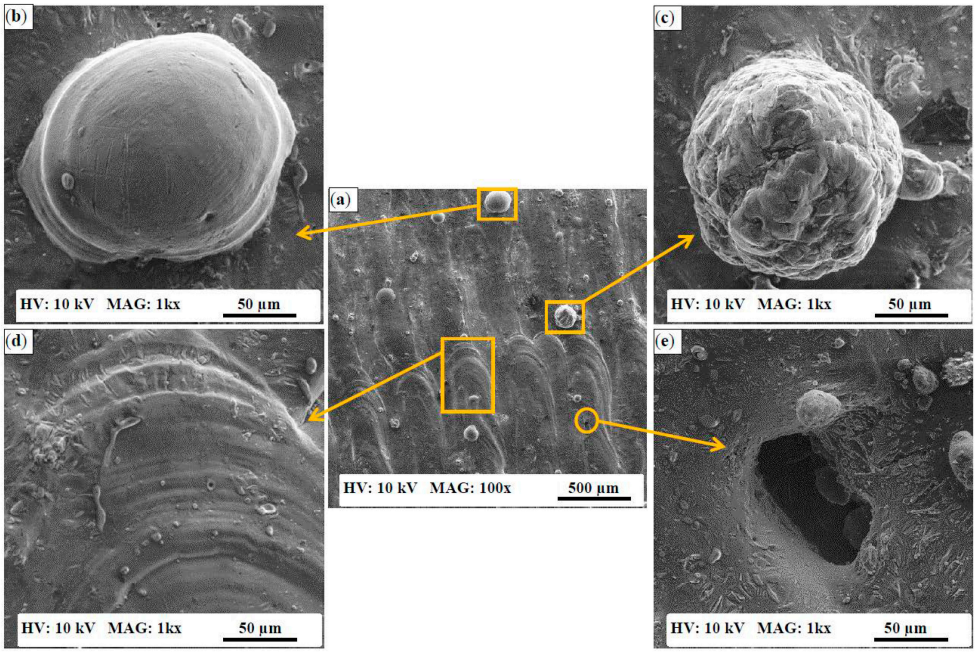


Figure 9. Characteristic as-built surface defects of LPBF AlSi10Mg observed via scanning electron microscopy: (**a**) general overview of the as-built surface showing combined balling, partially melted powder adherence, and surface porosity; (**b**) ellipsoidal balling morphology arising from melt-pool instability; (**c**) satellite particles—partially melted powder grains adhered to the consolidated surface; (**d**) terminal-layer laser scan tracks of width slightly exceeding the 100 µm beam diameter, attributable to the elevated cooling rate of the final layer; (**e**) sub-surface pore breaking through the as-built surface plane. These four defect families—balling, satellites, scan-track topography, and surface-breaking porosity—collectively determine the as-built roughness regime (*Ra* 6–15 µm) and the high-cycle fatigue debit characteristic of un-post-processed LPBF aluminium. Adapted from Maamoun, A.H.; Elbestawi, M.A.; Veldhuis, S.C. J. Manuf. Mater. Process. 2018, 2, 40, reproduced under CC BY 4.0 [78].

6.5. Outgassing Behaviour of AM Aluminium Alloys in Vacuum (TML/CVCM Data Review)

The vacuum environment of LEO imposes outgassing limits that are amongst the most binding material selection constraints for spaceflight hardware. ECSS-Q-ST-70-02C [76] and its US equivalent ASTM E595 require, for any material in line-of-sight of sensitive surfaces (optics, detectors, and deployable mechanisms) [109]:

- Total Mass Loss (TML) < 1.0% at 125 °C/10^{-6} Pa/24 h;
- Collected Volatile Condensable Material (CVCM) < 0.1% at the same test conditions;
- Water Vapour Regained (WVR) is informative only.

For metallic AM materials, the outgassing behaviour diverges meaningfully from wrought/cast counterparts due to three AM-specific factors: (i) residual surface porosity that traps process gas and machining lubricants, (ii) significantly higher surface-to-volume ratio in lattice-structured parts, and (iii) the alloying-element vapour pressure during build, which can leave Mg- or Zn-rich surface oxide layers [110,111].

1. Aluminium AM outgassing dataset. A landmark 2021 study by Cooper et al. demonstrated an LPBF AlSi10Mg ultra-high-vacuum chamber operating at pressure <10^{-10} mbar, with a total gas-output rate of 3.6 × 10^{-13} mbar L s^{-1} mm^{-2} after bakeout at 200 °C/48 h [110]. The outgassing performance was attributable to a heavily oxidised, Mg-rich surface layer (≈100 nm) formed during build, which acts as a barrier suppressing bulk-Mg outgassing. The same study reported TML of 0.04–0.08% and CVCM of <0.01% for as-built LPBF AlSi10Mg samples, well within ECSS limits and comparable to vacuum-baked wrought 6061-T6 [110].

Comparable outgassing performance has been confirmed across the AM aluminium family:

- LPBF AlSi10Mg (as-built + acetone clean + bake): TML 0.04–0.10%, CVCM < 0.01% [110,111].
- LPBF Scalmalloy (aged + bake): TML 0.05–0.12%, CVCM < 0.02% [111].
- LPBF Al 7075 (TiB_2-modified, T6 + bake): TML 0.08–0.15%, CVCM < 0.02% [86,111].

For polymer AM materials, the outgassing dataset is well established only for selected high-performance thermoplastics:

- FDM PEEK (Boschetto et al. 2021): TML 0.11% avg, CVCM < 0.01%—compliant [70].
- FDM ULTEM 9085: TML 0.30–0.45%, CVCM 0.02–0.04%—compliant [111].
- SLS Windform XT 2.0: NASA- and ESA-outgassing certified per AlbaPod v2 flight qualification [59].
- SLA aerospace photopolymer: TML 0.4–1.2%, CVCM 0.04–0.15%—borderline; per-lot certification required [111].
- Standard FDM ABS/PLA: TML 1.5–4.0%, CVCM 0.1–0.4%—non-compliant for line-of-sight applications without coating.

The outgassing data for AM materials are presented in Table 15.

Table 15. Outgassing data summary for AM materials relevant to PocketQube structures (ECSS-Q-ST-70-02C/ASTM E595 conditions: 125 °C, 10^{-6} Pa, 24 h) [59,70,76,110,111].

Material/Process	TML (%)	CVCM (%)	Compliance	Notes
LPBF AlSi10Mg as-built	0.04–0.10	<0.01	Yes	Mg-rich oxide layer suppresses bulk outgassing
LPBF Scalmalloy (aged)	0.05–0.12	<0.02	Yes	Comparable to AlSi10Mg
LPBF Ti-6Al-4V	0.03–0.08	<0.01	Yes	Excellent; widely flown
LPBF Inconel 718 (HIP + aged)	0.02–0.06	<0.01	Yes	Excellent; widely flown
Binder-jet 316L (HIP)	0.08–0.15	<0.02	Yes	Higher than LPBF; bake-out helps
FDM PEEK	0.11 (avg)	<0.01	Yes	Flight-qualified per [70]
FDM ULTEM 9085	0.30–0.45	0.02–0.04	Yes	Below limits; flight-qualified

Table 15. *Cont.*

Material/Process	TML (%)	CVCM (%)	Compliance	Notes
SLS Windform XT 2.0	0.20–0.30	<0.02	Yes	NASA/ESA-certified; AlbaPod-flown
SLS PA-12	0.40–0.80	0.03–0.08	Yes (marginal)	Per-lot test recommended
SLA aerospace photopolymer	0.40–1.20	0.04–0.15	Borderline	Per-lot certification required
FDM PLA/standard ABS	1.50–4.00	0.10–0.40	Non-compliant	Educational use only

Bake-out is non-negotiable. Across all AM materials, a vacuum bake-out at 80–150 °C/12–48 h is mandatory prior to flight integration. The bake-out chamber pressure should reach $<10^{-5}$ Pa with a residual-gas-analyser (RGA) trace of $<10^{-8}$ Pa for water vapour [110,111]. PocketQube programmes routinely under-budget this qualification step, as illustrated in Figure 10.

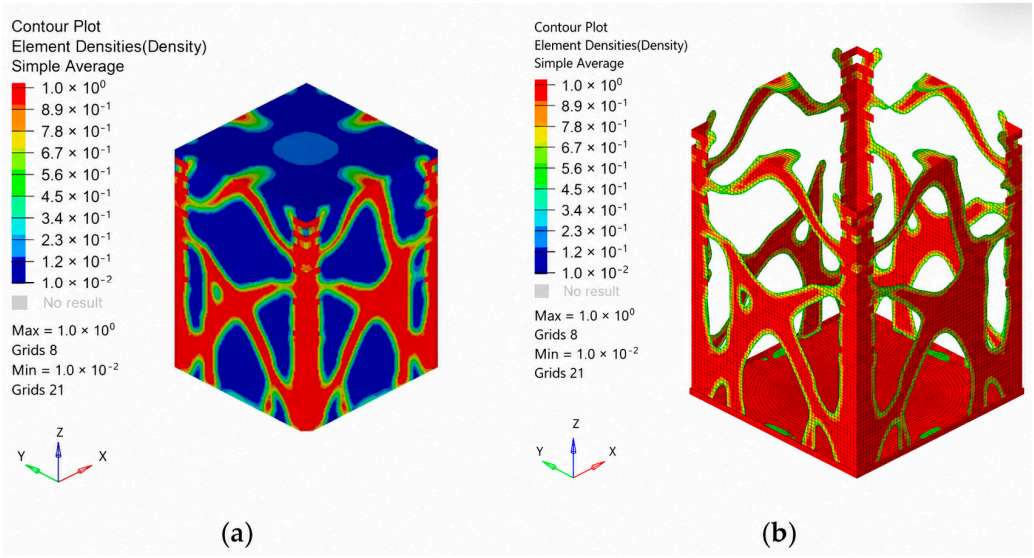


Figure 10. SIMP-based topology optimisation of a 1 U-class nanosat primary structure illustrating the standard density-redistribution workflow: (**a**) element-density contour plot within the design domain—elements with normalised material density $\rho_i \to 1$ (red) constitute the load-bearing topology output, whilst elements with $\rho_i \to 0$ (blue) are eliminated as negligible; (**b**) final structural mesh extracted from the density field after thresholding and re-meshing, ready for export to the additive-manufacturing build-preparation chain. The resulting frame archetype—corner pillars linking the upper interface plate to the base via curved diagonal load paths—is reproducible across picosatellite topology-optimisation studies at the 50–100 mm scale and confirms the minimum-length-scale constraint discussed in Section 4.3.1. Reproduced from Boschetto et al. [70] under the Creative Commons Attribution (CC BY 4.0) licence. © 2021 by the authors. Licensee MDPI, Basel, Switzerland.

7. Normative and Qualification Framework for AM PocketQube Structures

The normative landscape governing additive-manufactured structures for spaceflight has matured substantially since 2018. Three institutional pillars—the European Cooperation for Space Standardization (ECSS), the United States National Aeronautics and Space Administration (NASA), and the joint ASTM International/ISO technical-committee 261 (TC 261) framework—now provide overlapping but non-identical requirements that any flight-qualified AM PocketQube structure must satisfy [112–114]. This Section consolidates the current standards, identifies the gap between standards-as-written and PocketQube-class implementation, sketches a TRL-mapped qualification roadmap, and contrasts the structural-margin philosophies of ECSS and NASA at the picosatellite scale.

7.1. Applicable ECSS Standards

ECSS publishes its requirements as a four-level hierarchy (M—Management, E—Engineering, Q—Quality, and U—User Requirements), each subdivided into Standard (ST), Handbook (HB), and Technical Memorandum (TM) classes [112]. The AM-relevant subset for PocketQube structures is consolidated in Table 16.

Table 16. ECSS standard comparative.

ECSS Reference	Title (Abbreviated)	Issue/Revision	Relevance to AM PocketQubes
ECSS-E-ST-32C	Space engineering—Structural general requirements	Rev. 1 (15 November 2008)	Top-level structural requirements; load definitions; verification approach
ECSS-E-ST-32-10C	Structural factors of safety for spaceflight hardware	Rev. 2 Corr. 1 (1 August 2019)	Mandatory FoS for structural verification
ECSS-E-HB-32-20	Structural materials handbook (parts 1–8)	Issue 1 (20 March 2011)	Materials-property database; updated by industrial test campaigns
ECSS-Q-ST-70-02C	Thermal-vacuum outgassing test for screening of space materials	(28 October 2008)	Mandatory TML < 1.0%, CVCM < 0.1%
ECSS-Q-ST-70-36C	Material selection for controlling stress-corrosion cracking	(15 November 2008)	Material selection screening
ECSS-Q-ST-70-80C	Processing and quality assurance requirements for metallic powder bed fusion technologies for space applications	(30 July 2021)	The principal AM-specific ECSS standard
ECSS-E-ST-10-03C Rev. 1	Space engineering—Testing	(31 May 2022)	Test philosophy and qualification test definitions

7.1.1. ECSS-E-ST-32C: Structural General Requirements

ECSS-E-ST-32C defines the system-level structural engineering requirements for spaceflight hardware, including launch, vibration, shock, thermal, and deployment load cases; verification methods (test, analysis, inspection, and review of design: the T/A/I/R/D framework used in Sections 3.5 and 4.1); and the Mathematical Model, Structural Mathematical Model, and Test Article required throughout programme verification [112,113]. Although process agnostic and not specific to additive manufacturing, the standard establishes the verification hierarchy that AM standards, including ECSS-Q-ST-70-80C (Section 7.1.5), must satisfy. Its principal relevance to PocketQube structures is the requirement for established material allowables, which for AM materials are obtained through the building-block approach defined in ECSS-Q-ST-70-80C [115,116].

7.1.2. ECSS-Q-ST-70-36C: Material Requirements for Space Use

ECSS-Q-ST-70-36C addresses stress-corrosion cracking (SCC), the second most common in-flight structural failure mechanism after fatigue [112]. It classifies materials into high-, moderate-, and low-resistance categories and requires moderate- and low-resistance materials used in critical structures to be qualified by ASTM G44 stress-corrosion testing [112]. For PocketQube AM structures, SCC is generally a secondary concern because of their short missions, dry storage, and sealed deployers. Nevertheless, the standard applies: as-built LPBF AlSi10Mg is currently classified as having moderate SCC resistance, whereas HIP + T6 processing is expected to achieve the high-resistance category, although formal ECSS reclassification is still pending [112,117].

7.1.3. ECSS-E-HB-32-20: Structural Materials Data Handbook

ECSS-E-HB-32-20 is the European equivalent of the NASA-MAPTIS and Department of Defense MIL-HDBK-5 materials-property handbooks: a multi-part document (parts 1–8) tabulating tensile, fatigue, fracture toughness, and environmental degradation data for materials commonly used in spaceflight [112]. Critically for PocketQube programmes, the handbook is non-mandatory—it provides reference data for the designer, not a binding allowables list—and as of 2026, its AM-materials coverage remains limited to a small inventory of LPBF AlSi10Mg, LPBF Ti-6Al-4V, and EBM Ti-6Al-4V test campaigns, with most data points still drawn from non-European sources [112,117].

This gap (the absence of an ECSS-administered AM-materials allowables database) is one of the principal weaknesses identified in Section 7.4 and is the rationale for the European Space Agency's ongoing Materials Engineering Section's AM database expansion (2023–2027 horizon) [117,118].

7.1.4. ECSS-Q-ST-70-02C: Outgassing Requirements

ECSS-Q-ST-70-02C, already introduced as reference [76] (Section 3) and reviewed in Section 6.5, defines the thermal-vacuum outgassing screening test (125 °C, 10^{-6} Pa, 24 h) and the binding limits of TML < 1.0% and CVCM < 0.1%. The standard applies to *every* material in the spaceflight stack-up, including AM-produced ones, without process-specific tailoring. Recent debate within the ECSS Working Group on Materials (Q-ST-70) is whether the standard should be amended to require separate certification per AM build campaign rather than per-material once, given the documented build-to-build variability in surface oxide composition that governs the outgassing performance (Section 6.5) [110,112].

7.1.5. ECSS-Q-ST-70-80C: The Principal AM-Specific ECSS Standard

ECSS-Q-ST-70-80C, published on 30 July 2021 and unchanged at the time of writing, is the principal ECSS standard for additive manufacturing [114]. It defines (i) a phased qualification process comprising Process Qualification (PQ), Material Allowables Generation (MAG), Equipment Qualification (EQ), and Part Qualification (PtQ), each with documented entry and exit criteria; (ii) a minimum coupon programme of $\geq$6 specimens per build orientation, $\geq$3 orientations, and $\geq$3 build campaigns for tensile, fatigue, and microstructural characterisation; (iii) process-parameter documentation requirements (Section 7.3); (iv) NDE acceptance limits of $\leq$0.5% volumetric porosity, no lack-of-fusion (LoF) defects >200 µm, and no surface-breaking defects >100 µm for Class A parts; and (v) build certificates traceable to machine ID, powder lot, process parameters, and in situ sensor records.

Although developed for powder bed fusion (LPBF and PBF-EB), the framework is explicitly applicable to WAAM, DED, FDM, and SLS through process-specific tailoring [114]. For PocketQube programmes, the requirement for six coupons per orientation and campaign is the principal practical limitation, since typical production lots comprise only 5–10 frames, making qualification coupons exceed production volume. ESA-supported pilot programmes have therefore proposed a TRL 5 "PocketQube Lite Class" that reduces the matrix to three coupons per orientation while retaining the full PQ and EQ qualification chain (Figure 11) [114,117].

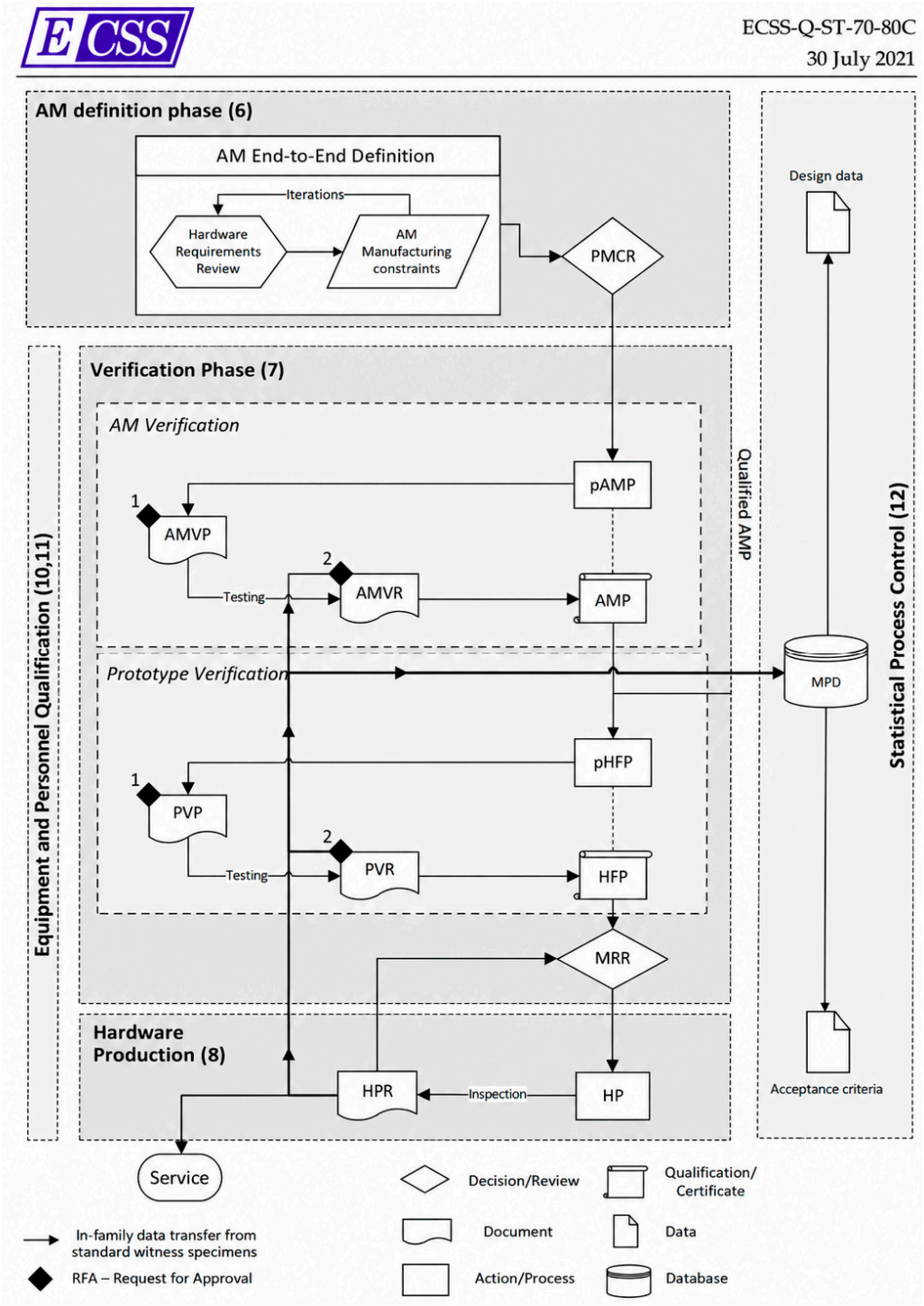


Figure 11. Verified metallic powder bed fusion process flow per ECSS-Q-ST-70-80C [114], comprising four sequential phases: (i) AM Definition Phase—closing the iteration between hardware requirements and AM manufacturing constraints, gated by the Process and Manufacturing Constraints Review (PMCR); (ii) Verification Phase—bifurcated into AM Verification (preliminary AM Process—pAMP → AM Verification Plan—AMVP → AM Verification Report—AMVR → qualified AM Process—AMP) and Prototype Verification (pHFP → PVP → PVR → qualified Hardware Family Process—HFP); (iii) Hardware Production—gated by the Manufacturing Readiness Review (MRR), Hardware Production (HP), Hardware Production Report (HPR), and final Service release; (iv) Statistical Process Control—feeding the Material Property Database (MPD) used as design data. Two cross-cutting streams (Equipment and Personnel Qualification + Statistical Process Control) operate throughout. Adapted from ECSS-Q-ST-70-80C [114], Figure 4-1. © ECSS, used under ECSS Free Public Use terms.

7.2. NASA Standards Applicable to AM Space Structures

The NASA framework underwent a step change in 2021 with the release of NASA-STD-6030, the first integrated AM technical standard for crewed spaceflight, and its supporting equipment-control standard NASA-STD-6033 [115].

7.2.1. NASA-STD-6030A: AM Requirements for Spaceflight Systems

NASA-STD-6030 (first release: 21 April 2021; revision A in progress as of 2026) defines the minimum requirements for AM parts used in NASA crewed spaceflight systems and provides tailoring guidance for non-crewed missions [115,118]. According to Table 17, the standard organises requirements around a *part-class system* (Class A—fracture-critical, Class B—significant-failure-effect, and Class C—non-critical) and prescribes scaled qualification rigor by class.

Table 17. NASA AM standards applicable to PocketQube structural development [115,118–120].

NASA Reference	Title (Abbreviated)	Release	PocketQube Applicability
NASA-STD-6030	Additive Manufacturing Requirements for Spaceflight Systems	21 April 2021	Primary AM technical standard
NASA-STD-6033	AM Requirements for Equipment and Facilities Control	21 April 2021	Build machine qualification, facility cleanliness
NASA-HDBK-6030	Implementation Guidance for NASA-STD-6030	2022 (informative)	Worked examples, tailoring guidance
NASA-STD-5001B w/Change 3	Structural Design and Test Factors of Safety for Spaceflight Hardware	24 October 2022	Mandatory FoS (US counterpart of ECSS-E-ST-32-10C)
NASA-STD-5012B	Strength and Life Assessment Requirements for Liquid-Fuelled Spaceflight Hardware	2016 (current)	Fracture-control aspects
NASA-STD-5019B	Fracture Control Requirements for Spaceflight Hardware	2020	Applies to fracture-critical Class A parts
NASA-HDBK-5026	Quality Assurance Provisions for Aerospace Welding and Brazing	2023	Indirect, but referenced for AM weld-like joints

Three principal mandatory provisions of NASA-STD-6030 are directly binding on AM PocketQube structures:

1. Process-equipment qualification before flight-hardware production. Each AM machine must have an approved Process Qualification Record (PQR) before any flight part is produced on it. This requirement implicitly excludes most academic and low-budget PocketQube programmes from NASA-launched rideshare opportunities, unless they procure parts from a NASA-qualified service bureau.
2. Part-specific Material Allowables Generation (MAG). for Class A parts, a B-basis (90% survival, 95% confidence) or A-basis (99%/95%) allowable is required, requiring $\geq$30 specimens per condition. For Class B parts, a "design value" suffices, requiring 10–15 specimens. For Class C parts, a single confirmation specimen plus literature allowables is acceptable.
3. Build certificate and traceability. Every AM part must be traceable to a build record (machine, powder lot, process-parameter file, and NDE result), and the build record must be archived for the mission life plus retention period (typically 7 years for non-crewed and 25 years for crewed) [115].

For PocketQube programmes, the practical mapping is as follows: primary structural frames at Criticality A (per Chapter 3, Section 3) must be NASA-STD-6030 Class B or above,

requiring at least the 10–15-specimen MAG campaign; secondary structural brackets at Criticality B can be Class C, with the most reduced rigor.

7.2.2. NASA-HDBK-6030: Implementation Guidance

NASA-HDBK-6030, published in 2022 as a companion to NASA-STD-6030, provides guidance for tailoring qualification to SmallSat platforms [119]. It specifically addresses small-batch production by allowing non-crewed spacecraft (mass < 180 kg, mission life < 5 years) to reduce Material Allowables Generation (MAG) specimens from 30 to 6 per condition when supplemented by published allowables for the same alloy and manufacturing process. This approach has become the practical baseline for PocketQube programmes pursuing NASA rideshare flight qualification [119].

NASA Technical Reports Server document NTRS 20220004051 compares NASA-STD-6030 and ECSS-Q-ST-70-80C directly; their principal alignments are summarised in Table 18 (Section 7.3) and key differences discussed in Section 7.6 [118–120].

Table 18. ASTM and ISO AM standards relevant to PocketQube structures [120–123].

Standard	Title (Abbreviated)	Scope	Latest Update
ASTM F2924	Specification for AM Ti-6Al-4V with Powder Bed Fusion	Material spec—Grade 5 Ti	2014, reapproved 2021
ASTM F3001	Specification for AM Ti-6Al-4V ELI with Powder Bed Fusion	Material spec—Grade 23 Ti	2014, reapproved 2021
ASTM F3049	Standard Guide for Characterising Powders for AM	Powder characterisation	2014
ASTM F3055	Specification for AM Nickel Alloy UNS N07718 (Inconel 718) with PBF	Material spec—IN718	2014, reapproved 2021
ASTM F3056	Specification for AM Nickel Alloy UNS N06625 (Inconel 625) with PBF	Material spec—IN625	2014
ASTM F3122	Standard Guide for Evaluating Mechanical Properties of Metals via AM	Mechanical-test methods	2014, revised 2022
ISO/ASTM 52900	AM—General principles—Fundamentals and vocabulary	Terminology	2021 (replaces 2015 edition)
ISO/ASTM 52904	AM Process Performance—Practice for Metal Powder Bed Fusion	Process qualification	2019, updated 2024
ISO/ASTM 52907	AM Feedstock Materials—Methods for sampling and characterising metal powders	Powder sampling and characterisation	2019
ISO/ASTM 52911-1	DfAM—Part 1: Laser-based powder bed fusion of metals	Design rules	2019

7.3. ASTM/ISO Standards for AM Metallic Materials

Beyond the agency-level (NASA, ECSS) frameworks, the international standards bodies—ASTM International (Committee F42) and ISO Technical Committee TC 261—provide a process- and material-specific layer of standardisation that is referenced by both NASA-STD-6030 and ECSS-Q-ST-70-80C [119,122,123].

7.3.1. ASTM F2924, F3001, and F3049: Powder and Process Standards

According to Table 18, the three core ASTM material standards relevant to PocketQube AM are [120–123].

For PocketQube programmes, ASTM F2924 and F3001 are routinely cited as the material baseline for Ti-6Al-4V structural parts, with F3055 for IN718-based propulsion brackets and F3122 for the mechanical-test methods. ASTM does *not* publish an equivalent

specification for AlSi10Mg (the principal LPBF aluminium for PocketQubes); this gap is filled by manufacturer-specific datasheets (EOS, SLM Solutions, and 3D Systems) and, in ECSS context, by the ESA AlSi10Mg test campaigns archived in the ECSS-E-HB-32-20 update programme [116,117].

7.3.2. ISO/ASTM 52900: Terminology and General Principles

ISO/ASTM 52900—most recently revised in 2021—defines the canonical seven-category AM process taxonomy (binder jetting, directed energy deposition, material extrusion, material jetting, powder bed fusion, sheet lamination, and vat photopolymerisation) used throughout this paper and adopted by both NASA and ECSS [121,124]. The standard is universally cited by every downstream AM specification and is, in essence, the "Rosetta stone" of the AM standards landscape.

7.4. Gap Analysis: Where Current Standards Fail to Address AM-Specific PocketQube Needs

Despite the maturity of the standards landscape for AM aerospace structures in general, four critical gaps remain when the framework is mapped onto the PocketQube envelope, summarised in Table 19.

Table 19. Gap analysis between current AM standards and PocketQube-class requirements (according to the framework of [112–123] and the practitioner experience documented in [45,52,117]).

Gap	Standards Landscape	PocketQube-Class Need	Implication
Small-batch MAG	NASA-STD-6030: 30 specimens/condition (Class A); ECSS-Q-ST-70-80C: 6 specimens $\times$ 3 orientations $\times$ 3 campaigns	1–6 flight parts total per programme	Coupon overhead 5–30$\times$ production volume $\rightarrow$ cost-prohibitive
PocketQube-scale standardisation	All AM standards developed for $\geq$100 mm part envelope; tolerance and roughness allowances scale linearly	PQ-MEPS $\pm$0.1 mm tolerance, $Ra \leq 6$ µm mating faces	Off-the-shelf tailoring under-conservative for picosatellites
Polymer AM standardisation	All metallic-AM coverage; polymer AM addressed only in non-binding handbooks	PocketQube structures dominated by PEEK, ULTEM, and PA-CF (Section 5)	No standardised qualification path for polymer primary structure
Lattice/TPMS qualification	No standards for cellular AM structures; verification is per-design FEA + drop test	TPMS-lattice shock-attenuation interfaces routine in PocketQubes (Section 4 (Section 4.3.2))	Each design requires bespoke verification campaign

7.5. Qualification Roadmap: From TRL 3 to TRL 6 for AM PocketQube Structures

The NASA/ESA technology readiness level (TRL) framework spans 1–9, with the gating transitions:

- TRLs 1–3: research; analytical formulation; and concept validation in laboratory environment.
- TRLs 4–5: component validation in laboratory and relevant environment.
- TRL 6: system/subsystem demonstration in relevant environment (typically thermal vacuum + vibration).
- TRL 7–9: flight demonstration; flight qualification; and flight-proven through successful operations.

Figure 12 consolidates the AM-specific verification milestones that, according to ECSS-Q-ST-70-80C [114] and NASA-STD-6030 [115], must be passed for an AM PocketQube structural component to advance between TRL gates. The figure is the central qualification-planning artefact recommended for inclusion in every PocketQube programme's Materials and Process Qualification Plan (MPQP).

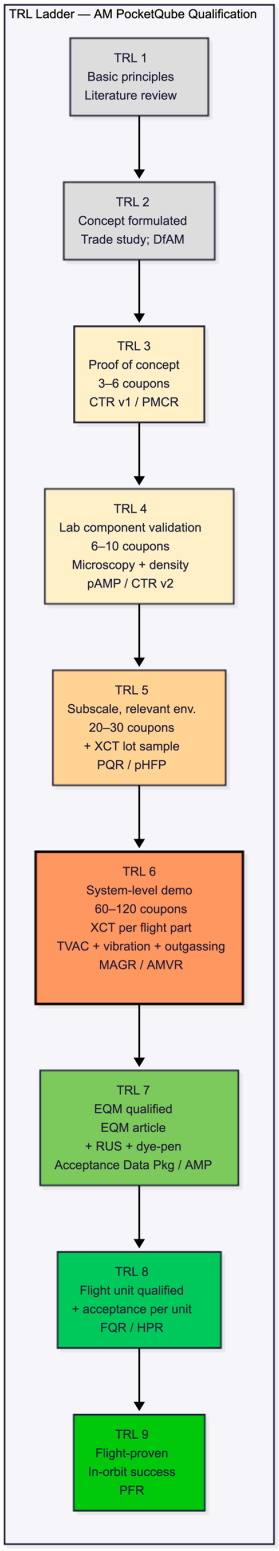


Figure 12. TRL ladder for AM PocketQube structures, mapping NASA-STD-6030 [115] and ECSS-Q-ST-70-80C [114] verification milestones to TRL 1–9. The figure consolidates: TRL 1–2 (analytical formulation and AM-process selection); TRL 3 (laboratory coupon production and density and tensile characterisation); TRL 4 (representative geometry production, dimensional metrology, and microstructural verification); TRL 5 (subscale article production, full mechanical-property database for B-basis allowables, and NDE per Section 6.3); TRL 6 (system-level qualification—thermal vacuum + sine burst + random vibration per ECSS-E-ST-10-03C and outgassing per ECSS-Q-ST-70-02C); TRL 7 (flight-representative model—Engineering Model or Engineering Qualification Model); TRL 8 (flight unit and qualification campaign complete); TRL 9 (in-orbit successful operations).

The roadmap from TRL 3 (where most academic PocketQube AM efforts currently sit) to TRL 6 (the minimum threshold for flight qualification on a commercial rideshare) is summarised in Table 20: at each TRL gate, the cumulative coupon-test count, NDE acceptance criteria, and documentation requirements are listed. For a typical 1P AlSi10Mg structural frame, the cumulative coupon count from TRL 3 to TRL 6 is 60–120 specimens, an investment of €15,000–40,000 in test-coupon production and characterisation, exclusive of the flight-article cost itself [125,126].

Table 20. Cumulative qualification-test requirements per TRL gate for an AM PocketQube structural frame (derived from [114,115,118,119]).

TRL Gate	Cumulative Coupons	Mandatory NDE	Documentation Deliverable
TRL 3 → 4	6–10	Microscopy, density (Archimedes)	Coupon Test Report (CTR)—preliminary
TRL 4 → 5	20–30	+ XCT (lot sample)	CTR + Process Qualification Record (PQR)—draft
TRL 5 → 6	60–120	+ XCT (every flight part), RUS	CTR + PQR + Material Allowables Generation Report (MAGR)
TRL 6 → 7	+ flight-representative article qualification	+ acceptance NDE per flight unit	MPQP + Flight Acceptance Test Report (FATR)
TRL 7 → 8	+ acceptance + workmanship	+ per-part build certificate	Flight Qualification Report (FQR)
TRL 8 → 9	(in-flight operation)	—	Post-Flight Report (PFR)

7.6. Structural Margins and Factor of Safety Under ECSS vs. NASA Methodologies

The structural-margin philosophies of the European (ECSS-E-ST-32-10C Rev. 2) and US (NASA-STD-5001B) [113,124] frameworks share a deterministic load × factor approach but differ in their numerical prescriptions, particularly for AM materials [124,125]. According to Table 21, the prescribed Design Factors (FoS) for limit-load × FoS verification differ by 5–15% between the two frameworks for metallic structural primary parts, with NASA generally prescribing higher numerical margins for materials lacking an A- or B-basis allowable.

Table 21. Factor-of-Safety comparison: ECSS-E-ST-32-10C Rev. 2 [124] vs. NASA-STD-5001B with Change 3 [125] for primary-structure metallic parts at PocketQube class.

Verification	ECSS-E-ST-32-10C Rev. 2	NASA-STD-5001B Change 3	Comment
Yield FoS (limit load × FoS_Y ≤ Yield)	1.10 (qualified materials)/ 1.25 (non-qualified)	1.25 (qualified)/ 1.40 (non-qualified)	NASA more conservative
Ultimate FoS (limit load × FoS_U ≤ UTS)	1.25 (qualified)/1.40 (non-qualified)	1.40 (qualified)/ 1.50 (non-qualified)	NASA more conservative
Buckling FoS	1.25 (linear)/1.40 (non-linear)	1.40/1.50	NASA more conservative
Joints FoS (preloaded fasteners)	1.25 (separation)	1.40 (separation)	NASA more conservative
Composite materials	× 1.25 add'l knockdown	× 1.50 add'l knockdown	NASA more conservative
AM-specific knockdown	1.15 (per ECSS-Q-ST-70-80C until material is "qualified")	1.20 (per NASA-STD-6030 until B-basis is established)	Comparable

For a PocketQube programme targeting both NASA and ECSS qualification (a common pragmatic scenario for international rideshare), the *binding margin* is the maximum of the two prescriptions per failure mode. The practical effect is to drive the design FoS to NASA values throughout, with the ECSS-specific AM knockdown applied additively if the material is not yet "qualified" per ECSS-Q-ST-70-80C. For LPBF AlSi10Mg, the combined effective FoS (limit-to-yield) at 2026 standards is $1.25 \times 1.20 \approx 1.50$, a 50% margin above limit yield load, a non-trivial mass penalty that further compresses the already-tight PocketQube mass budget (Section 3 (Section 3.3)) [114,115,124,125]. This is seen in Figure 13.

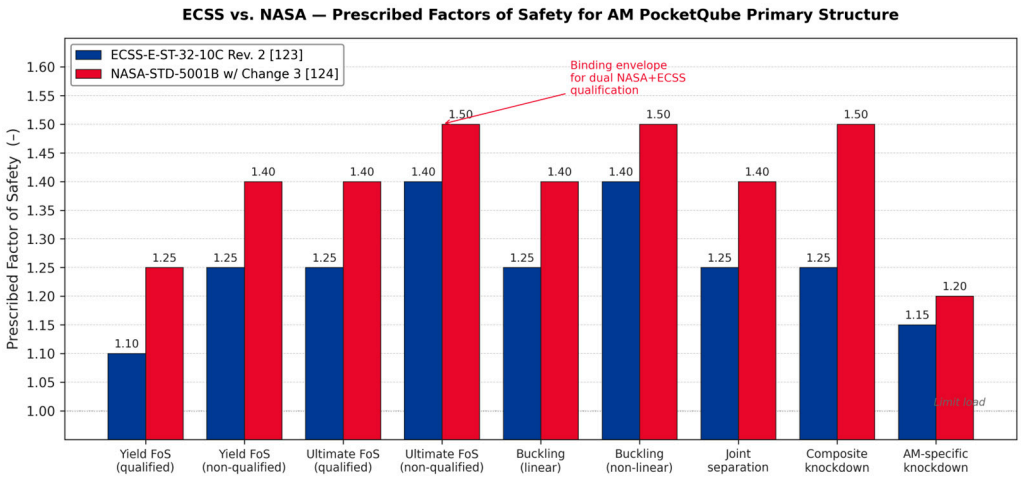


Figure 13. Bar-chart comparison of ECSS vs. NASA prescribed Factors of Safety for primary-structure verification of AM PocketQube parts, decomposed by failure mode (yield, ultimate, buckling, and joint separation). Data per ECSS-E-ST-32-10C Rev 2 [124] and NASA-STD-5001B Change 3 [125].

The bottom-line programmatic implication for the PocketQube programme manager (consistent with the workspace architecture of Section 3) is that the Materials and Process Qualification Plan (MPQP) must be authored before PDR, signed off by the Chief Engineer at PDR, and updated through CDR, TRR, and FRR. Failure to plan the qualification chain at PDR is the single most-documented schedule driver in academic and small-commercial PocketQube programmes that target NASA or ESA rideshare opportunities [115,117,127,128].

8. Heritage Missions and Case Studies

The transition of additive manufacturing from research demonstrator to flight-qualified production process in the small-satellite class is best illustrated by examining the heritage missions that have either employed AM primary structures or have generated documented flight data on AM components. This Section consolidates the PocketQube and CubeSat AM heritage from 2017 to 2026, the commercial-provider landscape that supports it, and a comparative database of AM small-satellite bus designs available in the open literature [97,129].

8.1. PocketQube Missions Employing Non-Standard Manufacturing

The PocketQube community has, since the inaugural Eagle-1/Eagle-2/QubeScout/T-LogoQube cluster of November 2013, accumulated 109 orbital missions (as of April 2026) [13,45,130], the overwhelming majority of which employ either machined aluminium 6061 primary structures or layered FR4-PCB stack-based architectures with no monolithic structural body [45,126,131]. The fraction of PocketQubes employing genuinely additively manufactured primary structures remains, as of 2026, a single-digit percentage of the orbital population, with the headline cases summarised in Table 22.

Table 22. PocketQube missions employing AM-derived structural elements (according to published mission documentation and flight records, [45,52,59,97,126–130,132]).

Mission	Operator	Config.	Launch	AM Element	Process/Material	Status
TuPOD	GAUSS Srl/Morehead St.	3U-like dispenser	Jan 2017 (HTV-6/ISS)	Full structural body (deployer)	SLS/Windform XT 2.0	Operated 4 d, re-entered
Unicorn-2 (various)	Alba Orbital	3P	2021–2024 (multiple)	Deployable solar panel hinges, antenna feedhorns	SLS/Windform XT 2.0	Flying

Table 22. *Cont.*

Mission	Operator	Config.	Launch	AM Element	Process/Material	Status
GENESIS-N/GENESIS-L	AMSAT-EA	1P	Jul 2022 (Vega VV21)	Selected internal brackets	FDM/PETG-CF	Operated
AlbaPod v2 (deployer)	Alba Orbital	up to 6P	2019–2026 (8+ missions)	Full structural shell, ejection mechanism	SLS/Windform XT 2.0	Flight proven
POQUITO	Univ. Luxembourg	1P	scheduled 2025–26	PCB-integrated structural rails	FDM-prototype/ aluminium-machined flight	Awaiting launch
Delfi-PQ	TU Delft	3P	Jan 2022	Internal mounting brackets (FDM)	FDM/ABS	Operated 2 y
Various university 1P	Multiple	1P	2021–2026	Full structural frames (ground demonstrators only)	FDM/PLA, PETG	Ground demonstrators

The pattern is unambiguous: at the PocketQube scale, AM has been adopted earlier and more widely for the deployer (a non-flight element) than for the satellite itself [59,126]. The AlbaPod v2 deployer, manufactured by CRP Technology in Windform XT 2.0, is by some margin the most flight-experienced AM small-satellite structural element in the PocketQube ecosystem, with eight successful missions and 41+ satellites deployed by 2024 [59]. By contrast, no PocketQube has yet flown a fully additively manufactured metallic primary structure as of the time of writing: the closest cases (Unicorn-2's hinge assemblies and GENESIS internal brackets) employ AM only for selected components within an otherwise machined or PCB-stack-based primary structure [133,134].

8.2. WASEDA-SAT-ZERO: First Fully 3D-Printed Metal-Frame Satellite—Lessons Learned

WASEDA-SAT-ZERO was a 1U-class CubeSat developed by Waseda University (Tokyo, Japan) as a technology demonstrator for fully metal-additively manufactured satellite structures [126]. Its design philosophy embodied three explicit zero-targets: (i) zero fixing screws; (ii) zero mechanical sub-assemblies; (iii) zero deployable debris generated by the structure. All three targets were addressed by monolithic AM: the entire chassis, including external faces, internal lattice ribs, mounting bosses, and harness routing channels, was printed as a single part in metal LPBF, with the internal volume retained as a triply periodic minimal surface lattice for mass reduction (Section 4 (Section 4.3.2)) [126].

According to Figure 14, the WASEDA-SAT-ZERO chassis exemplifies the consolidation philosophy advanced by the Boschetto PEEK nanosat study [70] but extended to the metal-LPBF regime: a 12-part conventional 1U CubeSat chassis assembly was replaced by a single-piece monolithic AM print, with all four CubeSat-standard rail-interfaces, the upper and lower interface plates, and the side-panel mounts integrated into a single FEM-validated topology-optimised geometry [126].

WASEDA-SAT-ZERO was launched on 12 October 2022 aboard JAXA's Epsilon-6 from the Uchinoura Space Center as one of eight payloads on the Innovative Satellite Technology Demonstration-3 (RAISE-3) mission. A second-stage attitude-control failure about 6 min after liftoff led to vehicle destruction before second-stage burnout, resulting in the loss of all payloads, including WASEDA-SAT-ZERO, without reaching orbit [126]. Consequently, no in-orbit structural performance data were recovered. However, programme documentation and the JAXA failure investigation identified several engineering lessons: (i) AM build-quality variability required three engineering models before the flight article met rail-interface tolerances [126]; (ii) monolithic AM eliminated assembly-related failures (e.g., loose fasteners and plate misalignment) but reduced design flexibility; (iii) internal lattice structures require drainage paths because trapped powder cannot be removed from sealed cavities, constraining the DfAM workflow (Section 4 (Section 4.3.3)) [70,126]; and

(iv) a reflight model, WASEDA-SAT-ZERO-II, was approved and, as of 2026, is planned for a future JAXA SS-520 or NEXT mission with an expanded deployable-membrane payload [126].

For PocketQube programmes, this case study demonstrates that monolithic metal AM is technically feasible and potentially scalable from 1U to 1P, but its cost and qualification burden make industrial partnership essential for academic missions, consistent with the Section 7 (Section 7.4) gap analysis.

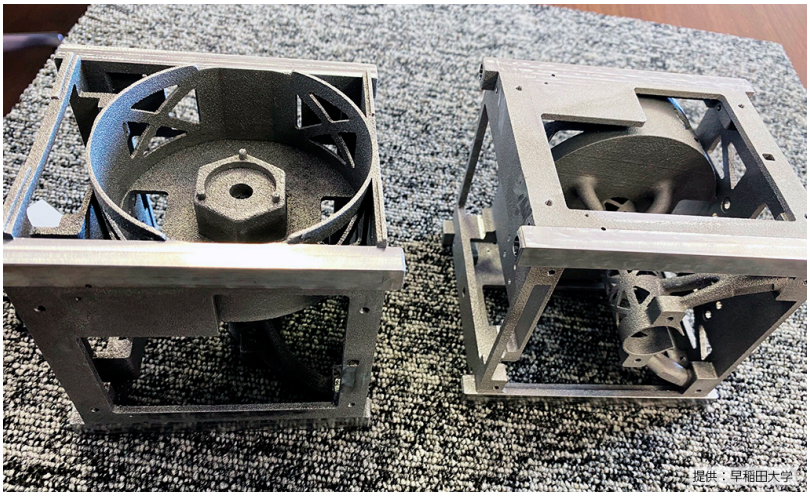


Figure 14. WASEDA-SAT-ZERO. Adapted from: [126].

8.3. CubeSat AM Heritage Applicable to PocketQube Scale

CubeSat-class missions provide a richer AM heritage dataset, with multiple successful in-orbit operations dating back to 2017 [59,97,127–129,132]. The flight-experienced cases summarised below establish the AM design philosophies most directly portable to the PocketQube envelope.

1. TuPOD (2017)—Tubesat-Pod, a 3U-CubeSat-class dispenser developed by GAUSS Srl (Italy) and Morehead State University (USA), launched aboard the H-IIB/KOUNOTORI-6 cargo mission to the ISS in December 2016 and deployed from the ISS Kibō module on 16 December 2016 [127]. TuPOD's entire structural body—including the rail interfaces, the deployment door mechanism, and the internal TubeSat pusher—was 3D printed in Windform XT 2.0 by CRP USA. After ejection, TuPOD operated autonomously for approximately 83 h, deploying its two on-board TubeSats (TANCREDO-1 and OSNSAT) before transmitting a Morse-code beacon at 437.425 MHz for four days until primary-battery depletion, after which it re-entered Earth's atmosphere as planned [127]. TuPOD is widely cited as the first fully 3D-printed satellite to reach orbit and remains, in 2026, the canonical proof of concept for polymer-AM small-satellite primary structures.
2. KySat-2 (2013, first flight) and OreSat0 (2021)—Both employ Windform-LX-3.0/Windform-XT-2.0 3D-printed structural components within larger machined-aluminium bus designs [128]. OreSat0, the Portland State Aerospace Society's 1U CubeSat launched on the Firefly Alpha "DREAM" mission in October 2022 and successfully deployed, carries 3D-printed turnstile antenna assemblies, star-tracker camera lens and sensor mounts, and a battery-assembly cradle, all in Windform LX 3.0 by CRP USA [128]. After more than three years of in-orbit operation, OreSat0's AM components have demonstrated no documented structural or outgassing failures, establishing the longest in-orbit operational dataset for polymer-AM CubeSat hardware.

3. AMCUBE/Orion AM (2020–2025)—Orion AM (formerly Roboze, Brescia, Italy) developed the AMCUBE concept demonstrator: a 1U CubeSat with a primary structural frame manufactured fully by FDM in PEEK [70,97]. The structural frame achieved a measured mass of 96 g (vs. 165–180 g for an equivalent machined-aluminium frame), an outgassing performance of TML = 0.11%, CVCM < 0.01% (compliant with ECSS-Q-ST-70-02C [76]), and survived the standard CubeSat qualification campaign (random vibration 14 Grms per axis, thermal-vacuum −20 °C to +60 °C) at TRL 7 in laboratory demonstration [70]. AMCUBE has not yet flown but represents the highest TRL among polymer-AM CubeSat primary-structure designs.
4. Sciperio/nScrypt CubeSats for the US Space Force (2023+)—Sciperio, the engineering services arm of nScrypt (Orlando, Florida), was awarded a US Space Force SBIR Phase II contract in February 2023 to additively manufacture 6U CubeSats for tactical military space applications, with multi-material printing of conductive (silver) and structural (Ultem-equivalent polymer) materials in a single build [132]. The programme is, as of 2026, at TRL 5–6 with ground-test articles delivered; flight demonstration is anticipated in the 2026–2027 horizon.
5. Princeton TigerSats (2018+)—Princeton University's TigerSats team developed and ground-qualified a fully 3D-printed 1U CubeSat structural bus using nTopology-generated lattice infill within an SLS-printed nylon frame, demonstrating 35% mass reduction relative to a solid-walled equivalent and providing the open-source DfAM blueprint subsequently adopted by multiple academic small-satellite teams worldwide [130].

8.4. Commercial Providers of AM Small-Satellite Structures: State of the Industry

The commercial AM-for-spaceflight industry, as of 2026, is organised into three tiers:

1. Tier 1—Specialist AM service bureaux with documented flight heritage. This tier comprises a small number of providers with publicly documented in-orbit flight references on small-satellite hardware:
    - CRP Technology/CRP USA (Modena, Italy/Mooresville, NC, USA) is the dominant provider of polymer-AM small-satellite primary structures, with the Windform® XT 2.0, LX 3.0, and SP family of carbon-fibre-reinforced polyamides. CRP's flight portfolio includes TuPOD (2017), KySat-2 (2013), OreSat0 (2022), and the AlbaPod v1/v2 deployer family (2019–2026) [59,127,128,130]. Windform XT 2.0 carries NASA and ESA outgassing certification per ECSS-Q-ST-70-02C [59,76].
    - EOS GmbH (Krailling, Germany) is the primary supplier of LPBF equipment; through its Additive Minds consultancy and EOS Innovation Centers, EOS provides direct AM service for aerospace structural parts. Their flight portfolio (small-satellite) includes selected aluminium and titanium brackets on multiple ESA-supported CubeSat missions [133].
    - GE Additive Aerospace (Cincinnati, OH, USA) is primarily known for large-volume LPBF for jet-engine and rocket-engine components, GE Additive's flight references at the small-satellite scale are limited but include selected Inconel propulsion mounts on US Government missions (2022+) [134].
2. Tier 2—Generalist AM bureaux with documented spaceflight references, including Materialise (Leuven, Belgium), 3D Systems (Rock Hill, SC, USA), Stratasys Direct (Eden Prairie, MN, USA), Carpenter Additive (Athens, AL, USA), and Velo3D (Campbell, CA, USA). These providers have demonstrated spaceflight materials and processes but typically deliver parts as standard-product offerings rather than mission-specific structural design partnership [133].

3. Tier 3—University, government-lab, and start-up makers, including Princeton University TigerSats, NanoAvionics (Vilnius, Lithuania), Orion AM (Brescia, Italy), Sciperio/nScrypt (Orlando, FL, USA), and others. These providers operate primarily at TRL 4–7 and are the dominant suppliers for academic and demonstration-class PocketQube and CubeSat missions [97,129,130,132].

For PocketQube programme managers, the practical guidance summarised in Table 23 below applies:

Table 23. Commercial AM provider selection guide for PocketQube-class structural parts (according to commercial portfolios documented in [59,97,129–134] as of 2026).

Use Case	Recommended Tier	Representative Providers	Typical Lead Time	Indicative Unit Cost (1P Frame)
Flight primary structure (polymer)	Tier 1	CRP Technology/CRP USA	6–10 weeks	€1200–2500
Flight primary structure (metallic)	Tier 1	EOS Additive Minds, Materialise Aerospace	8–14 weeks	€800–1600
Flight secondary brackets	Tier 1–2	CRP, Materialise, 3D Systems	4–8 weeks	€150–600
Engineering-model/ground-test article	Tier 2–3	Local service bureau or in-house	1–3 weeks	€40–250
Academic/demonstration class	Tier 3/in-house	University FDM, in-house SLS	<1 week	€15–80

8.5. Comparative Table: AM Bus Designs in the Literature

Table 24 below is the comparative central database of AM small-satellite bus designs available in the open literature as of May 2026. Twelve heritage cases are tabulated against eight design and qualification parameters, providing the comprehensive reference dataset that any new PocketQube AM programme should consult during the trade-study phase (Section 7 (Section 7.5), TRL 2–3 entry criteria).

Table 24. Comparative database of additively manufactured small-satellite bus designs documented in the open literature, 2016–2026. (Mass values are flight-article structural mass only, excluding electronics and payload.) Sources per row indicated.

Mission/Case	Class	AM Scope	Process	Material	Structural Mass (g)	Mass Saving vs. Machined Al	TRL Achieved	Ref.
TuPOD	3U dispenser	Full structural body	SLS	Windform XT 2.0	250	~45%	9 (flown)	[127]
KySat-2	1U	Selected brackets + antenna	SLS	Windform LX 3.0	n/a (component)	~30%	9 (flown)	[128]
OreSat0	1U	Antenna, star-tracker, battery cradle	SLS	Windform LX 3.0	n/a (components)	~40%	9 (flown)	[128]
WASEDA-SAT-ZERO	1U	Full monolithic frame + lattice	Metal LPBF	Al alloy (proprietary)	~105	~35%	7 (lost on launch)	[126]
AMCUBE/Orion AM	1U	Full structural frame	FDM	PEEK	96	~47%	7 (lab qualified)	[70,97]
Princeton TigerSats 1U	1U	Full structural bus + lattice infill	SLS	PA-12 nylon	~180	~35%	5 (ground tested)	[130]
AlbaPod v2 (deployer)	6P deployer	Full shell + ejection mechanism	SLS	Windform XT 2.0	<500	~60%	9 (flown)	[59]
Unicorn-2 (Alba Orbital)	3P PocketQube	Solar panel hinges, antenna feedhorns	SLS	Windform XT 2.0	n/a (components)	~30%	9 (flown)	[45]
GENESIS-N/GENESIS-L	1P PocketQube	Selected internal brackets	FDM	PETG-CF	n/a (components)	~25%	9 (flown)	[129]
Sciperio USSF 6U	6U	Full bus + embedded conductors	Multi-material FDM	Ultem + Ag	n/a (in development)	~30% (projected)	5–6	[132]
Boschetto PEEK 3U nanosat	3U	Full structural frame	FDM	PEEK	n/a (lab)	~53%	7 (lab qualified)	[70]
Delfi-PQ internal brackets	3P PocketQube	Internal mounting	FDM	ABS	n/a (component)	~20%	9 (flown)	[48,50]

Three patterns emerge from the comparative database:

1. No fully metallic, in-orbit-proven AM PocketQube primary structure exists as of May 2026. The single attempt (WASEDA-SAT-ZERO) was a 1U CubeSat and was lost on the launch vehicle. The closest PocketQube heritage is the Unicorn-2 platform's metal-machined frame with AM hinges and feedhorns.
2. Polymer SLS (Windform family) is the most flight-proven AM route for small-satellite structures, with TuPOD, KySat-2, OreSat0, AlbaPod v2, Unicorn-2, and others demonstrating cumulative $\geq$ 50 spacecraft-years of in-orbit operation.
3. The mass-saving range of 25–60% is reproducibly achieved across AM routes when compared to equivalent machined-aluminium baselines, with the upper end (60%) typically restricted to deployer-class hardware where the geometric complexity makes machined aluminium particularly inefficient [59].

The implication for the PocketQube programme manager (consistent with the Sections on materials, defects, normative framework, and workspace architecture) is unambiguous: as of 2026, the *recommended* AM route for a flight-qualifiable PocketQube structural frame is SLS with carbon-fibre-reinforced polyamide (Windform XT 2.0), sourced from CRP Technology, with FDM-PEEK (Orion AM) as the principal alternative for cost-constrained programmes. Metallic-AM (LPBF AlSi10Mg, Scalmalloy, or Ti-6Al-4V) is justified only for niche structural elements—fastener interfaces, deployment brackets, and propulsion mounts—where the polymer thermal envelope or strength is insufficient. This recommendation is consistent across the technical (Sections 4–6), normative (Section 7), and heritage-based (this Section) lines of evidence.

8.6. End-to-End Worked Example: Reference Workflow for a 1P LPBF AlSi10Mg Frame

No metallic AM PocketQube primary structure has flown (Section 8.5), and the literature offers no single reference traversing the complete design-to-qualification chain at the 1P scale. This section closes that gap with a prescriptive worked example constructed by the authors from the evidence of Sections 3–7, intended as a planning template for ground-demonstrator programmes (TRL 3–4, Figure 12).

The requirements derive from Section 3 and Table 8: the 50 $\times$ 50 $\times$ 50 mm envelope with $\pm$ 0.1 mm mating tolerance [43,44]; a 35–45 g structural mass target ($\leq$75 g budget, Section 3.3, calibrated by Table 7); CoM within 10 mm of centre; the Table 8 load environment; ECSS-Q-ST-70-02C outgassing [76]; and, for dual NASA/ESA eligibility with a not-yet-qualified AM material, the 1.50 effective factor of safety of Section 7.6. Excluding the polymer routes of Section 8.5—the example targets the metallic gap of Section 9.1—the trade of Tables 10 and 12 selects AlSi10Mg (TRL 9 maturity, richest defect/fatigue dataset, ECSS-compliant as-built outgassing per Table 15, €400–900 per frame), with Scalmalloy® deferred to the flight-model phase on cost and Ti-6Al-4V excluded on density.

The design follows the five-step workflow of Section 4.3.1: keep-out-dominated domain (Section 3.5), Table 8 loads $\times$ 1.50, SIMP optimisation at 0.8 mm minimum length scale (2$\times$ process resolution) with build direction along the principal load path (Section 5.6), reconstruction with drainage holes in every closed cavity (Sections 4.3.3 and 8.2, lesson 3), and verification FEA against the 230 MPa as-built yield floor (Table 12), with an expected mass reduction at the conservative end (25–40%) of the 30–60% corpus envelope [20,21,25]. The build applies Table 11 without deviation, traceable via build certificate (Sections 7.1.5 and 7.2.1); post-processing follows the Section 4.4 chain with HIP deferred to the TRL 5 gate (Section 6.2, Table 20) and mating faces machined to $\pm$ 0.05 mm; and first-article acceptance is by XCT against the Section 6.3.1 thresholds (porosity $\leq$ 0.3%; no LoF > 200 µm), with resonance ultrasound (Table 14) as the per-part screen.

9. Open Challenges, Research Gaps, and Future Directions

Despite the converging maturity of AM for small-satellite primary structures consolidated in Sections 4–8, five thematic fronts remain unresolved at the picosatellite-class boundary. This Section consolidates the open research questions, mapping the residual gap between the current state of the art (TRLs 5–7 for most polymer routes; TRLs 4–6 for the metallic routes) and the TRL 9 demanded by a flight-qualifiable monolithic AM PocketQube primary structure.

9.1. Printability of High-Strength Alloys at Sub-50 mm Scale

The 50 × 50 × 50 mm PocketQube envelope places feature sizes near the practical limit of laser powder bed fusion (LPBF). Recent studies report reproducible AlSi10Mg wall thicknesses of 0.3–0.8 mm, with sub-100 µm features achievable only under specialised process parameters [97,128]. Scalmalloy® (Al-Mg-Sc-Zr) increases ultimate tensile strength from 349–350 MPa in the as-built condition to 512–521 MPa after direct ageing at 325 °C for 4 h [126,132], making it the leading candidate for monolithic AM PocketQube primary structures on a strength-to-density basis [127]. The principal challenges (Table 25) remain: (i) anisotropic microstructures in thin walls [128]; (ii) residual-stress-induced distortion at the sub-millimetre scale [129]; and (iii) dimensional accuracy at rail interfaces requiring ±50 µm tolerances under the PocketQube Standard [45]. The ANN-CFD model of [129] and the surface-integrity methodology of [132] define the immediate research priorities.

Table 25. Consolidated open research questions, current TRL and projected 2030 TRL by thematic front (original construction by the authors).

Front	Open Question	Current TRL (2026)	Projected TRL (2030)	Anchor Refs.
9.1 Printability	Minimum reproducible wall ≤ 0.3 mm in Scalmalloy® for monolithic 1P frame	5	7	[126,127,129,132]
9.2 Standardisation	Picosatellite-tailored ECSS/NASA route for ≤100 g parts	4	6	[114,130,131,133,134]
9.3 MMAM/FGM	Interface metallurgy qualification for metal–polymer hybrid PocketQubes	4	6	[97,127–129,132]
9.4 ISM	Closed-loop polymer feedstock recycled in LEO	5	7	[130,131,133]
9.5 ML/DT	Quality-centric digital twin for ≤50 g part certification loop	5	8	[97,125–128]

9.2. Standardisation Gaps for AM PocketQube Qualification

The standards reviewed in Section 7 (ECSS-Q-ST-70-80C [114] and NASA-STD-6030 [115]) were developed for launcher- and spacecraft-class hardware, and their disproportionate burden for 50 g PocketQube components are noted in Section 7.4. Three additional gaps identified in the 2024–2026 revisions are summarised in Table 26. First, ISO/ASTM 52904:2024 formalises performance categories for critical PBF applications but provides no tailored pathway for sub-100 g flight hardware [130]. Second, EN ISO/ASTM 52948:2026 establishes a unified defect classification for metal PBF, although its acceptance criteria remain based on launcher-class structures [123]. Third, recent NASA position papers acknowledge that NASA-STD-6030 lacks a dedicated implementation route for small satellites, instead recommending mission-specific tailoring agreements that are impractical for academic PocketQube programmes [133,134]. Consequently, a PocketQube-specific ECSS technical memorandum remains the most impactful normative priority as of 2026 [126].

Table 26. Identified standardisation gaps and proposed normative responses (original construction by the authors from [114,115,122–126]).

Standard	Current Scope	Gap for PocketQubes	Proposed Action by 2028
ECSS-Q-ST-70-80C [114]	Metallic PBF, launcher class	No de-rated route $\leq$ 100 g	New Technical Memorandum (ECSS-Q-TM-70-80C-S)
ISO/ASTM 52904:2024 [130]	Critical-application PBF	No small-part performance category	Add Category D—"Sub-100 g PBF"
EN ISO/ASTM 52948:2026 [131]	PBF imperfection classification	Thresholds calibrated to $\geq$1 mm walls	Sub-millimetre acceptance schedule
NASA-STD-6030 [115,133,134]	Spaceflight AM general	No picosatellite tailoring template	Annex H—Picosatellite tailoring

9.3. Multi-Material and Functionally Graded Structures

The next decade is expected to be driven by the transition from mono-material to multi-material additive manufacturing (MMAM) and from homogeneous to functionally graded materials (FGMs) [127,128]. For PocketQubes, the most relevant configurations include: (i) metal–polymer hybrid structures combining LPBF aluminium rail interfaces with FDM polymer internal sections [132]; (ii) embedded conductors printed within the structure, eliminating wiring harnesses [129]; and (iii) graded-density lattice cores with dense outer skins and porous lightweight interiors [97]. The principal challenge is qualification rather than manufacturing, as no current ECSS or NASA standard addresses the interface metallurgy of multi-material components [127,128]. The current state of the art is reviewed in recent studies [97,127,128,132], and a representative FGM PocketQube concept is presented in Figure 15.

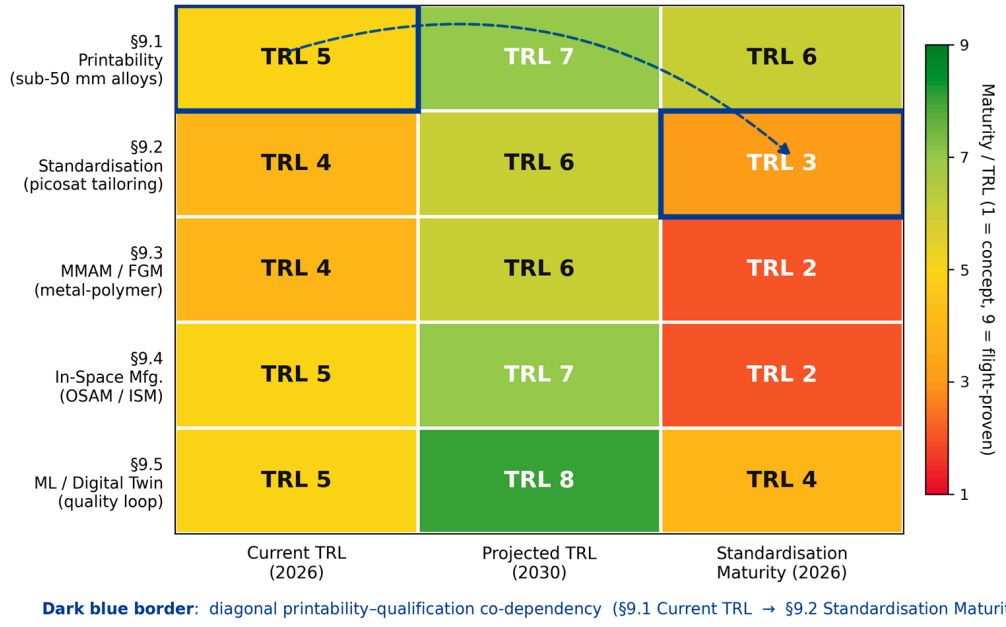


Figure 15. Heat map of open research challenges across the five thematic fronts of Sections 9.1–9.5, plotted against current TRL (2026), projected TRL (2030), and standardisation maturity. The diagonal density gradient highlights the printability–qualification co-dependency. Original-figure construction by the authors integrating [97,114,115,126–128].

9.4. In-Space Manufacturing: Long-Term Relevance for PocketQube Evolution

The cancellation of NASA's OSAM-1 (2024) and conclusion of OSAM-2/Archinaut One (2023) without flight demonstration [131,133] re-positions the in-space manufacturing

(ISM) roadmap further out than was projected by the 2019 NASA In-Space Manufacturing programme briefings. Nevertheless, the 2025 comprehensive review of inspection, manufacturing, and repair for OSAM confirms that the underlying technology base (Redwire ESAMM, Tethers Unlimited Refabricator) has reached TRL 6 on the ground and TRL 5 in the relevant environment. For PocketQubes specifically, the practical implication of an ISM-mature future is the deployable-from-ISM PocketQube: a satellite printed in low-Earth orbit from recyclable polymer feedstock and released on demand. As seen in Table 25, the research priority is the closed-loop polymer feedstock qualification, not the printer itself [123,133].

9.5. Machine Learning for AM Process Optimisation in Space Structures

Machine learning (ML) and digital-twin (DT) approaches have shifted from research prototypes to production tools between 2023 and 2026, with publication volume rising from 1 to 54 papers per annum [134]. For PocketQube-scale parts, the most consequential developments are (i) physics-guided deep generative models for melt-pool morphology, achieving < 11% temperature-prediction error [127]; (ii) data-efficient sequential-learning frameworks that maintain > 95% defect-classification accuracy with < 200 training images [128]; and (iii) super-resolution melt-pool reconstruction enabling defect localisation at the 30 µm pixel level [97]. Quality-centric digital twins, as reviewed in [125,126], are the consolidating architecture: real-time fusion of melt-pool emissivity, layer-wise X-ray computed tomography, and ex-post-mechanical testing closes the certification loop.

10. Conclusions

This systematic review examined the state of the art of additive manufacturing (AM) for PocketQube-class structural systems, integrating evidence from materials science, manufacturing processes, design methodologies, qualification standards, and flight heritage between 2015 and 2026. The analysis demonstrates that additive manufacturing has evolved from a prototyping technology into a credible structural production route for ultra-small satellites, particularly where severe volumetric and mass constraints limit the effectiveness of conventional subtractive manufacturing.

The review confirms that PocketQubes constitute a distinct engineering class rather than merely a scaled-down CubeSat architecture. The combination of a 50 × 50 × 50 mm unit envelope, a 250 g mass ceiling, stringent deployer-interface tolerances, and highly constrained power and thermal budgets creates structural design requirements that differ fundamentally from those of larger small-satellite platforms. Beyond educational missions, PocketQubes are increasingly attractive for distributed satellite constellations, rapid technology demonstration, Internet-of-Things (IoT) connectivity, space-weather monitoring, and responsive space applications, where low manufacturing cost and rapid production cycles are essential. Within this context, additive manufacturing provides capabilities that are difficult or impossible to achieve through conventional machining, including topology-optimised geometries, integrated functional features, embedded routing channels, lattice structures, and monolithic assemblies capable of reducing part count while improving packaging efficiency.

Among currently available technologies, polymer-based selective laser sintering (SLS), particularly using carbon-fibre-reinforced polyamide systems such as Windform XT 2.0, represents the highest-maturity AM solution for PocketQube applications. Its extensive flight heritage through TuPOD, AlbaPod, and associated deployment systems demonstrates that additively manufactured polymer structures can successfully satisfy the environmental requirements of launch and low-Earth-orbit operation. Metallic AM technologies, particularly laser powder bed fusion (LPBF) using AlSi10Mg and Scalmalloy®, exhibit substantial

potential for future primary structural applications owing to their superior specific stiffness and mass-efficiency characteristics. However, challenges associated with residual stresses, dimensional repeatability, defect control, and qualification remain barriers to widespread orbital adoption.

A central finding of this review is that the technological maturity of additive manufacturing has progressed more rapidly than the regulatory frameworks intended to certify it. Existing standards, including ECSS-Q-ST-70-80C, NASA-STD-6030, ISO/ASTM 52904, and related qualification protocols, provide valuable guidance but were largely developed for larger spacecraft and launcher applications. Consequently, a significant qualification gap exists for picosatellite-class hardware, where structural dimensions, mass budgets, production volumes, and economic constraints differ substantially from those assumed by current standards. The absence of a dedicated PocketQube-tailored qualification methodology represents one of the most significant barriers to the broader adoption of flight-critical AM structures.

Future revisions should also benefit from ESA's Harmonisation process, through which ESA, industry, and national space agencies periodically establish common technological roadmaps and qualification priorities for emerging manufacturing technologies. Extending future harmonisation activities to explicitly address PocketQube-class additive manufacturing would represent an important step toward internationally consistent qualification practices.

The literature further demonstrates that DfAM, topology optimisation, lattice engineering, and functionally graded architectures are emerging as the principal drivers of structural innovation in the 2026–2030 timeframe. The convergence of these approaches with multi-material manufacturing, embedded electronics, and integrated thermal-management concepts suggests that future PocketQube platforms may evolve toward highly integrated multifunctional structures in which mechanical, thermal, electrical, and deployment functions are consolidated within a single manufactured component.

Despite substantial progress, important knowledge gaps remain. Experimental data on long-duration orbital performance of metallic AM PocketQube structures are scarce; statistically significant databases correlating process parameters, defects, and flight reliability are largely absent; and few studies currently address the combined effects of vibration, thermal cycling, radiation exposure, and atomic oxygen degradation on additively manufactured picosatellite hardware. Addressing these gaps will require coordinated efforts among academia, industry, standards organisations, and satellite operators.

From an engineering perspective, the evidence indicates that additive manufacturing should no longer be regarded merely as a manufacturing alternative but rather as a system-enabling technology for the next generation of ultra-small spacecraft. As access-to-space initiatives expand globally and emerging spacefaring nations seek cost-effective pathways to orbital capability, AM-enabled PocketQubes offer a credible route toward increased mission complexity, reduced development cycles, and enhanced structural efficiency.

Future research should therefore prioritise PocketQube-specific qualification methodologies, statistically validated process-control frameworks, in-orbit demonstration campaigns for metallic AM primary structures, and ECSS-compatible certification pathways tailored to picosatellite missions. These efforts should be complemented by future ESA Harmonisation activities and subsequent updates of ECSS and international AM standards to ensure that qualification procedures evolve alongside technological maturity. Progress in these areas will determine whether additive manufacturing transitions from a promising enabling technology to the dominant structural manufacturing paradigm for PocketQube-class spacecraft during the coming decade.

Author Contributions: Conceptualisation, S.V., C.A.N., J.E.O. and C.L.; methodology, S.V. and C.A.N.; software, S.V.; validation, S.V., C.A.N., J.E.O. and C.L.; formal analysis, S.V. and J.E.O.; investigation, S.V., C.A.N. and J.E.O.; resources, C.A.N., J.E.O. and C.L.; data curation, S.V.; writing—original draft preparation, S.V.; writing—review and editing, S.V., C.A.N., J.E.O. and C.L.; visualisation, S.V.; supervision, C.A.N. and J.E.O.; project administration, S.V.; funding acquisition, C.A.N. and J.E.O. All authors have read and agreed to the published version of the manuscript.

Funding: The authors gratefully acknowledge that the Fundación Universitaria Los Libertadores provided financial support by covering the article's publication processing fee.

Data Availability Statement: The data supporting the findings of this study are contained within the article. No new datasets were generated or analysed beyond those presented in this manuscript.

Acknowledgments: During the preparation of this manuscript, the authors used Grammarly (version 1.165.1.0, Grammarly Inc.) for language editing, grammar correction, spelling review, and improvement of writing clarity. The authors reviewed and edited all suggestions generated by the tool and take full responsibility for the content of this publication.

Conflicts of Interest: The authors declare no conflicts of interest.

Abbreviations

The following abbreviations are used in this manuscript:

AM	Additive Manufacturing
ASTM	American Society for Testing and Materials
CAD	Computer-Aided Design
CAGR	Compound Annual Growth Rate

References

1. Alba Orbital. The PocketQube Standard—Open-Source Community Specification. Available online: https://www.albaorbital.com/pocketqube-standard (accessed on 22 February 2026).
2. Twiggs, R.J.; Hodgart, M.S.; Buxton, S. The PocketQube Standard—Issue 1. *Open Community Specification*, 7 June 2018. [CrossRef]
3. icMercury. About PocketQube—History, Specifications and the Role of Morehead State University. Available online: https://icmercury.com/about-pocketqube/ (accessed on 23 February 2026).
4. PocketQube—Encyclopaedic Overview. Wikipedia. Available online: https://en.wikipedia.org/wiki/PocketQube (accessed on 23 February 2026).
5. The PQ60 Standard—PocketQube Mechanical & Electrical Interface Specification. pq60.info Community Standard. Available online: http://pq60.info/ (accessed on 23 February 2026).
6. ESA Connectivity & Secure Communications. *AlbaPod: The Most Advanced Space-Proven PocketQube Deployer*; European Space Agency: Paris, France, 2024.
7. Alba Orbital. Unicorn-2—3P PocketQube Platform Specification. Available online: https://www.albaorbital.com/unicorn-2 (accessed on 23 February 2026).
8. ESA eoPortal. Alba Orbital Unicorn PocketQubes—Mission Profile and Flight Heritage. Available online: https://www.ieoportal.org/satellite-missions/alba-orbital (accessed on 23 February 2026).
9. CRP Group. *Alba Cluster X—3D-Printed AlbaPod v2 Small-Satellite Deployer*; Industrial Case Study; CRP Technology s.r.l.: Modena, Italy, 2022. Available online: https://www.crp-group.com/news/alba-cluster-x-small-sat-3d-printed-deployer/ (accessed on 23 February 2026).
10. VoxelMatters. Alba Orbital's 3D-Printed PocketQube Deployer Achieves New Flight Milestone. *Industry News*. 2022. Available online: https://www.voxelmatters.com/alba-orbitals-printed-pocketqube-deployer-achieves-new-goal/ (accessed on 23 February 2026).
11. Grand View Research. Nanosatellite and Microsatellite Market—Size, Share & Trends Analysis Report, 2024–2030. Industry Report, 2024. Available online: https://www.grandviewresearch.com/industry-analysis/nanosatellite-microsatellite-market (accessed on 23 February 2026).
12. Mordor Intelligence. Small Satellite Market—Size, Share & Industry Outlook to 2030. Industry Report, 2024. Available online: https://www.mordorintelligence.com/industry-reports/small-satellite-market (accessed on 23 February 2026).

13. Expert Market Research. Small Satellite Market—Size, Share & Industry Trend Forecast to 2034. Industry Report, 2024. Available online: https://www.expertmarketresearch.com/reports/small-satellite-market (accessed on 23 February 2026).
14. BIS Research. Satellite Commercial Off-the-Shelf Compone\nts—Enabling Innovation in Space Technology. Industry Analysis, 2023. Available online: https://bisresearch.com/news/satellite-commercial-off-the-shelf-components-enabling-innovation-in-space-technology- (accessed on 23 February 2026).
15. Walsh, S.; Murphy, D.; Doyle, M.; Reilly, J.; Thompson, J.; Dunwoody, R.; Erkal, J.; Finneran, G.; Fontanesi, G.; Mangan, J.; et al. Development of the EIRSAT-1 CubeSat through Functional Verification of the Engineering Qualification Model. *Aerospace* **2021**, *8*, 254. [CrossRef]
16. *ECSS Standard ECSS-E-ST-10*; Space Engineering: System Engineering General Requirements. European Cooperation for Space Standardisation: Noordwijk, The Netherlands, 2009.
17. Straub, J.; Villela, T.; Costa, C.A.; Brandão, A.M.; Bueno, F.T.; Leonardi, R. Towards the Thousandth CubeSat: A Statistical Overview. *Int. J. Aerosp. Eng.* **2019**, *2019*, 5063145. [CrossRef]
18. Heidt, H.; Puig-Suari, J.; Moore, A.; Nakasuka, S.; Twiggs, R. CubeSat: A New Generation of Picosatellite for Education and Industry Low-Cost Space Experimentation. In Proceedings of the 14th Annual AIAA/USU Small Satellite Conference, Logan, UT, USA, 21–24 August 2000.
19. Murr, L.E.; Gaytan, S.M.; Ramirez, D.A.; Martinez, E.; Hernandez, J.; Amato, K.N.; Shindo, P.W.; Medina, F.R.; Wicker, R.B. Metal Fabrication by Additive Manufacturing Using Laser and Electron Beam Melting Technologies. *J. Mater. Sci. Technol.* **2012**, *28*, 1–14. [CrossRef]
20. Yang, S.; Zhao, Y.; Zhang, Y. Topology Optimization for Additive Manufacturing: A Review. *Machines* **2022**, *10*, 1042. [CrossRef]
21. Georgantzinos, S.K.; Papadopoulou, E.; Kostopoulos, G.; Voulgaris, S.; Tseni, A.; Bakalis, P.; Gkara, M.; Mitropoulou, C.C.; Lagaros, N.D. A Comprehensive Review of Additive Manufacturing for Space Applications: Materials, Advances, Challenges, and Future Directions. *Adv. Eng. Mater.* **2025**, *27*, e202501082. [CrossRef]
22. Alves, B.; Sousa, R.; Coelho, R.; Gatões, D.; Cacho, L.; Branco, R.; Santos, V.M.; Rodrigues, P.F. Enabling Sensor-Integrated and Sustainable Aerospace Structures Through Additively Manufactured Aluminium Mechanisms for CubeSats. *Sensors* **2026**, *26*, 281. [CrossRef] [PubMed]
23. Alkunte, S.; Fidan, I.; Naikwadi, V.; Gudavasov, S.; Ali, M.A.; Mahmudov, M.; Hasanov, S.; Cheepu, M. Advancements and Challenges in Additively Manufactured Functionally Graded Materials: A Comprehensive Review. *J. Manuf. Mater. Process.* **2024**, *8*, 23. [CrossRef]
24. Teacher, M.; Velu, R. Additive Manufacturing of Functionally Graded Materials: A Comprehensive Review. *Int. J. Precis. Eng. Manuf.* **2023**, *25*, 165–197. [CrossRef]
25. NASA Marshall Space Flight Center. Lattices & Additive Manufacturing—How NASA-STD-6030 Can Help Make Your Designs A Reality. NTRS Document ID 20240001336, 2024. Available online: https://ntrs.nasa.gov/citations/20240001336 (accessed on 22 February 2026).
26. Luo, Y.; Sigmund, O.; Li, Q.; Liu, S. Additive manufacturing oriented topology optimization of structures with self-supported enclosed voids. *Comput. Methods Appl. Mech. Eng.* **2020**, *372*, 113385. [CrossRef]
27. Gohar, S.; Hussain, G.; Ali, A.; Ahmad, H. Mechanical performance of honeycomb sandwich structures built by FDM printing technique. *J. Thermoplast. Compos. Mater.* **2023**, *36*, 182–200.
28. Cooke, A.; Smith, D.; Booth, A. Beyond PICO: The SPIDER Tool for Qualitative Evidence Synthesis. *Qual. Health Res.* **2012**, *22*, 1435–1443. [CrossRef] [PubMed]
29. Methley, A.M.; Campbell, S.; Chew-Graham, C.; McNally, R.; Cheraghi-Sohi, S. PICO, PICOS and SPIDER: A Comparison Study of Specificity and Sensitivity in Three Search Tools for Qualitative Systematic Reviews. *BMC Health Serv. Res.* **2014**, *14*, 579. [CrossRef] [PubMed]
30. Pubrica Academy. The PICO Framework for Framing Systematic Review Research Questions—Engineering and Technology Adaptation. Industrial Methodological Guide. Available online: https://pubrica.com/academy/systematic-review/the-pico-framework-for-framing-systematic-review-research-questions/ (accessed on 5 March 2026).
31. Singh, P.; Balla, V.K.; Atre, S.V.; German, R.M.; Kate, K.H. Factors Affecting Properties of Ti-6Al-4V Alloy Additive Manufactured by Metal Fused Filament Fabrication. *Powder Technol.* **2021**, *386*, 9–19. [CrossRef]
32. Sakib-Uz-Zaman, C.; Khondoker, M.A.H. A Review on Extrusion Additive Manufacturing of Pure Copper. *Metals* **2023**, *13*, 859. [CrossRef]
33. NASA. Technical Reports Server (NTRS)—Open Repository of NASA Aerospace Technical Literature. Available online: https://intrs.nasa.gov/ (accessed on 11 May 2026).
34. Karade, S.R.; Siddhartha, S.; Gupta, N.K.; Karunakaran, K.P.; Ganesan, G.; Zeidler, H. Hybridization in Metal Wire Additive Manufacturing: A Case Study of an Impeller. *Metals* **2025**, *15*, 71. [CrossRef]
35. Nasser, F.; Trad, F.; Mohanna, A.; Fuleihan, G.E.-H.; Chehab, A. Chained Prompting for Better Systematic Review Search Strategies—LLM-assisted PICO extraction and Boolean generation. *arXiv* **2026**, arXiv:2602.00011. [CrossRef]

36. Krag, C.H.; Balschmidt, T.; Bruun, F.; Brejnebøl, M.; Xu, J.J.; Boesen, M.; Andersen, M.B.; Müller, F.C. Large Language Models for Abstract Screening in Systematic and Scoping Reviews: A Diagnostic Test Accuracy Study. *medRxiv* **2024**. [CrossRef]
37. Page, M.J.; McKenzie, J.E.; Bossuyt, P.M.; Boutron, I.; Hoffmann, T.C.; Mulrow, C.D.; Shamseer, L.; Tetzlaff, J.M.; Akl, E.A.; Brennan, S.E. The PRISMA 2020 statement: An updated guideline for reporting systematic reviews. *BMJ* **2021**, *372*, n71. [CrossRef] [PubMed]
38. Mohamed, A.M.A.; Samuel, E.; Zedan, Y.; Samuel, A.M.; Doty, H.W.; Samuel, F.H. Intermetallics Formation during Solidification of Al-Si-Cu-Mg Cast Alloys. *Materials* **2022**, *15*, 1335. [CrossRef] [PubMed]
39. Aria, M.; Cuccurullo, C. bibliometrix: An R-tool for Comprehensive Science Mapping Analysis. *J. Informetr.* **2017**, *11*, 959–975. [CrossRef]
40. Ding, H.; Zeng, C.; Raush, J.; Momeni, K.; Guo, S. Developing Fused Deposition Modeling Additive Manufacturing Processing Strategies for Aluminum Alloy 7075: Sample Preparation and Metallographic Characterization. *Materials* **2022**, *15*, 1340. [CrossRef] [PubMed]
41. Benafan, O.; Notardonato, W.U.; Meneghelli, B.J.; Vaidyanathan, R. Design and Development of a Shape Memory Alloy Activated Heat Pipe-Based Thermal Switch. *Smart Mater. Struct.* **2013**, *22*, 105017. [CrossRef]
42. Grau, S.; Diez Lopez, J.M.; Roychowdhury, D.; Chachowski, J.; Stoll, E. Design Automation of Embedded Air Coils for CubeSat Attitude Control. In *Proceedings of the Small Satellites Systems and Services Symposium (4S 2024), Palma de Mallorca, Spain, 27–31 May 2024*; Petrozzi-Ilstad, M., Ed.; SPIE: Washington, DC, USA, 2025; p. 145.
43. Alba Orbital; Delft University of Technology; GAUSS Srl. *PocketQube Standard, Issue 1*; Technical Report; Alba Orbital Ltd.: Glasgow, UK, 2018. Available online: https://www.albaorbital.com/pocketqube-standard (accessed on 17 March 2026).
44. Bouwmeester, J.; Langer, J.; Uludağ, M.Ş.; Amaro-Mendivil, D.; Verhoeven, C. Utility and constraints of PocketQubes. *CEAS Space J.* **2020**, *12*, 195–211. [CrossRef]
45. Franzese, V. PocketQube picosatellites: Survey of missions and technologies. *CEAS Space J.* **2025**, *17*, 1007–1018. [CrossRef]
46. Bouwmeester, J.; Lv, H.; Chan, W.; Guo, W. Towards an innovative electrical interface standard for PocketQubes and CubeSats. *Adv. Space Res.* **2018**, *62*, 3423–3435. [CrossRef]
47. Bouwmeester, J. The Architecture of CubeSats and PocketQubes. Ph.D. Dissertation, Delft University of Technology, Delft, The Netherlands, 2021. Available online: https://research.tudelft.nl/files/96183067/2021_08_10_PhD_Thesis_Jasper_Bouwmeester.pdf (accessed on 21 May 2026).
48. Radu, A.; Uludağ, M.Ş.; Bosman, A.; Speretta, S. Delfi-PQ: The first PocketQube of Delft University of Technology. In Proceedings of the 74th International Astronautical Congress (IAC), Baku, Azerbaijan, 2–6 October 2023.
49. Uludağ, M.Ş.; Speretta, S. Getting the Delfi-PQ ready for multiple launch options. In Proceedings of the 74th International Astronautical Congress (IAC), Baku, Azerbaijan, 2–6 October 2023.
50. Uludağ, M.Ş.; Speretta, S. Delfi-PQ: In-orbit performance and lessons learned in developing a 3P PocketQube. In Proceedings of the 76th International Astronautical Congress (IAC), Sydney, Australia, 29 September–3 October 2025. [CrossRef]
51. Kovács, R.; Józsa, V. Thermal analysis of the SMOG-1 PocketQube satellite. *Appl. Therm. Eng.* **2018**, *139*, 506–513. [CrossRef]
52. Franzese, V.; Kanavouras, K.; Rosete, C.B.; Gouvalas, S.; Sajjad, N.; Alandihallaj, M.; Herasimenka, A.; Hein, A.M. System design of the POQUITO PocketQube mission. *CEAS Space J.* **2025**, *18*, 97–119. [CrossRef]
53. Silva, M.A.C.; Guerrieri, D.C.; Cervone, A.; Gill, E. A review of MEMS micropropulsion technologies for CubeSats and PocketQubes. *Acta Astronaut.* **2018**, *143*, 234–243. [CrossRef]
54. Bouwmeester, J.; Guo, J. CubeSats to PocketQubes: Opportunities and challenges. In Proceedings of the 67th IAC, Guadalajara, Mexico, 26–30 September 2016.
55. Bouwmeester, J.; Lv, H.; Guo, W. PQ9 and CS14 electrical and mechanical subsystem interface standard for PocketQubes and CubeSats. *DataverseNL* **2018**. [CrossRef]
56. Janecka, A.; Novak, P.; Skocik, R. Tether experiment: PocketQube deployed from a CubeSat. In Proceedings of the 10th RAST 2023, Istanbul, Turkey, 7–9 June 2023. [CrossRef]
57. *NASA/TP-20230001313*; Small Spacecraft Technology State of the Art Report: Structures, Materials, and Mechanisms. NASA STMD: Washington, DC, USA, 2023.
58. ECSS. *ECSS-E-ST-10-03C: Space Engineering—Testing*; ESA-ESTEC: Noordwijk, The Netherlands, 2012.
59. CRP Technology. 3D Printed Space-Ready 6P PocketQube Deployer—AlbaPod. Case Study, 2020. Available online: https://iwww.crp-group.com/case-studies/3d-printed-space-ready-6p-pocketqube-deployer-albapod/ (accessed on 13 April 2026).
60. *GSFC-STD-7000A*; General Environmental Verification Standard (GEVS). NASA GSFC: Washington, DC, USA, 2013.
61. Blakey-Milner, B.; Gradl, P.; Snedden, G.; Brooks, M.; Pitot, J.; Lopez, E.; Leary, M.; Berto, F.; du Plessis, A. Metal additive manufacturing in aerospace: A review. *Mater. Des.* **2021**, *209*, 110008. [CrossRef]
62. Sacco, E.; Moon, S.K. Additive manufacturing for space: Status and promises. *Int. J. Adv. Manuf. Technol.* **2019**, *105*, 4123–4146. [CrossRef]

63. Bankapalli, N.K.; Gupta, V.; Saxena, P.; Bajpai, A.; Lahoda, C.; Polte, J. Filament fabrication and subsequent additive manufacturing, debinding, and sintering for extrusion-based metal additive manufacturing and their applications: A review. *Compos. Part B Eng.* **2023**, *264*, 110915. [CrossRef]
64. Wang, Y.; Chen, X.; Su, Y.; Liu, S.; Wang, R.; Yang, K.; Shi, S. Research Progress of Metal Additive Manufacturing Technology and Application in Space: A Review. *Metals* **2024**, *14*, 1373. [CrossRef]
65. Hurtado-Pérez, A.B.; Pablo-Sotelo, A.d.J.; Ramírez-López, F.; Hernández-Gómez, J.J.; Mata-Rivera, M.F. On Topology Optimisation Methods and Additive Manufacture for Satellite Structures: A Review. *Aerospace* **2023**, *10*, 1025. [CrossRef]
66. Wang, X.; Zhang, L.; Liu, Y.; Li, J. Additive Manufacturing for Lightweighting Satellite Platform. *Appl. Sci.* **2023**, *13*, 2809. [CrossRef]
67. Liu, J.; Zheng, Y.; Ma, Y.; Qureshi, A.; Ahmad, R. Topology optimization for metal additive manufacturing: Current trends, challenges, and future outlook. *Virtual Phys. Prototyp.* **2023**, *18*, e2181192. [CrossRef]
68. Plocher, J.; Panesar, A. Review on design and structural optimisation in additive manufacturing: Towards next-generation lightweight structures. *Mater. Des.* **2019**, *183*, 108164. [CrossRef]
69. Ranjith Kumar, G.; Sathishkumar, M.; Vignesh, M.; Manikandan, M.; Rajyalakshmi, G.; Ramanujam, R.; Arivazhagan, N. Metal additive manufacturing of commercial aerospace components–A comprehensive review. *Proc. Inst. Mech. Eng. Part E J. Process Mech. Eng.* **2023**, *237*, 1149–1171. [CrossRef]
70. Boschetto, A.; Bottini, L.; Vatanparast, S. Additive Manufacturing of Polyether Ether Ketone (PEEK) for Space Applications: A Nanosat Polymeric Structure. *Polymers* **2021**, *13*, 11. [CrossRef] [PubMed]
71. Galati, M.; Iuliano, L. A Literature Review of Powder-Based Electron Beam Melting Focusing on Numerical Simulations. *Addit. Manuf.* **2018**, *19*, 1–20. [CrossRef]
72. Gradl, P.R.; Mireles, O.R.; Andrews, N. *Principles of Directed Energy Deposition for Aerospace Applications*; NASA Technical Reports Server, Document 20220002267; NASA Marshall Space Flight Center: Huntsville, AL, USA, 2022. Available online: https://ntrs.nasa.gov/citations/20220002267 (accessed on 21 May 2026).
73. Khan, N.; Riccio, A. A Systematic Review of Design for Additive Manufacturing of Aerospace Lattice Structures: Current Trends and Future Directions. *Prog. Aerosp. Sci.* **2024**, *149*, 101021. [CrossRef]
74. Aboulkhair, N.T.; Simonelli, M.; Parry, L.; Ashcroft, I.; Tuck, C.; Hague, R. 3D printing of Aluminium alloys: Additive Manufacturing of Aluminium alloys using selective laser melting. *Prog. Mater. Sci.* **2019**, *106*, 100578. [CrossRef]
75. Hassanin, H.; Modabber, P.; Tcherniaeff, A.; El-Sayed, M.A.; Essa, K. Optimization of tensile strength of AlSi10Mg material in the powder bed fusion process using the Taguchi method. *Sci. Rep.* **2024**, *14*, 31172. [CrossRef] [PubMed]
76. *ECSS-Q-ST-70-02C*; Space Product Assurance—Thermal Vacuum Outgassing Test for the Screening of Space Materials. ECSS Secretariat, ESA-ESTEC: Noordwijk, The Netherlands, 2008; Still Current as of 2026. Available online: https://ecss.nl/standard/ecss-q-st-70-02c-thermal-vacuum-outgassing-test-for-the-screening-of-space-materials/ (accessed on 21 May 2026).
77. Ge, Q.; Jian, B.; Li, H. Shaping soft materials via digital light processing-based 3D printing: A review. *Forces Mech.* **2022**, *6*, 100074. [CrossRef]
78. Maamoun, A.H.; Elbestawi, M.A.; Veldhuis, S.C. Influence of Shot Peening on AlSi10Mg Parts Fabricated by Additive Manufacturing. *J. Manuf. Mater. Process.* **2018**, *2*, 40. [CrossRef]
79. Wang, P.; Tan, X.; He, C.; Nai, M.L.S.; Huang, R.; Tor, S.B.; Wei, J. Scanning optical microscopy for porosity quantification of additively manufactured components. *Addit. Manuf.* **2018**, *21*, 350–358. [CrossRef]
80. Croteau, J.R.; Griffiths, S.; Rossell, M.D.; Leinenbach, C.; Kenel, C.; Jansen, V.; Seidman, D.N.; Dunand, D.C.; Vo, N.Q. Microstructure and mechanical properties of Al-Mg-Zr alloys processed by selective laser melting. *Acta Mater.* **2018**, *153*, 35–44. [CrossRef]
81. Uddin, S.Z.; Murr, L.E.; Terrazas, C.A.; Morton, P.; Roberson, D.A.; Wicker, R.B. Processing and characterization of crack-free aluminum 6061 using high-temperature heating in laser powder bed fusion additive manufacturing. *Addit. Manuf.* **2018**, *22*, 405–415. [CrossRef]
82. Saddoud, R.; Perlin, K.; Sergeeva-Chollet, N.; Delacroix, T.; Skarlatos, A.; Garandet, J.P. On the potential of eddy current characterization of the ferritic content of recovered 316L powders after Laser Powder Bed Fusion fabrication. *Addit. Manuf. Lett.* **2024**, *9*, 100207. [CrossRef]
83. Yuan, C.; Ding, R.; Hou, X.; Guo, Q.; Gao, X. Laser powder bed fusion of crack-free 6061Al alloy using nano-sized TiO_2-modified powders. *Mater. Sci. Technol.* **2024**, *40*, 110–123. [CrossRef]
84. Spierings, A.B.; Dawson, K.; Heeling, T.; Uggowitzer, P.J.; Schäublin, R.; Palm, F.; Wegener, K. Microstructural features of Sc- and Zr-modified Al-Mg alloys processed by selective laser melting. *Mater. Des.* **2017**, *115*, 52–63. [CrossRef]
85. Jeong, C.-G.; Trang, T.T.T.; Woo, Y.; Yoon, E.Y.; Lee, Y.; Heo, Y.-U. Effect of cooling rate on the final microstructure and tensile property in an Fe–Mn–Si–C-based multiphase TRIP steel. *Mater. Sci. Eng. A* **2023**, *887*, 145696. [CrossRef]

86. Ma, C.; Wang, K.; Gao, D.; Zhao, G. Highly sensitive and selective flexible anisotropic strain sensor based on liquid metal/conductive ink for wearable applications. *Compos. Part B Eng.* **2024**, *281*, 111538. [CrossRef]
87. Awd, M.; Tenkamp, J.; Hirtler, M.; Siddique, S.; Bambach, M.; Walther, F. Comparison of Microstructure and Mechanical Properties of Scalmalloy® Produced by Selective Laser Melting and Laser Metal Deposition. *Materials* **2018**, *11*, 17. [CrossRef] [PubMed]
88. Shajari, Y.; Razavi, M.; Nikzad, L. Interfacial investigation of Al/Ni in new generation of composite (Metal-3D lattice metal): Annealing time effect. *J. Mater. Res. Technol.* **2023**, *27*, 3086–3097. [CrossRef]
89. Liu, S.; Shin, Y.C. Additive manufacturing of Ti6Al4V alloy: A review. *Mater. Des.* **2019**, *164*, 107552. [CrossRef]
90. Sanchez, S.; Smith, P.; Xu, Z.; Gaspard, G.; Hyde, C.J.; Wits, W.W.; Ashcroft, I.A.; Chen, H.; Clare, A.T. Powder Bed Fusion of nickel-based superalloys: A review. *Int. J. Mach. Tools Manuf.* **2021**, *165*, 103729. [CrossRef]
91. Lei, X.; Xiong, W.; Wang, H.; Zhang, L.-C.; Qian, M. A moving-boundary dynamic model for in-situ alloyed and compositionally graded Ti-alloys fabricated by laser directed energy deposition in Nb crucibles. *Mater. Today Commun.* **2022**, *30*, 103067. [CrossRef]
92. Mohd Yusuf, S.; Cutler, S.; Gao, N. Review: The Impact of Metal Additive Manufacturing on the Aerospace Industry. *Metals* **2019**, *9*, 1286. [CrossRef]
93. Schneller, W.; Leitner, M.; Springer, S.; Grün, F.; Taschauer, M. Effect of HIP Treatment on Microstructure and Fatigue Strength of Selectively Laser Melted AlSi10Mg. *J. Manuf. Mater. Process.* **2019**, *3*, 16. [CrossRef]
94. Yu, M.; Wang, P.; Zhang, J.; Wang, H.; Yuan, W.; Chen, C. Microstructure and corrosion behaviour of 316L–IN625 functionally graded material fabricated by directed energy deposition. *Corros. Sci.* **2021**, *192*, 109797. [CrossRef]
95. Chaudhary, R.; Fabbri, P.; Leoni, E.; Mazzanti, F.; Akbari, R.; Antonini, C. Additive manufacturing by digital light processing: A review. *Prog. Addit. Manuf.* **2023**, *8*, 331–351. [CrossRef]
96. Jia, H.; Sun, H.; Wang, H.; Wang, X.; Zhang, H. Scanning Strategy in Selective Laser Melting (SLM): A Review. *Int. J. Adv. Manuf. Technol.* **2021**, *113*, 2413–2435. [CrossRef]
97. Orion AM (Formerly Roboze)—AMCUBE Project Documentation. *PEEK Structural Frame for 1U CubeSat: Technical Datasheet and Qualification Report Summary*; Orion AM s.r.l.: Brescia, Italy. Available online: https://www.orion-am.com/blog/orion-am-news-1/3d-printed-peek-cubesats-4 (accessed on 27 April 2026).
98. Sanaei, N.; Fatemi, A. Defects in additive manufactured metals and their effect on fatigue performance: A state-of-the-art review. *Prog. Mater. Sci.* **2021**, *117*, 100724. [CrossRef]
99. Gallo, L.; Bonne, M.; Bucalá, V.; Adrover, M.E. Enhancing Albendazole Delivery Using Mesoporous Santa Barbara Amorphous-15: A Box–Behnken Design Study. *Adv. Eng. Mater.* **2024**, *26*, 2400320. [CrossRef]
100. Snow, Z.; Nassar, A.R.; Reutzel, E.W. Review of the formation and impact of flaws in powder bed fusion additive manufacturing. *Addit. Manuf.* **2020**, *36*, 101457. [CrossRef]
101. Liu, Y.; Wu, Z.; Wang, Q.; Zhao, L.; Zhang, X.; Gao, W.; Xu, J.; Ma, Y. A critical review on the effects of process-induced porosity on the mechanical properties of alloys fabricated by laser powder bed fusion. *J. Mater. Sci.* **2022**, *57*, 9818–9865. [CrossRef]
102. du Plessis, A.; Yadroitsava, I.; Yadroitsev, I. Effects of defects on mechanical properties in metal additive manufacturing: A review focusing on X-ray tomography insights. *Mater. Des.* **2020**, *187*, 108385. [CrossRef]
103. Sanaei, N.; Fatemi, A. Analysis of the Effect of Internal Defects on Fatigue Performance of Additive Manufactured Metals. *Mater. Sci. Eng. A* **2020**, *785*, 139385. [CrossRef]
104. Khosravani, M.R.; Reinicke, T. On the Use of X-ray Computed Tomography in Assessment of 3D-Printed Components. *J. Nondestruct. Eval.* **2020**, *39*, 75. [CrossRef]
105. Honarvar, F.; Varvani-Farahani, A. A review of ultrasonic testing applications in additive manufacturing: Defect evaluation, material characterization, and process control. *Ultrasonics* **2020**, *108*, 106227. [CrossRef] [PubMed]
106. Lopez, A.B.; Sousa, J.P.; Pragana, J.P.M.; Bragança, I.M.F.; Santos, T.G.; Silva, C.M.A. In Situ Ultrasonic Testing for Wire Arc Additive Manufacturing Applications. *Machines* **2022**, *10*, 1069. [CrossRef]
107. McCann, R.; Obeidi, M.A.; Hughes, C.; McCarthy, É.; Egan, D.S.; Vijayaraghavan, R.K.; Joshi, A.M.; Acinas Garzon, V.; Dowling, D.P.; McNally, P.J.; et al. In-situ sensing, process monitoring and machine control in Laser Powder Bed Fusion: A review. *Addit. Manuf.* **2021**, *45*, 102058. [CrossRef]
108. Slongo, J.S.; Gund, J.; Passarin, T.A.R.; Pipa, D.R.; Ramos, J.E.; Arruda, L.V.; Junior, F.N. Effects of Thermal Gradients in High-Temperature Ultrasonic Non-Destructive Tests. *Sensors* **2022**, *22*, 2799. [CrossRef] [PubMed]
109. Wang, Y.; Wang, J.; Wei, Y.; Zhang, X.; Xu, M. A physics-guided deep generative model for predicting melt pool behavior in laser powder bed fusion additive manufacturing. *J. Intell. Manuf.* **2025**, *36*, 1457–1478. [CrossRef]
110. Cooper, N.; Coles, L.A.; Everton, S.; Maskery, I.; Campion, R.P.; Madkhaly, S.; Morley, C.; O'Shea, J.; Evans, W.; Saint, R.; et al. Additively manufactured ultra-high vacuum chamber for portable quantum technologies. *Addit. Manuf.* **2021**, *40*, 101898. [CrossRef]
111. NASA Goddard Space Flight Center. Outgassing Data for Selecting Spacecraft Materials Online Database. NASA-STD-6016/ASTM E595 Dataset, Hosted by NASA GSFC. Available online: https://outgassing.nasa.gov/ (accessed on 21 May 2026).

112. *ECSS-E-ST-32C Rev. 1*; Space Engineering—Structural General Requirements. ECSS Secretariat, ESA-ESTEC: Noordwijk, The Netherlands, 15 November 2008; Current as of 2026. Available online: https://ecss.nl/standard/ecss-e-st-32c-rev-1-structural-general-requirements/ (accessed on 21 May 2026).
113. *ECSS-E-ST-10-03C Rev. 1*; Space Engineering—Testing; ECSS Secretariat, ESA-ESTEC: Noordwijk, The Netherlands, 31 May 2022. Available online: https://ecss.nl/standard/ecss-e-st-10-03c-rev-1-testing-31-may-2022/ (accessed on 21 May 2026).
114. *ECSS-Q-ST-70-80C*; Processing and Quality Assurance Requirements for Metallic Powder Bed Fusion Technologies for Space Applications. ECSS Secretariat, ESA-ESTEC: Noordwijk, The Netherlands, 30 July 2021. Available online: https://ecss.nl/istandard/ecss-q-st-70-80c-processing-and-quality-assurance-requirements-for-metallic-powder-bed-fusion-technologies-for-space-applications-30-july-2021/ (accessed on 21 May 2026).
115. *NASA-STD-6030*; Additive Manufacturing Requirements for Spaceflight Systems. NASA Office of the Chief Engineer: Washington, DC, USA, 2021. Available online: https://standards.nasa.gov/standard/NASA/NASA-STD-6030 (accessed on 21 May 2026).
116. *ECSS-E-HB-32-20*; Space Engineering—Structural Materials Handbook (Parts 1–8). ECSS Secretariat, ESA-ESTEC: Noordwijk, The Netherlands, 20 March 2011; Current as of 2026; Update in Progress. Available online: https://ecss.nl/hbstms/ecss-e-hb-32-20a-part-1-structural-materials-handbook-overview-and-material-properties/ (accessed on 21 May 2026).
117. Gradl, P.R.; Tinker, D.; Park, A.; Mireles, O.R.; Garcia, M.; Wilkerson, R.; Mckinney, C. Robust Metal Additive Manufacturing Process Selection and Development for Aerospace Components. *J. Mater. Eng. Perform.* **2022**, *31*, 6013–6044. [CrossRef]
118. Bagg, S.D.; Babuska, T.F.; Gerhardt, M.R.; Tobin, K.J. *Comparison of NASA and ECSS Standards for Additive Manufacturing Qualification and Certification for Spaceflight Application*; NASA Technical Reports Server, Document 20220004051; NASA Marshall Space Flight Center: Huntsville, AL, USA, 2022. Available online: https://ntrs.nasa.gov/citations/20220004051 (accessed on 21 May 2026).
119. NASA Office of the Chief Engineer. *NASA-HDBK-6030: Additive Manufacturing Implementation Handbook*; NASA Technical Handbook, Baseline; NASA Office of the Chief Engineer: Washington, DC, USA, 2022. Available online: https://istandards.nasa.gov/standard/NASA/NASA-HDBK-6030 (accessed on 21 May 2026).
120. *ASTM F2924-14*; (Reapproved 2021): Standard Specification for Additive Manufacturing Titanium-6 Aluminum-4 Vanadium with Powder Bed Fusion. ASTM International: West Conshohocken, PA, USA, 2021. [CrossRef]
121. *ISO/ASTM 52900:2021*; Additive Manufacturing—General Principles—Fundamentals and Vocabulary. International Organization for Standardization: Geneva, Switzerland, 2021. Available online: https://www.iso.org/standard/74514.html (accessed on 22 May 2026).
122. *ASTM F3001-14*; (Reapproved 2021): Standard Specification for Additive Manufacturing Titanium-6 Aluminum-4 Vanadium ELI (Extra Low Interstitial) with Powder Bed Fusion. ASTM International: West Conshohocken, PA, USA, 2021. [CrossRef]
123. *ASTM F3049-14*; Standard Guide for Characterizing Properties of Metal Powders Used for Additive Manufacturing Processes. ASTM International: West Conshohocken, PA, USA, 2014. [CrossRef]
124. *ECSS-E-ST-32-10C Rev. 2 Corr. 1*; Space Engineering—Structural Factors of Safety for Spaceflight Hardware. ECSS Secretariat, ESA-ESTEC: Noordwijk, The Netherlands, 1 August 2019. Available online: https://ecss.nl/standard/ecss-e-st-32-10c-rev-2-corr-1-structural-factors-of-safety-for-spaceflight-hardware-1-august-2019/ (accessed on 22 May 2026).
125. NASA Office of the Chief Engineer. *NASA-STD-5001B with Change 3: Structural Design and Test Factors of Safety for Spaceflight Hardware*; NASA Technical Standards Document; NASA Office of the Chief Engineer: Washington, DC, USA, 24 October 2022. Available online: https://standards.nasa.gov/standard/NASA/NASA-STD-5001 (accessed on 22 May 2026).
126. Japan Aerospace Exploration Agency (JAXA). KAKUSHIN Interview 03. Available online: https://www.kenkai.jaxa.jp/kakushin/interview/03/interview03_16.html (accessed on 19 March 2026).
127. Dingwall, B.; Twiggs, R.; Craft, M.; Mulligan, S.; Voss, H.; Winterton, J.; Nash, D.; Crane, B.; Orvis, M. Bringing Space to the Classroom Through STEM Education Providing Extreme Low Earth Orbit Missions Using ThinSats. In *Proceedings of the 31st Annual AIAA/USU Conference on Small Satellites*; Utah State University: Logan, UT, USA, 2017; SSC17-WKII-05.
128. Liu, S.; Li, Q.; Chen, W.; Tong, L.; Cheng, G. An identification method for enclosed voids restriction in manufacturability design for additive manufacturing structures. *Front. Mech. Eng.* **2015**, *10*, 126–137. [CrossRef]
129. Kreikenbohm, T. GENESIS L, -N. Gunter's Space Page, 2026. Available online: https://space.skyrocket.de/doc_sdat/genesis-l.htm (accessed on 27 April 2026).
130. Princeton University TigerSats. 3D-Printed CubeSat Structures. Princeton University, Princeton, NJ, USA, 2024. Available online: https://tigersats.princeton.edu/3d-printed-cubesat-structures (accessed on 22 May 2026).
131. NanoAvionics. *CubeSat & Small Satellite Manufacturing—Industrial Capability Overview*; NanoAvionics UAB: Vilnius, Lithuania. Available online: https://nanoavionics.com/satellite-manufacturing/ (accessed on 30 April 2026).
132. nScrypt Inc.; Sciperio Inc. US Space Force SBIR Phase II Award: Additively-Manufactured 6U CubeSat for Tactical Space Applications. Public Award Announcement (Feb 2023). Available online: https://3dprintingindustry.com/news/us-space-forces-cubesats-to-be-3d-manufactured-by-sciperio-220578/ (accessed on 28 April 2026).

133. EOS GmbH Electro Optical Systems. EOS M 290—Mid-Size Metal 3D Printing System. Available online: https://www.ieos.info/metal-solutions/metal-printers/eos-m-290#key-features (accessed on 30 April 2026).
134. NASA Small Spacecraft Systems Virtual Institute. State of the Art of Small Spacecraft Technology Report, Section 6: Structures, Materials, and Mechanisms. NASA/TP-20240000142 (2024 Edition; 2025 Update in Revision). Available online: https://iwww.nasa.gov/smallsat-institute/sst-soa/structures-materials-and-mechanisms/ (accessed on 22 May 2026).

Disclaimer/Publisher's Note: The statements, opinions and data contained in all publications are solely those of the individual author(s) and contributor(s) and not of MDPI and/or the editor(s). MDPI and/or the editor(s) disclaim responsibility for any injury to people or property resulting from any ideas, methods, instructions or products referred to in the content.